TESTING A TB VACCINE IN HUMANIZED MICE IN THE CONTEXT OF HIV

COMBATING THE HIV/TB CO-INFECTION SYNDEMIC: TESTING A NOVEL RESPIRATORY MUCOSAL ADENOVIRAL TUBERCULOSIS VACCINE IN NAÏVE AND HIV-INFECTED HUMANIZED MICE

By ALEXIS CHACON, BSc. (Hons)

A Thesis Submitted to the School of Graduate Studies in Partial Fulfilment of the Requirements for the Degree Master of Sciences

McMaster University MASTER OF SCIENCES (2023) Hamilton, Ontario (Medical Sciences - Infection & Immunity)

TITLE: Combating the HIV/TB Co-infection Syndemic: Testing a Novel Respiratory Mucosal Adenoviral Tuberculosis Vaccine in Naïve and HIV-Infected Humanized Mice. AUTHOR: Alexis Chacon, BSc. (Honours) (McMaster University) SUPERVISOR: Dr. Amy Gillgrass NUMBER OF PAGES: xx, 146.

Lay Abstract

HIV and TB are major diseases that can occur together, severely worsening patients' health and challenging global healthcare systems. The current TB vaccine, BCG, isn't ideal for people living with HIV (PLWH), causing this vulnerable population to be at greater risk of getting TB infection. Therefore, developing a new TB vaccine that is safe and effective in PLWH is an urgent global issue. We used humanized mice that develop human immune cells to test a novel TB vaccine delivered to the lungs (Tri:ChAd68) to see if it could protect against TB and overcome immune challenges from HIV. We saw increased immune responses and lower TB infection in our vaccinated humanized mice and the vaccine appeared to also be beneficial in the mice that had prior HIV infection. This suggests the Tri:ChAd68 vaccine may be able to offer protection against TB in PLWH; however, more studies are needed to conclude this.

Abstract

HIV and Tuberculosis (TB) co-infection place an immense burden on health care systems as they act in synergy to worsen disease prognoses. TB is the most common cause of death in people living with HIV (PLWH) and in turn, HIV is the most significant risk factor for progressing from latent to active TB disease. While HIV and TB are endemic in sub-Saharan Africa, they also disproportionately affect marginalized populations in Canada. Unfortunately, the only licensed TB vaccine, BCG, does not protect from adult pulmonary TB and is not recommended for PLWH. Thus, the development of novel TB vaccines, which are safe and effective in PLWH, remains an urgent global necessity. We have found that humanized mice (hu-mice) are ideal models to research this as they can be successfully infected with HIV, TB and HIV/TB and recapitulate human disease pathology.

A next-generation respiratory mucosal (RM) trivalent chimpanzee adenoviral-vectored vaccine (Tri:ChAd68) was developed and tested in our naïve and HIV-infected hu-mice. When immunizing naïve hu-mice, a trend of increased *M.tb*-specific CD4+ T cells producing IFNγ and TNFα in the lungs and spleen was observed. After subsequent *M.tb* infection, the vaccinated naïve hu-mice also exhibited significantly reduced lung mycobacterial burden, tissue dissemination and lung pathology. We then investigated the vaccine immunogenicity and ability to protect from TB in the context of HIV. Our immunized HIV-infected hu-mice were also able to produce *M.tb*-specific T cells and when challenged with *M.tb*, we observed a decreased trend in mycobacterial load in the lungs, indicating that the vaccine may be able to offer protection against TB when a prior HIV infection is present. These findings demonstrate the protective potential of the RM

Tri:ChAd68 vaccine against TB disease for PLWH. In the future, we will test this vaccine in antiretroviral treated HIV-infected hu-mice to increase clinical significance.

Acknowledgements

I am beyond grateful to have had the opportunity and privilege to do my M.Sc at McMaster University in the Gillgrass Lab. I have learned so much about myself and about all the work that goes into research, giving me a greater appreciation and new perspective on science research. I am incredibly thankful for all the experiences I've had and the friendships I've made these past two years. There are many individuals I would like to acknowledge that have played a great part in my academic career during graduate school.

First and foremost, I would like to thank my supervisor Dr. Amy Gillgrass for the endless support, mentorship and guidance she has given me throughout my masters. Her passion for science and dedication to her students helped motivate me (especially when experiments did not go as planned) and she always remained positive and eager to help me find a solution any problem that arose.

I would like to thank my supervisory committee, Dr. Charu Kaushic and Dr. Zhou Xing for their advice, expertise and contributions. They have played a significant role in helping my thesis project get to where it is today, and for that I am extremely grateful.

I would like to thank the past and current members of the Gillgrass Lab, who have help shaped this amazing experience for me. I'd like to thank Jack Yang, although you are no longer in the lab, I cherish all the fun memories we had together while running experiments. I'd like to thank Madeleine Lepard, for always being there to help out and being so knowledgeable whenever we had questions. I'd like to thank Victoria Lee, for always being so cheerful and bubbly, even during our all-nighters in the lab. I'd like to thank Margaret Choi, for all her help with the histology quantification and for always being so kind.

I would like to thank Dr. Sam Afkhami, for all his help with my project and his constant encouragement. Thank you for always being willing to lend a helping hand, even when he was super busy. I really appreciate our friendship and the support and guidance he had given me. I would also like to thank Mittens for being a good boy.

I would like to thank Dr. Aisha Nazli, for all her help with containment level 2+ training and for always being a ray of sunshine any time of day. I would also like to thank Anna Zganiacz, for all her help in the containment level 3 facility and guiding us through challenges with the TB and BCG.

I'd like to thank all the friends I've made at MIRC, namely Yona Tugg, Emily Grydziuszko, Dominika Boron, Emily Feng, Alicia Kang, and Jori. Having friends that can relate to the struggles of grad school but still push through has been so comforting and reassuring. I would also like to thank all the past and current Kaushic Lab members, who have all been super supportive and friendly during and outside of lab meetings.

I would also like to thank my two best friends, Neeti Jain and Farseema Delgosha. Even though we were all in different provinces (soon countries ☹) they gave me their never-ending support and encouragement. From first year undergrad students living in the same residence, I'm so glad we have remained so close over these years.

I would like to thank my boyfriend, Mitch Weisner, for being my rock, my cheerleader and someone I could always call when life got too overwhelming. Words can't express how much you have helped me mentally throughout grad school, and I am eternally grateful to have you by my side.

Finally, I would like to thank my family. From the bottom of my heart, I'd like to thank my mom and stepdad Kevin for being an amazing support system for me and always believing in me. Thank you for your constant words of encouragement and your unconditional love and support. I would like to thank my sister Chelsea and Auntie Myra (and Shadow), who have supported me throughout my entire academic journey, and I know will always be there for me. I would like to thank Klyde, the best roommate and buddy I could ask for.

And most of all, I would like to thank the mice.

Table of Contents

List of Figures

List of Tables

List of Supplementary Figures

List of Supplementary Tables

List of Abbreviations

A2	NRG mice transgenic for HLA class I (A*02:01)
ACK	Ammonium-Chloride-Potassium lysing buffer
Ad	Adenovirus
AdHu5	Human serotype 5 adenoviral-vector
AFB	Acid-fast bacillus
Ag	Antigen
Ag85A	Antigen 85A
AIDS	Acquired Immunodeficiency Syndrome
AMØ	Alveolar macrophage
ANOVA	Analysis of variance
APC	Antigen presenting cell
ART	Antiretroviral therapy
AUP	Animal Utilization Protocol
BAL	Bronchoalveolar lavage
BCG	Bacille Calmette-Guérin
BLT	Bone Marrow Liver Thymus
BSA	Bovine serum albumin
cART	Combination antiretroviral therapy
CBMC	Cord blood mononuclear cells
CCR5 (or R5)	C-C chemokine receptor type 5
CD	Cluster of differentiation
CFCB	Culture filtrate and crude BCG
CFU	Colony forming units
cGy	Centigray
Ch	Chimpanzee
ChAd68	Chimpanzee serotype 68 adenoviral-vector
CL3	Containment level 3
CO_2	Carbon dioxide
COVID-19	Coronavirus disease 2019
CTL	Cytotoxic T lymphocyte
CXCR4 (or X4)	C-X-C chemokine receptor type 4
DC	Dendritic cell
DMPA	Depot-medroxyprogesterone acetate
DMSO	Dimethyl sulfoxide
DNA	Deoxyribonucleic acid
DRAG	NRG mice transgenic for HLA Class II (DRB1*04:01)
EDTA	Ethylenediaminetetraacetic acid
ELISA	Enzyme-linked immunosorbent assay
Env	Envelope
FBS	Fetal bovine serum
Fc	Fragment crystallizable
FMO	Fluorescence minus one

FRT	Female reproductive tract
FTC	Emtricitabine
Gag	Group-specific antigen
Gp120/41	Envelope glycoprotein
GvHD	Graft-versus-host disease
GWAS	Genome-wide association studies
h	Human
H&E	Hematoxylin and eosin
hCD	Human cluster of differentiation
HEPA	High efficiency particulate air
HEPES	Hydroxyethyl piperazineethanesulfonic acid
HiREB	Hamilton Integrated Research Ethics Board
HIV	Human immunodeficiency virus
HLA	Human leukocyte antigen
HSC	Hematopoietic stem cells
HSV	Herpes simplex virus
Hu	Human
Hu-mice/mouse	Humanized mice/mouse
huDRAG-A2	humanized DRAG-A2 mice
huDRAGA	humanized DRAGA mice
huNRG	humanized NRG mice
huNSG	humanized NSG mice
Hu-BLT	humanized NSG using the BLT-method
IFN	Interferon
Ig	Immunoglobulin
IGRA	Interferon gamma release assay
IH	Intrahepatic
IHC	Immunohistochemistry
IL	Interleukin
IM	Intramuscular
IMØ	Interstitial macrophage
IN	Intranasal
IP	Intraperitoneal
IRIS	Immune reconstitution inflammatory syndrome
IU	Infectious unit
IV	Intravenous
kg	Kilograms
LMIC	Low-to-middle income country
LTBI	Latent tuberculosis infection
M. bovis	*Mycobacterium bovis*
MDR-TB	Multi-drug resistant TB
MFI	Mean fluorescent index
mg	Milligrams
MHC	Major histocompatibility complex

mL	Milliliter
MSM	Men who have sex with men
M. tb	*Mycobacterium tuberculosis*
NAT	Nucleic acid tests
NHEJ	Non-homologous end joining
NHP	Non-human primates
NK	Natural killer
NNRTI	Non-nucleoside reverse transcriptase inhibitors
NOD	Non-obese diabetic
NOG	NOD.Cg-Prkdr^{scid}Il2rγ^{tm1sug}
NRG	NOD.Cg-Rag1^{tm1MoM}Il2rγ^{tm1sug}
NSG	NOD.Cg-Prkdr^{scid}Il2rγ^{tm1Wjl}
OADC	Oleic acid-albumin-dextrose-catalase
PBS	Phosphate buffered saline
PCR	Polymerase chain reaction
PEP	Pre-exposure prophylaxis
PFA	Paraformaldehyde
PFU	Plaque forming unit
PLWH	People living with HIV
PMA	Phorbol myristate acetate
Pol	DNA polymerase
PrEP	Pre-exposure prophylaxis
Prkdc	Protein kinase, DNA-activated, catalytic polypeptide
qPCR	Quantitative polymerase chain reaction
Rag	Recombination-activating gene
RAL	Raltegravir
RBC	Red blood cell
RIF	Rifampicin
RNA	Ribonucleic acid
RpfB	Resuscitation promoting factor B
RPMI	Rotations per minute
RPMI	Roswell Park Memorial Institute culture media
RT	Reverse transcriptase
RT-qPCR	Reverse transcription quantitative polymerase chain reaction
SCID	Severe combined immunodeficiency
SEM	Standard error of mean
SHIV	Simian human immunodeficiency virus
SIV	Simian immunodeficiency virus
sRPMI	Supplemented RPMI 1640 media
SSA	Sub-Saharan Africa
STI	Sexually transmitted infection
TB	Tuberculosis
TBE	Tris Borate EDTA buffer
TCR	T cell receptor

TDF	Tenofovir disoproxil fumarate
Tg	Trangenic
Th	T helper
TII	Trained innate immunity
TNF	Tumour necrosis factor
Tri	Trivalent
TST	Tuberculin skin test
UCB	Umbilical cord blood
V(D)J	Variability, diversity, and joining
WHO	World Health Organization
XMDR-TB	Extreme multi-drug resistant TB
^{o}C	Degrees Celsius
α	Alpha
γ	Gamma
µg	Microgram
µL	Microliter
µM	Micromolar
µm	Micrometer/micron

Declaration of Academic Achievement:

I declare that this thesis dissertation has been composed by myself and based solely on original research conducted in the lab. This thesis was written entirely by myself, with editing and feedback from my supervisor, Dr. Amy Gillgrass. I confirm that the work submitted is an accurate representation of the experiments and findings that I have contributed to during my time as a M.Sc candidate. I confirm that the work is my own, and listed below is the work conducted in collaboration with others.

Alexis Chacon
Mouse breeding, animal monitoring, cord blood processing, cord blood DNA extraction, HLA-typing, CFU plating, humanizing mice, HIV-1 preparation and infections, vaccine preparations, sample collection and processing, ART preparation, flow cytometry, T cell stimulation, RNA extraction, RT-qPCR, histology processing, experimental planning, data generation and analysis

Madeleine Lepard
Mouse breeding, animal monitoring, cord blood processing, CFU plating, humanizing mice, HIV-1 preparation and infections, *M.tb* preparation, sample collection and processing, histology processing, flow cytometry, RNA extraction, RT-qPCR, data analysis

Jack (Xiaozhi) Yang
Mouse breeding and genotyping, animal monitoring, cord blood processing, CFU plating, humanizing mice, *M.tb* preparation, mouse immunization, sample collection and processing, flow cytometry, T cell stimulation, RT-qPCR, data analysis

Dr. Amy Gillgrass
Experimental designs and planning, protocol specific training, CFU plating, tissue processing, data analysis

Dr. Sam Afkhami
M.tb infection, mouse immunization, sample collection and processing, data analysis

Victoria Lee
Mouse breeding, sample collection and processing, flow cytometry, ART preparation

Dr. Aisha Nazli
RT-qPCR optimization and HIV-1 preparation

Anna Zganiacz
BCG preparation and CFU plating

Margaret (Wa Yan) Choi
Histology imaging and quantification

CHAPTER 1: INTRODUCTION

CHAPTER 1.1. Human Immunodeficiency Virus

1.1.1. Epidemiology and Significance

Human immunodeficiency virus (HIV) is a spherical enveloped retrovirus that persists as a chronic infection but can develop into the clinical syndrome, acquired immunodeficiency syndrome (AIDS), characterized by the weakening of the immune system and increased susceptibility to opportunistic infections[1]. It is categorized into two distinct subtypes, HIV-1 and HIV-2. While both subtypes share similar transmission routes, HIV-2 has a lower global prevalence mainly due to being less pathogenic, lower transmissibility and likelihood to progress to AIDS[2]. In 2022, 39 million people around the world were living with HIV-1 and of those individuals, 630,000 people died from AIDS-related illnesses[3]. Since the beginning of the HIV/AIDS epidemic, it has claimed over 40 million lives with ongoing transmission in all countries globally, with sub-Saharan Africa (SSA) remaining the region most severely impacted by the epidemic[4]. Two thirds of people living with HIV-1 (PLWH) reside in SSA, with countries such as Eswatini, Lesotho, Botswana and South Africa having the largest HIV-positive population[4]. In Canada, about 62,790 people were living with HIV, with an estimated 1,520 new HIV infections at the end of 2020[5]. Of these new infections, the proportion among people who inject drugs, Indigenous people and women slightly increased from previous years. Moreover, about 90% of PLWH in Canada were diagnosed cases, with 87% of them on treatment with suppressed viral load[5].

While HIV-1 can affect anyone, it disproportionally affects women and adolescent girls, as well as men who have sex with men (MSM). Globally, women account for more than half the number of people living with HIV-1, which can be due to factors such as gender inequality, violence against women, low socioeconomic status and restricted social autonomy[6]. Moreover, a risk factors analysis suggested that being under the age of 25, having had a previous sexually transmitted infection (STI), and being unmarried significantly increased the risk of HIV-1 acquisition among SSA women[7,8]. Studies have also shown that women who use Depot Medroxyprogesterone Acetate (DMPA), a progestin-based hormonal contraceptive widely used in SSA, increases the likelihood of them acquiring HIV-1 by 40-50%[9]. This may be due to DMPA impairing the vaginal epithelial barrier, increasing vaginal target cells, and altering genital immunity and defense thus enhancing the women's susceptibility to HIV-1[9]. Fortunately, in 2022 over 75% of PLWH were accessing treatment in the form of antiretroviral therapy (ART); however, there are still millions of people who do not have access to this life changing medication[3].

1.1.2. Transmission and Pathogenesis

HIV is transmitted through contact with a variety of bodily fluids from HIV-positive individuals such as blood, semen, vaginal secretions, and breast milk[4]. Individuals who engage in condomless anal or vaginal sex, share contaminated needles, receive contaminated blood transfusions and/or had a previous STI such as herpes simplex virus (HSV) and chlamydia, as well as bacterial vaginosis are at a greater risk of contracting HIV[4]. The virus can also be transmitted from mother to child during pregnancy and through breast feeding[4]. HIV infectivity and clinical outcomes among people varies, as it depends

on the hosts' susceptibility, social environment, route of transmission and diverse genetic variants of the virus[10]. Interestingly, human leukocyte antigens (HLA) have been shown by genome-wide association studies (GWAS) to be the most significant host genetic variant of viral susceptibility, contributing to 10-15% of variation in clinical outcomes[11].

During the primary stage of infection, the virus is actively replicating in the body and may produce flu-like symptoms weeks after entering the host[12]. HIV weakens the immune system by targeting and attacking CD4+ T cell populations and impairing macrophage signaling[12,13]. The CD4+ T cells can get infected through the mucus membranes of the vagina or the rectum, or directly in the bloodstream[14]. To gain entry into the cells, HIV encodes the *env* gene to develop the envelope glycoprotein 120 (gp120) that binds to the host CD4+ T cell receptor and a chemokine receptor, either CCR5 or CXCR4, to undergo a series of confirmational changes which determines the viral tropism[15]. CCR5 receptors bind to the R5 strain of HIV, which is a macrophage-tropic virus, and represent the dominant viral population during primary clinical HIV infection[16]. CCR5 co-receptors are not only expressed on macrophages and dendritic cells, but also on memory T lymphocytes[17]. On the other hand, CXCR4 co-receptors are expressed on both activated and resting T cells and are able to bind to the X4 strain of HIV, which is a T-lymphocyte-tropic virus. Viruses can also be dual-tropic (R5X4), allowing them to bind to both CCR5 and CXCR4 co-receptors[16].

HIV transmembrane glycoprotein (gp41), also encoded by the *env* genes, mediates fusion between the HIV envelope with the host cell wall, allowing the viral capsid to enter the CD4+ T cell[18]. Since the virus is a retrovirus, when HIV RNA enters the cell, it must

be reverse transcribed via its *pol* gene and reverse transcriptase enzyme into pro-viral DNA before it can integrate into the host cells' DNA[19,20]. Once integrated, it uses the host cells' machinery to undergo transcription and translation to make new core viral proteins that are assembled from the Gag and Gag-Pol polyproteins into HIV virions, with the help of regulatory proteins Vif, Vpr, VPu and Nef[21,22]. The virion is able to then bud from the host cell wall to begin infecting other cells in the rest of the body. As time goes on without treatment, the HIV plasma load continues to increase as CD4+ T cells diminish. While healthy individuals have CD4+ T cell counts well over 500 cells/mm^3, a person who has developed AIDS can reach as low as 200 CD4+ T cells/mm^3 [23]. In addition, macrophages play a key role in regulating the progression of HIV disease by acting as major reservoirs for HIV in tissues and organs such as the brain, lungs, lymph nodes and blood and serving as vehicles for dissemination throughout the body[24].

1.1.3. Clinical Presentation

While there is no cure for HIV, early detection of the virus through various diagnostic techniques can lead to a more favourable prognosis as treatments can be administered sooner. There are three main types of HIV diagnosis tests: antibody tests, antigen/antibody tests and nucleic acid tests (NAT). Antibody tests look for anti-HIV in the blood or oral fluid, while the antigen/antibody test looks for both the anti-HIV and p24 antigen, an immunodominant capsid protein encoded by the *gag* gene[25]. The NAT test detects the viral load in the blood and can be detected closer to the HIV exposure date than the other two tests[25]. To test for HIV infection, and enzyme-linked immunosorbent assay (ELISA) and/or a Western Blot Assay are commonly used, with ELISA being the preferred assay since has

a greater sensitivity, making it able to detect low-abundance HIV proteins while Western Blot analysis has higher specificity, thus is often used to confirm the results of the ELISA[26].

During the initial/eclipse phase of infection when the HIV is first transmitted, it begins to infect target cells while spreading through the lymphoid system and establishing viral reservoirs. After this phase which lasts about 0-3 weeks, HIV RNA levels first become detected in the blood during the acute phase[17]. This phase can last up to 9 weeks and is often associated with flu-like symptoms such as fever, swollen lymph nodes, muscle aches and/or malaise; however, many do remain asymptomatic[17]. The HIV RNA levels in the plasma then reaches its highest peak at approximately 10^6-10^7 copies per mL, while CD4+ T cells in the blood rapidly decline[17]. Once the adaptive immune response develops, it is thought that HIV-specific CD8+ cytotoxic T lymphocytes (CTLs) contribute to the viral load decreasing by 100-fold to a steady-state level, and CD4+ T cell counts rebounding close to normal levels[17]. The chronic phase occurs next, and as time progresses without treatment, viral load steadily increases as there is progressive CD4+ T cell loss and chronic inflammation, eventually leading to AIDS[17]. Not only is HIV able to cause cell death through direct cytopathic mechanisms and indirectly through inflammation, but it also negatively impacts the ability of the immune system to regenerate new CD4+ T cells, thus further contributing to its decline[17].

Treatment options are available for those at a greater risk of getting HIV and for PLWH in the form of pre-exposure prophylaxis (PrEP) and post-exposure prophylaxis (PEP) respectively. PrEP is highly effective for preventing HIV in HIV-negative individuals by using antiretroviral agents to prevent HIV from replicating and establishing

in the body[27]. PEP also uses antiretroviral therapy (ART) medications to treat HIV-positive individuals by decreasing their viral load and risk of transmission[27].

1.1.4. Combined Antiretroviral Therapy

Advances in antiretroviral therapy in recent years have led to significant improvements in overall quality of life and life expectancy of PLWH. One form of ART, known as combination ART (cART) involves a combination of three or more medications that prevents HIV from multiplying in the body. They do this by inhibiting steps in its replication cycle, thus reducing its viral load and the risk of transmission[28]. More specifically, they can block viral RNA transcription by inhibiting reverse transcriptase, block viral enzyme protease and inhibit the viral DNA from integrating into the host genome by binding to the active site of integrase[29]. Clinical and observational studies have demonstrated a profound decrease in mortality and morbidity in HIV-infected patients undergoing cART. Physicians highly recommend that cART is initiated within a couple days of confirmed HIV diagnoses, regardless of CD4+ T cell count and clinical symptoms. Currently, there are more than 25 different medications in six different classes, with the standard of care usually being a combination of two non-nucleoside reverse transcriptase inhibitor (NNRTIs), typically tenofovir disoproxil fumarate (TDF) and emtricitabine (FTC) and one protease or integrase inhibitor such as raltegravir (RAL)[30]. Most of the medications are administered once a day orally, and their HIV RNA viral load and CD4+ T cell count should be monitored every 3-6 months to assess the progress of the treatment[30].

Although cART provides life-saving benefits among HIV-infected individuals, many challenges still remain. While it aims to suppress viral replication and increase CD4+

T cell counts and function in the body, it does not completely reverse the effect of HIV on its increased risk of opportunistic infections and some antiretroviral medications cause long term toxicity such as oxidative stress and increased risk of cardiovascular diseases[31]. cART is most effective in individuals who begin therapy before the onset of advanced immunodeficiency; however, in places where clinical screening and diagnosis is challenging, that is not always an option[32]. Studies have shown that initiation of cART in patients with a CD4+ T cell count lower than 200 cells/μL (indicative of AIDS) results in less robust immunological recovery and poorer disease outcomes[33]. In many low-to-middle income countries (LMICs), economic cost of the medications, distribution, as well as social stigma including sex bias against women makes access to cART particularly difficult[34]. Recently, a long-acting injectable antiretroviral regimen called Cabenuva, that consists of cabotegravir, an integrase inhibitor and rilpivirine, a NNRTI, was approved in by Health Canada in 2020 for the treatment of HIV suppression in adults who have a fully suppressed viral load of less than 50 HIV copies/mL in their blood[35]. This represents a revolutionary alternative to traditional ART regimens, offering convenience and potential for improved clinical outcomes.

1.1.5. Animal Models for Research

Animal models are essential for understanding HIV disease pathogenesis and to pre-clinically test treatments and therapies to help PLWH. With that being said, there are often many challenges that occur with HIV testing in animals. First, small animals such as conventional inbred mice, rats, hamsters, guinea pigs, and rabbits are unable to be infected with or sustain HIV[36]. This is due to the cellular proteins in these species not supporting

viral replication as they lack important proteins and receptors such as CD4, CCR5 and CXCR4[36]. Due to the lack of success in small animal models, *in vivo* HIV research is often conducted on non-human primates (NHP), but since they also lack the proteins needed for HIV infection, they are infected with Simian Immunodeficiency Virus (SIV) via the oral, vaginal or rectal routes[37].

HIV and SIV are closely related lentiviruses that are similar in genomic variation and morphology as they both invade host cells to utilize their transcriptional machinery to replicate[37]. However, when African monkeys are infected with natural SIV it is often asymptomatic and the disease does not develop, therefore experimental models of SIV infection uses non-natural host Asian macaques to allow SIV to develop into a disease that is similar to AIDS (referred to as Simian AIDS)[38]. The most common NHP used for HIV research include the rhesus macaques, cynomolgus macaques, and pig-tailed macaques, with rhesus macaques of Indian-origin being the most widely used for HIV and AIDS research. These models are able to be infected with both SIV and a recombinant human simian immunodeficiency (SHIV) that expresses the HIV *env* gene[38]. Most of the pathophysiological features in HIV in humans are recapitulated in the rhesus macaques model including CD4+ CCR5+ T cells for viral targeting, depletion of CD4+ T cells at mucosal sites and in the peripheral blood, and the eventual development of opportunistic infections[38].

NHP have greatly contributed to our understanding of HIV/AIDS pathogenesis and treatment developments. For instance, research using NHP have led to the discovery that loss of central memory T cells is closely associated with disease progression and that

resting memory T cells are a major target of HIV[39]. Studies using NHP are able to use the same markers for plasma RNA levels and CD4+ T cell counts that are used in humans, allowing them to effectively monitor disease progression and the effect of antiretroviral treatments[40]. They also contributed to the understanding that that upon infection at mucosal sites, HIV can cross the epithelial barrier to infect cells and spread to draining lymph nodes[41,42]. During this time, the adaptive immune system is not effective in controlling the spread as CD8+ T cells responses are too late to control the viral dissemination of the HIV[43]. Moreover, these models have been able to provide information into using broadly neutralizing antibodies as therapeutic approaches as well as to explore different HIV vaccine approaches. The establishment of ART models in the SIV-infected NHP have demonstrated that these regimens are effective in suppressing virus replication and transmission, similar to what is observed in humans[44].

While NHPs infected with SIV have contributed greatly to the knowledge and understating of HIV/AIDS pathogenesis as well as the development of treatments and therapeutics, there are still many limitations with their application. These include their high cost, relative availability, labour in maintenance and low sample sizes[42]. There are also differences between HIV-1 and SIV/SHIV, as SIV resembles HIV-2 more than HIV-1, thus not allowing researchers to make definitive comparisons among both SIV and HIV as well as among humans and NHPs[42]. Therefore, *in vivo* models for HIV research still requires an ideal pre-clinical animal model that can be infected with HIV and replicate HIV infection in humans, such as humanized mouse models, to further advance our understanding and research progress.

CHAPTER 1.2. TUBERCULOSIS

1.2.1. Epidemiology and Significance

To date, nearly one quarter of the world's population, or 1.8 billion people, are infected with the obligate-anerobic, acid-fast bacteria *Mycobacterium tuberculosis* (*M.tb*), the causative agent of TB[45]. Most individuals infected with *M.tb* have latent TB infection (LTBI), meaning they do not produce any clinical symptoms, provide microbiological evidence or transmit the disease to other people[46]. Nonetheless, there is a 5-10% lifetime risk of developing an active infection, causing the disease to be highly transmissible and creating life-threatening symptoms[47]. As one of the world's top infectious killers, it is believed that every year 10 million people develop TB disease with 1.6 million people dying from it[48]. Over 80% of TB cases are in low to middle income countries (LMICs), with majority of cases being in Asian and African countries such as India, China, Indonesia, Pakistan, Nigeria and South Africa[48]. People living in environments where there is over-crowding and poor ventilation have increased risk of exposure to TB, and the risk of disease progression increases even more if the individual has a weakened immune defense from factors such as tobacco smoke, malnutrition, alcoholism, diabetes, and/or HIV infection[49]. The incidence rate of TB in Canada has remained fairly unchanged over the last decade, with the rate of 5.0 active TB cases per 100,000 people[50]. In 2021, there were about 1,904 active TB cases in Canada, with foreign-born and Indigenous people accounting for majority of the cases[50].

While TB can be treated with a combination of antibacterial medications for a 6 month regimen, *M.tb* can develop resistance to antimicrobial drugs, often called multi-drug

resistant TB (MDR-TB), making it much more challenging to treat[47]. MDR-TB is often resistant to multiple anti-tuberculosis medications, including the two standard and most-effective medications Rifampicin and/or Isoniazid[51]. While majority of MDR-TB is caused by infection with MDR-TB pathogens, they can also occur through factors such as antibiotic abuse, inadequate dosage and incomplete treatment[51]. A more severe type of MDR-TB known as extreme multi-drug resistant TB (XMDR-TB) is diagnosed when resistant to as least four anti-tuberculosis medications, including the two standard ones mentioned above[51]. In 2021, there was an estimated 450,000 cases of MDR-TB, which increased by 3.1% from the previous year potentially due to the increase in TB incidence rates as a result of the impact of the COVID-19 pandemic on TB detection[52].

1.2.2. Transmission and Pathogenesis

TB is transmissible when a patient with active pulmonary TB coughs, sneezes or talks and another individual inhales the infected aerosolized droplet containing the viable bacilli[53]. The droplet can remain suspended in the air for several hours, causing the risk of infection among household members of TB patients to be about 30%[53]. There are many factors influencing the transmission success including the bacterial load of the source and proximity and duration of the exposure. Following inhalation of the infectious droplet, *M.tb* enters the lung via the respiratory tract and travels to the alveolar space in the lower respiratory tract[54]. It encounters alveolar macrophages, which are thought to be the first cells infected, and the bacilli becomes engulfed through receptor-mediated phagocytosis[54].

M.tb possesses several virulence factors that allow it to ensure its survival in the macrophage by inhibiting phagosome fusion with the lysosome and disrupting the

phagosomal membrane, causing the release of mycobacterial DNA into the cytosol of the macrophage and potentially promoting the growth of *M.tb*[54]. Although the exact mechanisms are unknown, it is proposed that *M.tb* ends up in the lung parenchyma by *M.tb*-infected alveolar macrophages migrating to it[55]. This leads to the recruitment of cells to the site of infection generating a granuloma, which is a host defense mechanism consisting of a variety of CD4+/CD8+ T cells, B cells, neutrophils, dendritic cells (DCs) and natural killer (NK) cells, with an abundance of macrophages forming its core[55]. While the dynamic structure of the granuloma can immunologically restrain *M.tb* proliferation and contain bacterial dissemination, *M.tb* has adopted strategies to circumvent host defenses, creating conditions within the granuloma that are suitable for its survival and proliferation[56].

After the establishment of the primary infection, either infected DCs or inflammatory monocytes transport the bacilli to pulmonary lymph nodes for T cell priming. *M.tb* is able to delay the adaptive immune system for roughly 5-10 days by interrupting the T cell priming process and their movement into the lung[57]. Cell-mediated immunity is essential for control of *M.tb* infection by activating CD4+ and CD8+ T cells. The T cells recruited to the infected tissue release activated pro-inflammatory cytokines such as interferon gamma (IFNγ) and tumour necrosis factor alpha (TNFα). These cytokines enhances macrophage activation by inducing the transcription of genes that produce antimicrobial molecules, such as oxygen free radicals and nitric oxide, representing one of the best mechanisms for eliminating *M.tb*[58]. However, protective immune responses against TB are still not well understood.

1.2.3. Clinical Presentation

Some of the most common physical symptoms of pulmonary TB include a chronic cough which can sometimes lead to hemoptysis, weight loss, night sweats and fevers. Re-activation of latent TB infection often forms lesions and cavities in the upper portion of the lung, which can be visualized by a chest x-ray. Tuberculosis can be diagnosed through a variety of tests and assays including tuberculin skin test (TST), interferon gamma release assay (IGRA) and sputum smear microscopy[59]. The TST involves injecting a protein derivative from *M.tb* under the skin, and a positive response indicated prior TB exposure due to the interaction of memory T cells with antigens presented in the skin cells[59]. However, drawbacks include increased risk of false-negative results in immunocompromised patients and potential false-positives in those immunized with the BCG vaccine[60]. On the other hand, IGRA stimulated blood cells with *M.tb* antigens to measure IFNγ production, but it is more expensive than TST[61]. Sputum smear microscopy is another common TB diagnosis method, involving sputum staining to detect TB bacilli, and while it is rapid and cost-effective, it can't differentiate drug-susceptible from drug-resistant TB[62]. Therefore, the WHO suggests molecular tests like Xpert MTB/RIF and Xpert Ultra, with Xpert Ultra showing better sensitivity for TB in HIV-positive and negative individuals[63].

While TB most commonly affects the lungs, it can spread to other parts of the body such as the brain, kidneys or spine[64]. Pulmonary TB is the most common form of TB and is characterized by local granulomatous inflammation in the periphery of the lung. On the other hand, extrapulmonary TB is characterized by TB involving organs other than the lung,

such as miliary TB, pleural TB and skeletal TB[64]. Pulmonary TB can also cause various pathological lesions such as necrotic lesion, cavitation, bronchiectasis, fibrosis and pneumonia[65]. While these pathologies can co-exist in the same patient and manifest distinct differences, conventional assays on clinical samples cannot accurately capture the temporal changes of the disease or treatment progression.

1.2.4. Past and Current Vaccines in Development

The Bacille Calmette-Guérin (BCG) vaccine continues to be one of the most widely used vaccines globally and the only currently available vaccine for TB[66]. While this vaccine has been used for over a century, it remains controversial in terms of vaccine efficacy and variability in BCG sub-strains. BCG is often administered through the intradermal route shortly after birth in countries that are at high risk for TB. This vaccination provides effective protection against childhood disseminated TB; however, it is ineffective against highly transmissible adult pulmonary TB[66]. While it is not fully understood why the vaccine efficacy against TB in adults is highly variable, some researchers propose it is due to the BCG strains evolving away from each other and from the original strain, while other researchers infer it has to do with prior exposure to environmental non-tuberculosis mycobacterium impacting BCG-specific immune responses through cross-reactivity[66,67].

Furthermore, BCG is a live attenuated form of *Mycobacterium bovis*, creating long-lasting and protective immune response in healthy individuals. However, this vaccine can be dangerous in immunocompromised individuals such as PLWH, as increasing T cell activation can accelerate HIV disease progression, thus potentially increasing their susceptibility to active TB, disseminated BCG disease and the development of AIDS[68].

Therefore, the World Health Organization (WHO) does not recommend BCG immunization in untreated children and adults infected with HIV[69]. However, if HIV-infected individuals are receiving ART and are immunologically stable, it is safer for them to be vaccinated with BCG as it may reduce the risk of both BCG and TB disease[70]. TB vaccines are rarely tested in the context of HIV due to lack of effective animal models, difficult implementation, and challenges in investigating the complexity of the immune system interactions and mechanisms when infected with both TB and HIV. Research in vaccine efficacy and safety in the context of HIV is highly relevant on a global scale to public health, with TB endemic areas overlapping with many regions of high HIV prevalence.

Recent advances in TB vaccines have led to the development of many promising candidates in the TB vaccine clinical pipeline. These include vaccines currently in phase 3 of development, such as GamTBvac, a protein adjuvant vaccine, Immuvac (MIP), an inactivated vaccine, and MTBVAC, a live attenuated vaccine[71]. The University of Oxford also created a vaccine that is in phase 2b of their clinical trial, called ChAdOx1.85A, which uses a chimpanzee adenoviral vector expressing an immunodominant *M.tb* antigen Ag85A[71]. This vaccine is delivered through the respiratory mucosal route, and increasing evidence suggests that greater immune protection can be achieved when administered mucosally through the respiratory tract compared to the parenteral route[72].

Here at McMaster University, a phase 1b clinical trial conducted by Dr. Jeyanathan et al. evaluated the safety and immunogenicity of a novel recombinant replication-deficient human serotype 5 adenoviral-vector (AdHu5) vaccine expressing Ag85A[72]. The

AdHu5Ag85A vaccine was delivered to human participants via inhaled aerosol generated by the Aeroneb Solo nebulizer and compared it to intramuscular injection (IM). The results showed that the aerosol delivery of the vaccine was able to induce robust Ag-specific tissue-resident memory CD4+ and CD8+ T cells within the respiratory tract with polyfunctionality[73]. Furthermore, the aerosol delivered vaccine led to transcriptional changes in the airway-resident alveolar macrophages, thus preparing them for defensive immune responses[73]. This data shows that the inhaled aerosol delivery of the AdHu5Ag85A is a safer and superior way in establishing protective respiratory mucosal immunity.

While recombinant AdHu5-based vaccines have proven to be effective in protecting against pulmonary TB in pre-clinical and clinical data, the high prevalence of pre-existing anti-AdHu5 immunity in the human population is a significant limitation in the application of AdHu5-based vaccines in humans, as it may dampen the potency of the vaccine[74]. Furthermore, wild-type AdHu5 virus is a human respiratory pathogen that many people encounter, causing a concentration of AdHu5 antibodies in the lung mucosa which could have negative effects on the vaccine when administered through the respiratory mucosal (RM) route[74]. There is also an implied safety concern for people living with HIV or in HIV high-risk populations who have high levels of pre-existing anti-AdHu5 immunity, since according to Step HIV vaccine trials, the vaccine may alter the course of infection, causing accelerated disease progression and enhanced susceptibility to HIV[75].

1.2.5. Next Generation Tri:ChAd68 Vaccine

Recently, a novel replication deficient chimpanzee serotype 68 adenovirus expressing Ag85A (AdCh68Ag85A) vaccine was constructed and is an ideal alternative to

human adenoviral vectored vaccines. There is a lack of neutralizing anti-AdCh immunity seen in humans and the viral vector uses the same cell entry receptors as AdHu5, meaning it has similar immunogenicity to AdHu5 without dampening the potency of the vaccine or creating negative effects from pre-existing antibodies[76]. This vaccine represents a promising novel TB vaccine platform, as it may even be effective and safe to use on people living with HIV. Moreover, even more protection is expected to occur when immunizing with a trivalent AdCh68-vectored TB vaccine expressing three major TB antigens, Ag85A, TB10.4 and RpfB (termed Tri:ChAd68). Ag85A is a replication-associated antigen and is expressed during acute and active phases of TB, TB10.4 is a virulence-associated antigen and is expressed during chronic infection, and RpfB (resuscitation promoting factor B) is a resuscitation-associated antigen and is expressed during latency of the bacteria, helping the dormant bacteria become active[77]. Thus, these three TB antigens allow this vaccine to target different stages of the *M.tb* life cycle, targeting both replicating and non-replicating bacilli and have broader protection than monovalent vaccines[78]. Conventional mouse models that were RM immunized with the Tri:ChAd68 vaccine induced robust and sustainable tissue-resident multifunctional CD4+ and CD8+ T cell responses in the lungs and provided significant protection against both actively replicating and dormant non-replicating *M.tb* bacilli[78].

Recent evidence has suggested that a strategy to overcome *M.tb*-immune suppression on lung macrophages and DCs is to "train" the innate immune cells that the *M.tb* bacilli targets in the lung before *M.tb* exposure[79]. The idea is that training circulating monocytes through vaccination will cause them to undergo epigenetic and transcriptional

changes and persist as "memory" innate immune cells, enhancing host defense responses to *M.tb* exposure[79]. It is believed that the most effective vaccination strategy to contribute to trained innate immunity (TII) is through RM vaccination[79]. The respiratory mucosa is exposed to a large range of pathogens and thus requires a robust innate immune system, including alveolar macrophages (AMØs) and interstitial macrophages (IMØs)[79]. A recently study demonstrated that memory AMØs induced by RM vaccination of the AdHu5Ag85A vaccine in a conventional mouse model was able to alter the airway innate immune cells and provide TII capable of protection against *M.tb* in early stages of infection, and that it was independent of T cell immunity[80]. The findings of previously tested RM Ad-vectored as well as the RM Tri:ChAd68 vaccine indicate great prophylactic potential in inducing both trained innate and adaptive immunity to confer protection against TB.

1.2.6. Animal Models for Research

While *M.tb* often only occurs in humans, it can infect almost all mammals; however, the majority of them cannot easily transmit the infection. Nevertheless, animal models used for TB research have provided significant insight into the understanding of TB immunopathogenesis, host/pathogen interactions, and efficacy of treatments. The most commonly used experimental small animals of TB include mice, rabbits, guinea pigs, with non-human primates (NHPs) being extremely useful in TB research as well[81]. In rabbit models, *M. bovis* is often used as a surrogate for *M.tb*, since rabbits are significantly more susceptible to infections from *M. bovis* and the pulmonary pathology developed from inhaled bovine tubercle infection more closely resembles human *M.tb* infection than that seen in other animal models[81]. Unlike mice and guinea pigs, rabbits are able to develop

pulmonary cavitation, which can result in bronchial spread of the pathogen[81]. Rabbits can also be used as a model to study latent TB as they are more resistant to *M.tb*; however, unlike humans they tend not to spontaneously reactivate unless they were experimentally immunocompromised[82]. Guinea pigs on the other hand are exceptionally susceptible to TB infection, thus are well suited to study airborne transmission[83]. Guinea pigs are also able to replicate aspects of TB disease in humans such as the formation of granulomas, pulmonary lesions, dissemination and caseation necrosis, making them good models to study vaccine and treatment efficacy[83].

Mice strains are generally more resistant to TB infection than rabbits, guinea pigs and even humans as they are able to tolerate a large bacterial burden within their lungs. Unlike what we see in humans, mice do not suppress bacterial growth to form a latent infection, but instead develop noncaseating granulomas which manifests as a chronic infection[84]. This helps researchers understand the effects of chronic exposure to mycobacterial antigens on T cell functions, more specifically their CD4 and CD8 T cell responses[84]. Researchers are also able to find parallels between murine and human innate immune responses. For example, these studies have shown that murine macrophages also use TLRs on their cell surface to recognize mycobacterial antigens and trigger cytokine production, as well as they can demonstrate T cell-independent, NK cell production of IFNγ for defense against TB which is also seen in humans[85,86].

Furthermore, the availability of inbred, transgenic and knockout strains of mice have helped elucidate the role of various specific cell types and cytokines in TB disease and bacterial growth or suppression. Since mice do not naturally acquire latent TB when

infected, the Cornell mouse model was developed to combat that issue and help researchers investigate latent TB in a murine model. In this model, mice are infected intravenously with *M.tb* and treated with oral antimycobacterial drugs (isoniazid and pyrazinamide), which reduced the number of bacilli in the tissues up to undetectable levels, rendering them "sterile"[87]. Afterwards, reactivation of the infection occurred either spontaneously or in response to immunosuppressive agents, such as steroids[87]. While this is an attractive model for LTBI in mice, the use of antibiotics to suppress the bacterial burden does not accurately mimic naturally occurring latent TB in humans.

Non-human primate models (mainly rhesus macaques and cynomolgus macaques) are another important model of TB[88]. NHPs are the closest genetically to humans of any of the experimental animals used in research, allowing them to have remarkable immunological similarities to humans. One key advantage of this model is its ability to recapitulate a wide variety of granulomatous structures and lesions that occur in humans including classical granulomas with a caseating necrotic core, non-necrotizing granulomas, fibrotic and cavitary lesions as well as the formation of multinucleated giant cells in the periphery[88]. Another advantage of macaques in TB research is their ability to develop human-like latent infection characterized by the absence of clinical signs and symptoms which can be measured by antigen-specific immunological diagnostic tests such as TST or IGRA made for primates[89]. While this reinforces the significance of using macaque models to study TB pathology and latent infections, there are many limitations to the model such as high cost, low abundance of animals and ethical considerations.

CHAPTER 1.3. HIV/TB CO-INFECTION

1.3.1. Epidemiology and Significance

While both pulmonary TB and HIV alone present significant health concerns for individuals living with these diseases, the dual burden of HIV/TB co-infection can exacerbate their respective pathogenesis and complicate specific therapies and treatments, leading to a higher mortality rate. In fact, TB is the leading cause of death among PLWH, with untreated HIV-infected patients being up to 18 times more likely to develop active TB, either through primary infection or reactivation of latent TB infection, compared to uninfected individuals[90,48]. Although ART has been shown to reduce the risk of active TB in PLWH by 67%, those undergoing treatment still face a greater risk then HIV-negative individuals[91]. In 2021, approximately 187,000 people worldwide died of HIV-associated TB, with SSA having the highest prevalence of HIV/TB co-infection[92]. While there has been a steady decline in the estimated number of incident TB cases among PLWH, less than half of the estimated 787,000 PLWH who developed TB globally in 2020 received proper diagnosis and care[93]. Furthermore, not only does HIV have a profound effect on TB, but it increases rates of drug resistance and mortality among patients with MDR-TB and XDR-TB[94].

Like mentioned in the previous paragraph, HIV/TB co-infection can complicate treatments for one another, making it challenging to receive the appropriate course of action to treat the diseases. Firstly, the WHO does not recommend PLWH to be vaccinated by the BCG vaccine, since their low T cell responses may not be able to control the live attenuated bacteria to the site of infection, causing disseminated BCG disease in the patient[95].

Moreover, the BCG vaccine can also drive T cell activation, potentially increasing HIV viral load and accelerating HIV disease progression[96]. This means that the only available vaccine to combat TB cannot be used in the population most vulnerable to getting the disease. Therefore, preventing TB disease by screening for and treating LTBI at the time of HIV diagnosis, along with initiating ART as soon as possible are necessary actions that need to be taken[62].

The two main methods recommended for diagnosis LTBI in PLWH are the TST and IGRA, as methods such as sputum smear microscopy has too low sensitivity among PLWH and will only detect about half of sputum culture positive cases people with HIV-associated pulmonary TB[62,97]. However, reagents for TST are sometimes in short supply and IGRA testing is expensive and not often available in LMCIs as well as the accuracy is limited and cannot distinguish between LTBI and active TB disease[62]. Thus, WHO guidelines do not require LTBI diagnosis testing before initiating TB preventative therapy for PLWH[62].

With that being said, many people still do not take either TB preventative therapy or ART due to many factors such as poor patient adherence, drug toxicity and social stigma[98]. Moreover, a phenomenon termed immune reconstitution inflammatory syndrome (IRIS) can occur upon initiating ART, and an excessive immune response against *M.tb* during or after the completion of anti-TB therapy is known as TB-IRIS[99]. The two forms of IRIS include paradoxical, which is characterized by worsening of a previously diagnosed infection after ART is initiated and unmasking IRIS refers to a previously undiagnosed asymptomatic TB disease following ART[100]. Unfortunately, there are no specific tests that

can establish the diagnosis of TB-IRIS, therefore clinical features such as improvement of symptoms on TB treatment prior initiating ART followed by the deterioration of symptoms soon after starting ART may suggest a diagnosis of TB-IRIS[99]. The immunopathogenesis is not completely understood, so it is clear that there needs to be further investigation on HIV/TB co-infection to develop effective vaccines, therapeutics and treatments.

1.3.2. Pathogenesis and Human Pathology of Diseases

The extrapolation of evidence from pre-clinical and clinical studies have shaped our basic understanding of how HIV and TB increase susceptibility and exacerbate pathology for one another through immunological mechanisms[101]. It has been proposed that the increased in pathology is associated with a functional disruption within the granuloma, decreasing its ability to contain *M.tb* and leading to its bacterial growth and dissemination[102]. This can be attributed to HIV increasing its viral load within tissues leading to a decrease in number of CD4+ T cells and disruption of macrophage functions, causing detrimental changes to the granuloma[103]. The interactions between HIV and TB are complex, and there still remains many outstanding questions regarding their influence on one another.

Infection with HIV highlights the importance of T cell-mediated immunity against *M.tb*, as when CD4+ T cells are depleted, the proportions of polyfunctional *M.tb*-reactive CD4+ and CD8+ T cells which produce pro-inflammatory cytokines IFNγ , TNFα, IL-2 and IL-17 are also depleted[103]. This depletion is inferred to contribute to the higher risk associated of developing active TB in HIV-infected people than in HIV-uninfected people[103]. This has also been evident in the transcriptional profiling of biopsy samples from

HIV/TB co-infected patients which confirmed their T cell recruitment and IFNγ activity were substantially reduced, and their blood CD4+ T cell counts were less then 200 per mL, suggestive of AIDS[104]. Furthermore, even before HIV disease progresses to AIDS and the CD4+ T cells are depleted, HIV-infected T cells may still contribute to the increased risk of TB[104]. In early HIV infection, *M.tb*-specific T cells are preferentially depleted as HIV DNA is detected more frequently in these cells since they produce high levels of IL-2, making them more permissive to HIV infection[105]. Other T cell populations may also contribute to HIV-associated TB including Th17 and Th22 cells[106]. Another study demonstrated that in the BAL fluid of the lung in HIV/TB co-infected individuals, there was a larger increase in HIV viral RNA copies/mL and pro-viral DNA compared in individuals who were only infected with HIV[107].

While *M.tb* has evolved to survive and replicate within macrophages, evidence has shown that depletion of macrophages is associated with increased mycobacterial burden, indicating that macrophages are able to restrict bacterial growth, mainly through processes like phagocytosis[108]. HIV has been reported to inhibit macrophage phagocytosis through its accessory protein Nef, by blocking the maturation of autophagosomes to inhibit the autophagy pathways[109,110]. HIV-infected macrophages that are also infected with *M.tb* have been associated with increased mycobacterial growth, and studies have shown that vitamin D treatment of the co-infected macrophages restricted both *M.tb* and HIV replication via an autophagy-dependent mechanism[111]. HIV infection is also known to upregulate *M.tb* entry receptors on macrophages and impair TNFα mediated macrophage apoptotic responses, thus helping increase the chances of its survival[112]. Interestingly, in patients co-

infected with HIV and pulmonary TB the presence of fewer necrotic granulomas and less pulmonary cavitation was observed, supporting the hypothesis that T cell responses to *M.tb* contribute to cellular necrosis and tissue damage, as they are reduced in patients with AIDS due to the low levels of CD4+ T cells they possess[113].

HIV viral load in both the lungs and peripheral blood increases in patients with pulmonary TB, as HIV replication occurs in activated T cells that are recruited to sites of granulomatous inflammation, which then may facilitate rapid virus propagation leading to a vast increased viral load[114]. Evidence has shown that in HIV-infected macrophages co-infected with *M.tb in vitro*, HIV transcription levels initially decrease, followed by a substantial increase[115]. This increase was synchronous with sustained pro-inflammatory responses as a result of HIV reducing early IL-10 responses, which has been reported to inhibit HIV transcription[115]. Conversely, other pro-inflammatory cytokines including TNFα, IL-6 and IL1B have been known to upregulate HIV transcription[116,117]. Moreover, macrophages that enter the cell cycle are able to arrest in a G1-like state to facilitate reverse transcription and thereby allowing the synthesis of HIV DNA[118]. Pro-inflammatory cytokine responses to *M.tb* which is facilitated by HIV reduction of immune regulation, and their recruitment of activated T cells act in synergy with modulation of the macrophage cell cycle to enhance virus replication and propagation[118]. With many gaps still in the literature to truly understand how these two pathogens interact, animal models are required to address outstanding questions to better develop therapies and treatments to combat this syndemic.

1.3.3. Animal Models for Research

Finding appropriate animal models that can be infected with and sustain both TB and HIV co-infection can be very challenging. Although small animals such as mice can be infected with *M.tb*, they do not possess the right cells to be infected with HIV, thus cannot be used to model co-infection. In contrast, NHPs, mainly macaques, can be infected with *M.tb* with pathology similar to humans, as well as infected with SIV, mentioned in Chapter 1.2.6. macaques have also provided valuable insight into SIV-infections when co-infected with *Mycobacterium avium* complex and BCG as well at mimicking LTBI in SIV-infected macaques[119].

Mattila et al. showed that when compared with SIV-only infected cynomolgus macaques, the co-infected macaques had much fewer CD4+ T cells in the lungs and their granulomas histopathological characteristics were similar to chronically active TB seen in humans[120]. Furthermore, they also found that both pro- and anti-inflammatory cytokine responses in the co-infected macaques was correlated to reactivation of latent TB[120]. Another study using rhesus macaques conducted by Mehra et al. was able to show that SIV infection not only reactived latent TB, but also increased *M.tb* dissemination leading to their shorter survival time and higher bacterial load in multiple organs[121]. Confocal microscopy helped demonstrate that *M.tb* and SIV can infect the same cell, as there were many SIV-positive cells located in and around *M.tb* infected cells[121].

Research by Kuroda et al. demonstrated that SIV infection not only reactivated latent *M.tb* in rhesus macaques, but also contributed to higher lung monocyte/macrophage turnover rates that was associated with severe lung tissue damage and disease progression

in the co-infected NHPs[122]. Since HIV damages important factors in maintaining granuloma organization like CD4+ T cells and TNFα, it results in the disruption of the granuloma structure and is unable to contain the mycobacterium or the infection[112]. While TNFα production is required to restrict *M.tb* growth, it is also able to activate HIV replication in macrophages, indicating that the host immune response initiated against TB promotes the replication of HIV[123]. There is also evidence that HIV infection affects macrophage and DCs' ability to become active and impairs their antigen presenting function, thus contributing to the pathogenesis and dissemination of both diseases[123]. While NHPs have been a significant tool in researching *M.tb*/SIV infections, there are still key differences between SIV and HIV and previously mentioned limitations can make using this model challenging, thus a smaller, more applicable model such as a humanized mouse model is crucial to accurately explore the gaps in knowledge and research questions fully.

CHAPTER 1.4. HUMANIZED MOUSE MODEL

1.4.1. Applications in Research

The use of humanized mouse (hu-mice) models is a growing field in research and offers solutions to previous barriers and limitations that conventional animal models often held such as their small size, cost effectiveness and translatability to humans. This model allows researchers to effectively study human-specific diseases, immune responses, and treatment regimens *in vivo*.

Hu-mice models are immunodeficient mice that can be successfully engrafted with human cells or tissues and provide a more practical approach for pre-clinical research on many human diseases. The wide application of hu-mice can be used to study infectious

diseases including HIV, TB and HSV, cancer, autoimmune diseases, drug and vaccine testing, stem cell research, transplantation, and allergies[124]. Hu-mice provide a unique opportunity to bridge the gap between *in vitro* experiments and human clinical trials.

1.4.2. Development of Various Hu-Mouse Models

The advancement of various immunodeficient mouse strains has been crucial in establishing effective techniques for successful engraftment of human cells into mice. To humanize the mice, radiation follow by xenogeneic transplantation of human stem cells and/or tissue is required, therefore highly immunodeficient mouse recipients are needed to prevent rejection of the engraftment.

The development began with severe combined immunodeficiency (SCID) mice, carrying a mutation of the Prkdc gene, which encodes a DNA protein kinase and thus causes defects in the DNA repair machinery. This in turn does not allow the mouse to effectively recover from the double-stranded DNA breaks caused by the radiation[125]. This $Prkdc^{scid}$ mutation also causes causing abnormal V(D)J recombination that led to deficient T and B lymphocytes[126]. However, despite the lack of mature T and B cells, they still retained their NK cell and macrophage functions, and "leakage" was observed in some of the mice, meaning they were able to recover their T and B lymphocytes as they aged[127,128]. Therefore, the SCID mutation was introduced into non-obese diabetic mice (NOD), which have defects in their innate immune system including suppressed NK and macrophage phagocytic activity as well as absence of circulating complement[129]. While this did allow the SCID/NOD mice to have NK defects, they still exhibited partial NK activity thus the rg^{null} mutation was introduced[130]. This was developed by knocking out the IL-2 receptor

gamma chain, termed IL2rγ, to hinder cytokine binding[130]. Since SCID mice are highly sensitive to radiation due to their lack of effective DNA repair machinery, Rag^{null} mice were created by knocking out recombinant activated genes Rag1 or Rag2[131,132]. These Rag genes are able to induce V(D)J recombination by cleaving the DNA in lymphocyte receptor formations which are then processed and joined by proteins of the non-homologous end joining (NHEJ) pathways[133]. A mutation in the RAG genes disrupt the recombination process, leading to a lack of functional T and B cells[133]. While the RAG-knockout mice still produce the same SCID-like phenotype, they do not have a DNA repair mutation therefore allowing them to be less susceptible to radiosensitivity than the SCID mice[133].

The most common immunodeficient mice used are NOG (NOD.Cg-$Prkdr^{scid}Il2r\gamma^{tm1sug}$), NSG (NOD.Cg-$Prkdr^{scid}Il2r\gamma^{tm1Wjl}$), and NRG (NOD.Cg-$Rag1^{tm1MoM}Il2r\gamma^{tm1sug}$) which have all lost the ability to produce an adaptive immune response and show major deficits in their innate immune system[134]. The main differences between these mouse strains are their mutations. For example, NOG and NSG differ in their IL2rγ chain mutation, with the IL2rγ in NSG completely knocked out, whereas the IL2rγ mutation in NOG is truncated which produces a protein that binds to cytokines but cannot transduce a signal[135]. NRG on the other hand doesn't have the $Prkdr^{scid}$ mutation and instead replaces it with Rag1 to allow it to tolerate higher dosage of radiation[135]. These mice are either engrafted with CD34+ hemopoietic stem cells (HSCs) that were extracted from sources such as human umbilical cord blood or bone marrow, or surgically implanted with human fetal liver and thymus tissues following injection of matched CD34+ HSCs, which is known as the bone marrow liver thymus (BLT) model[136]. Both methods of engraftment

allow for successful reconstitution of human CD4+ and CD8+ T cells, monocytes, DCs and B cells in blood and tissues[136]. While the HSC-only method demonstrates better human B cell and myeloid cell development, the BLT methods yields higher cell counts and CD3+ T cell reconstitution in various tissues[137].

To improve human immune cell function in previously established HSC-only hu-mice models, a next generation mouse model was created by using mice with the NRG background that express human leukocyte antigen (HLA) transgenes. These HLA-transgenic NRG mice are then engrafted with HLA-matched HSCs, either HLA-A2 (Class I), HLA-DR4 (Class II) or both HLA-A2 and -DR4 matched HSCs[136]. HLA class I molecules are expressed on the surface of nucleated cells, while HLA class II molecules are expressed exclusively on antigen presenting cells (APCs) including B cells, monocytes, macrophages and DCs[138]. Studies have shown that compared to transgenic HLA-A2 only mice (hu-A2), mice transgenic for HLA-DR4 only (hu-DRAG) and both HLA-DR4 and HLA-A2 (hu-DRAGA2) demonstrated significantly better human CD4+ and CD8+ T cell reconstitution and function as well as B cell immunoglobin class switching than the hu-A2 model as well as other previously established hu-mouse models[139]. While there are many benefits to using hu-mice for research, one setback is they are at risk for developing graft-versus-host disease (GvHD) which is caused by the cross-reactivity of the human T cell receptor (TCR) to the murine major histocompatibility complex (MHC), initiating TCR:MHC interactions and often resulting in increased pathology and eventually death[140].

1.4.3. Hu-Mouse with HIV Research

As discussed in Chapter 1.1.5., NHP have led the emergence of research in HIV/SIV due to the lack of small animal models that can be effectively infected with HIV. Although NHPs have significantly contributed to our foundational knowledge and understanding of HIV, their widespread use is hindered by practicality issues and limitations. Nonetheless, in the past few decades there has been a surge of HIV studies using humanized mouse models, particularly treatment and therapeutics testing. The robust reconstitution and distribution of human immune cells in their blood and tissues including their reproductive and gastro-intestinal tract have allowed them to be successfully infected via parenteral, rectal, vaginal and/or oral HIV exposure[141]. Infection in these hu-mice can be readily monitored by detecting their viral load in their peripheral blood plasma and depletion of CD4+ T cells in their blood and tissues[142].

In a recently published study conducted by our lab, both hu-NRG and next generation hu-DRAGA2 were intravaginally infected with HIV and at both 2 and 4 weeks post infection, viral load was detectable in both the blood plasma and vaginal wash[143]. This not only demonstrated successful HIV infection, but also viral dissemination into the blood stream and peripheral tissues. Furthermore, there was a significant decrease in the frequency and number of human CD4+ T cells in the blood of both models, which is a hallmark of HIV infection in humans. Using immunohistochemistry (IHC), we were able to see a depletion on CD4+ T cells and CD68+ macrophages in both the vaginal mucosa and lung 8 weeks post-infection in both hu-NRG and hu-DRAGA2, with not much difference between the two models[143].

Similarly to our lab, a research study by Kim et al. 2017 used hu-DRAG mice to determine the presence of HIV in various tissues and organs after being infected via the vaginal route. They were able to identify HIV RNA and DNA present in the bone marrow, spleen, blood, gut, lymph nodes, female reproductive tract (FRT), with the last tissue/organ being infected being the brain[144]. Moreover, the trafficking of the virus from the FRT to other organs was consistent with studies that used SHIV in NHPs.

Interestingly, studies have demonstrated that many hu-mouse strains can be treated with the same antiretroviral agents that are used in humans, with the most common combination of ART medications being tenofovir disoproxil fumarate (TDF), emtricitabine (FTC) and raltegravir (RAL). These drugs are mainly administered either via daily IP injections, or orally through drinking water or food. Most of the studies that treat their mice with this combination of ART result in systemic recovery of CD4+ T cells and a decrease in HIV viral load[145,146,147,148,149].

1.4.4. Hu-Mouse with TB Research

Humanized mouse models are also a viable solution for investigating TB immune responses and testing novel TB vaccines as they are susceptible to *M.tb*, generate human-like T cell responses and show similar pathological damage to lung tissue as seen in humans. While other animal models including conventional mouse, rabbits, guinea pig and NHPs have shaped our understating of TB and have made essential contributions to TB research, hu-mice offer some advantages that those animal models lack.

In another experiment conducted by our lab exploring immune responses of hu-NRG and hu-DRAGA2 on *M.tb* infection, the mice were intranasally infected with the

H37Rv strain of *M.tb* and 4 weeks later they showed high bacterial load and dissemination to the spleen[143]. In the lungs of both hu-mice models, we were able to see the development of classically organized granulomas with a focal caseating necrotic core at the center[143]. Moreover, acid-fast bacilli (AFB) staining showed the bacilli being contained within the granuloma structure, and IHC showed hCD4+ T cells surrounding the granuloma in a halo structure with hCD68+ macrophages scattered throughout it[143].

Other studies have been able to successfully infect a wide array of hu-mouse strains to effectively study TB pathogenesis and treatments. One study using hu-BLT mice found that mice infected intranasally with *M.tb,* showed increasing lung bacterial infection and dissemination to the spleen and liver[150]. Lung infections displayed organized granulomas, caseous necrosis, bronchial obstruction, and cholesterol crystallization[150]. Human T cells were present in sites of inflammation, surrounding granulomas in the lung, liver, and spleen near bacterial growth sites[150]. Another study using *M.tb*-infected hu-NSG mice also showed caseous necrotic granulomas that had cellular phenotypic special-organization that resembled that of active TB patients[151]. Interestingly, they found that their hu-NSG mice had significantly lower lung bacterial burdens when compared to their non-humanized PBS-NSG mice, suggesting that the human immune cells may have partially controlled the bacterial growth[151]. This study also tested two anti-TB drug regimens, where they were able to conclude that both regimens were able to reduce bacterial loads at similar rates, demonstrating that this hu-mouse model is feasible for pre-clinical TB drug testing[151].

Hu-mice are great tools for TB vaccine testing, and in a study by Yao et al., a novel AdHuAg85A TB vaccine was tested in hu-NRG mouse models. The results showed that

RM immunization induced greater Ag-specific IFNγ CD4+ T cell responses in the lung while parenteral immunization induced more Ag-specific IL-2 CD4+ T cells in the spleen[152]. Moreover, the data indicated that RM immunization induces a much stronger polyfunctional T cell response in the lungs, producing a greater amount of important *M.tb*-specific cytokines such as IFNγ, TNFα and IL-2 than parenteral immunization[152]. In contrast to that, unimmunized hu-mice lacked any Ag-specific T cells before subsequent *M.tb* infection demonstrating that this vaccine contributes to *M.tb*-specific immune responses[152].

1.4.5. Hu-Mouse with Co-infection Research

As mentioned above, using humanized mice is an ideal model to study *in vivo* interactions during HIV and TB co-infections, mainly due to the human trophism of HIV and their ability to recapitulate human immune responses. In a study conducted by Nusbaum et al., it was observed that when hu-BLT mice were infected with pulmonary *M.tb* after prior infection with HIV, the HIV-infected cells were localized at the periphery of granulomas in the lung where *M.tb*-driven inflammation and mycobacterial replication took place[153]. This was thought to have disrupted the pro-active innate and adaptive immune functions required for the containment of *M.tb*, accelerating progression of TB disease in the HIV-infected hu-mice. The number of bacteria and TB lesions were significantly increased in the lung of the co-infected mice, and the percent of lung occupied by necrotic granulomatous tissue was greater compared to the TB-only infected mice[153]. HIV/TB co-infection caused increased mycobacterial burden and loss of prominent granuloma structure in the lungs of the hu-mice, which is consistent with what is seen in

human patients.

Furthermore, HIV was shown to increase neutrophil infiltration and tissue necrosis in the lung, causing it to activate pro-inflammatory cytokines and chemokines further promoting tissue damage[153]. Several of the co-infected mice developed TB pneumonia and vascular occlusions caused by inflammatory cells, consistent with TB pneumonia seen in individuals with AIDS[154]. This suggests that HIV-infection may quicken the TB disease pathogenesis in hu-mice by promoting specific cells responsible for non-protective inflammation.

Hu-BLT mice have also been used to understand HIV-associated TB relapse to develop effective interventions and drug therapies. Hu-BLT mice were used to model post-chemotherapy TB relapse with HIV infection, and it was observed that after Rifampin and Isoniazid treatment, HIV infection increased *M.tb* burden post-drug cessation[155]. Organized granulomas formed during acute TB and were resolved with drug therapy, and at relapse, there were fewer granulomas and mycobacteria were mainly at sites of inflammation[155]. It was postulated that this occurs as a result of HIV-related influences which causes a breakdown of the existing granulomas and encourage dissemination. Furthermore, mice with post-drug TB relapse displayed higher viral replication in the lung and liver, but not in the periphery, when compared to mice with HIV mono-infection, demonstrating the fundamental role hu-mouse models have for understanding TB relapse in the context of HIV[155].

In a pilot co-infection experiment conducted with hu-NRG mice in our lab, they were first successfully infected with HIV, followed by subsequent *M.tb* infection 3.5 weeks

later. At 8 weeks post HIV infection, hu-NRG in both the *M.tb*-only and co-infected groups developed multiple granulomatous lesions in the lungs, with the co-infected mice trending towards a higher percentage of granulomatous tissue in the whole lung[143]. It was demonstrated that these hu-mice models can be successfully infected with HIV, TB and HIV/TB and replicate similar disease progression to humans including depletion of CD4+ T cells during HIV infection and the production of organized granulomas in TB disease. This gives researchers more knowledge about co-infection disease pathogenesis and allowing vaccines to be effectively tested on them.

CHAPTER 1.5. RATIONALE AND HYPOTHESIS

HIV and TB co-infection place an immense burden on health care systems as they act in synergy to worsen disease prognoses. TB is the most common cause of death in PLWH and in turn, HIV is the most significant risk factor for progressing from latent to active TB disease. While HIV and TB are endemic in sub-Saharan Africa, they also disproportionately affect marginalized populations in Canada[92]. Unfortunately, the only licensed TB vaccine, BCG, does not protect from adult pulmonary TB and is not recommended for the vulnerable PLWH population[68]. Thus, the development and testing of novel TB vaccines, which are safe and effective in PLWH, remains an urgent global necessity.

In the past, it has been extremely difficult to study HIV and TB co-infections *in vivo* due to a lack of practical and affordable animal models. Humanized mice are an extremely useful tool in understanding disease pathogenesis, immune responses, and cell interactions

as they are able to recapitulate the human immune system. Both our hu-NRG and our transgenic hu-A2, hu-DRAG and hu-DRAGA2 mice are able to be successfully infected with HIV, TB and HIV/TB co-infection and replicate many hallmarks of human diseases[143].

The Xing Lab at McMaster University has created a novel trivalent ChAd68 TB vaccine that can be delivered via the respiratory mucosal route to induce robust T cell and trained innate immunity[78]. Our hu-mice are an optimal model to quantify the type of human *M.tb*-specific immune responses with the RM delivery of the vaccine, and investigate the impact of HIV immune suppression on *M.tb* protection. Once optimized, we would like to look at the protection and immune responses that this vaccine can provide in the context of HIV infection with and without ART. It is hypothesized that intranasal administration of the Tri:ChAd68 vaccine will be effective at promoting *M.tb*-specific immune cells, providing protection from TB challenge and overcoming HIV immune suppression to confer protection against TB in humanized mice.

CHAPTER 1.6. SPECIFIC AIMS

Aim 1. **Examine the immunogenicity and protective efficacy of respiratory mucosal administration of Tri:ChAd68 vaccine against pulmonary *M.tb* infection in a humanized mouse model**

Aim 1.1. Investigate the frequency and amount of M.tb-specific CD4+ and CD8+ T cells in the lung and spleen after intranasal administration of the Tri:ChAd68 vaccine in naïve humanized mice

Aim 1.2. Determine if the intranasally delivered Tri:ChAd68 vaccine will confer protection against TB infection

Aim 2. **Examine the immunogenicity and protective efficacy of respiratory mucosal administration of Tri:ChAd68 vaccine against pulmonary *M.tb* infection in HIV-infected humanized mice**

Aim 2.1. Investigate the frequency of M.tb-specific CD4+ and CD8+ T cell T cells in the lung and spleen after intranasal administration of the Tri:ChAd68 vaccine in HIV-infected humanized mice

Aim 2.2. Examine the Tri:ChAd68 vaccine's protective efficacy and effect on disease progression of immunized HIV-infected humanized mice when subsequently challenged with TB infection

Aim 3. **Establish and optimize an efficient method for delivering ART to humanized mice to use for future experiments**

Aim 3.1. Establish a regimen to process and safely administer ART in DietGel Boost

Aim 3.2. Investigate the efficacy of the ART regimen

CHAPTER 2. METHODS

CHAPTER 2.1. GENERATING HUMANIZED MOUSE

2.1.1. Breeding and Genotyping of NRG, DRAG, A2 and DRAG-A2 mice

NRG mice (NOD.Cg-Rag1^{tm1MoM}Il2rγ^{tm1sug}) and heterozygous DRAG mice (NRG mice transgenic for HLA-DRB1*04:01) mice were purchased from The Jackson Laboratory (JAX, strain # 007799, and strain # 017914, respectively). Homozygous NRG-A2 mice (transgenic for HLA-A*02:01) were obtained from Dr. Ali Ashkar and Dr. Yonghong Wan (McMaster University, Hamilton, ON). These NRG-A2 mice were generated by back-crossing the HLA-A*02:01 transgene from the NSG-A2 strain (JAX, strain # 009617) onto the NRG background. To generate homozygous DRAG mice,

heterozygous DRAG mice were mated for multiple generations and their offspring were genotyped until the entire litter was 100% homozygous. To genotype, the DRAG mice were ear tagged and a small sample of ear tissue was obtained to use in the DNeasy Blood & Tissue Kit (QIAGEN, cat# 69506) to extract purified DNA. The confirmed homozygous NRG-DRAG mice were then crossed with NRG-A2 mice to develop DRAGA2 mice. These mice were housed in pathogen free ultra-clean rooms with vented cages that are equipped with high efficiency particulate air (HEPA) filters within the Central Animal Facility at McMaster University. To humanize mice, enriched CD34+ hematopoietic stem cells (HSC) isolated from human umbilical cord blood (UBC) were used.

2.1.2. CD34+ Hemopoietic Stem Cells for Engraftment

Umbilical cord blood was obtained with ethics approval (HiREB:ID 15552) and parental consent from the Labour and Delivery Department in the McMaster Children's Hospital. The cord blood was processed within 24 hours, the red blood cells were removed from nucleated cells through erythrocyte aggregation (HetaSep, StemCell Technologies, cat: 07906) and T cells were removed by negative selection (RosetteSep, StemCell Technologies, cat: 15066). This was followed by separation using density gradient centrifugation (Lymphoprep, StemCell Technologies, cat: 07851) and the final enriched and purified CD34+ HSCs were then cryopreserved in a commercially available medium (CryoStor, StemCell Technologies, cat: 07930) and stored in liquid nitrogen until they were needed. Additionally, 1mL of each UCB sample was aliquoted to be processed to isolate for cord blood mononuclear cells (CBMCs) using only the Lymphoprep density gradient centrifugation and cryopreserved for future use. Approximately 100µl of the CBMC and

CD34+ HSCs from each UBC sample was aliquoted for flow cytometric analysis where we could determine the purity of the sample and detect population of HLA-A2 cells. After the erythrocyte aggregation step, a 1mL aliquot of the UBC was set aside and kept in -20ºC for DNA extraction and HLA typing.

2.1.3. HLA Tissue Typing of UCB Samples and Engraftment of Mice

DNA was extracted from the blood aliquoted using the Qiagen Blood & Cell Culture DNA Midi Kit (QIAGEN, cat#: 13343) and then screened for the DRAG allele (HLA-DRB1*04:01) and the A2 allele (HLA-A*02:01). Samples were first screened for the DRAG allele using the MicroSSP Allele Specific HLA-typing class II DNA typing trays-DRB1*04:01 (OneLambda, cat#: SSPR2-104). If the flow analysis showed a population for HLA-A2, then the samples were screened for the A2 allele using the MicroSSP Allele Specific HLA-typing class I DNA typing trays (OneLambda, cat#: SSPR1-A2). Tissue typing trays were run with the PCR protocol recommended by the manufacturer. After PCR, gel electrophoresis was performed using 2.5% agarose gel (ThermoFisher Scientific, cat#: 16500500) in 1x Tris Borate EDTA buffer (1x TBE) (ThermoFisher Scientific, cat#: AM9863). Agarose Gel was prepared with the addition of 1µL/mL GelRed Nucleic Acid Gel Stain (Biotium, cat#: 41003). The unique gel dock used for electrophoresis is the Micro SSP Gel System (One Lambda, cat#: MGS108). The final photographed image is analyzed with the HLA Fusion software (version 4.2.0).

The HLA type determined which mice the HSC sample will be used for. For samples that were negative for both DRAG and A2, they were used to humanize NRG mice, and samples that were positive for both alleles were used for DRAG-A2 mice. Samples that

were positive for DRAG and negative for A2 were used for DRAG mice and vice versa with A2 mice. Newborn pups were irradiated 24-72 hours after being born with two doses of 3cGy separated by three hours, followed by intrahepatic (IH) injection of at least $1x10^5$ CD34+ enriched HSCs. Flow cytometry analysis was conducted 12, 16 and/or 20 weeks following humanization to determine how well engrafted the mice were by looking at the percentage and absolute number of human CD45 T cells.

CHAPTER 2.2. INFECTION AND IMMUNIZATION

2.2.1. Intraperitoneal Infection with HIV

All mouse studies were carried out with AREB Approval (AUP# 21-12-39). Hu-mice were first anesthetized with gaseous isoflurane and either $1x10^5$ IU (infectious units) of HIV-1 (sucrose-purified JRCSF) was administered into the peritoneum in 100µL volume of sterile phosphate-buffered saline (PBS). The mice were then checked daily for a week following infection to monitor for acute health reactions, followed by weekly checks and weights until endpoint. All work with HIV was carried out under Level 2+ precautions.

2.2.2. Intranasal Immunization with Tri:ChAd68 or Empty Adenoviral Vaccine

Hu-mice were first anesthetized with gaseous isoflurane until an unconscious plane of 1 breath every 2 seconds was reached. $1x10^7$ PFU Tri:ChAd68 (titer = 5.2x105 PFU/µL) or empty-adenoviral vector (titer = 5.5x105 PFU/µL) vaccine in a total volume of 25µL of PBS was pipetted on the nose while they were held in a vertical position. The mouse's mouth was held closed and upon fully aspirating the vaccine, continued to be held closed for 10-20 more seconds to ensure that the vaccine was aspirated into the lower respiratory

tract. Any bubbling of the liquid was noted, and the mice's breathing was carefully monitored until they were conscious and moving again.

2.2.3. Intranasal Challenge of *M.tb*

Hu-mice were first brought into the Containment Level 3 (CL3) facility at McMaster University one week prior to infection. Mice were anesthetized with gaseous isoflurane until an unconscious plane of 1 breath every 2 seconds was reached. *Table 1* shows the CFU of H37Rv *M.tb* (ATCC27294) given to each mouse, which was in a total volume of 25µL of PBS and was pipetted on the nose while they were held in a vertical position. The mouse's mouth was closed to ensure the mice breathed in only through their nostrils and the vaccine was aspirated into their respiratory tract. Any bubbling of the liquid was noted, and the mice's breathing was carefully monitored until conscious and moving again. The infection dose and stock of *M.tb* was tittered, plated and counted after 2.5 to 3 weeks of incubation to confirm the accurate dose of infection.

Table 1. ***M.tb*** **H37Rv information for each experiment.** Stock *M.tb* was given from Dr. Zhou Xing (McMaster University, Hamilton, ON)

Experiment	*M.tb* Lot #	Estimated Dosage	Actual Dosage	Estimated Titer	Actual Titer
Aim 1.2	17	$1x10^4$ CFU	8,385 CFU	30,000 CFU/µL	41,750 CFU/µL
Aim 2.2. Exp 1	18	$1x10^3$ CFU	1,137 CFU	20,000 CFU/µL	19,783 CFU/µL
Aim 2.2. Exp 2	19	$1x10^3$ CFU	1,427 CFU	15,000 CFU/µL	10,750 CFU/µL

CHAPTER 2.3. PROCESSING AND PREPARATION

2.3.1. Mononuclear Cell Isolation

Whole blood was either extracted from facial vein (~50µL), retro-orbital (~100-200µL) or vena cava (~500-1000µL) into EDTA-coated tubed (VWR, cat# CABD365974L). Facial and retro-orbital bleeds were used for survival bleeds, and vena cava was used for endpoint bleeds. Red blood cells (RBCs) were lysed with two rounds of ACK lysis buffer treatment (Quality Biological, cat# 10128-802). The lung and spleen were extracted from the mice and placed in a tube containing RPMI 1640 media. The lung was cut up into small pieces and digested with collagenase type 1 (Fisher Scientific, cat#: 17100017) (150U/mL) for 45 minutes to 1 hour at 37ºC. After digestion, the lung pieces were crushed through 100 µm pore size filters (VWR, cat#: 352360), and red blood cells (RBCs) were lysed with ACK lysing buffer (Quality Biological, cat# 10128-802) before being strained through 70 µm pore size filters. The spleen was crushed through 70 µm pore size filters, followed by removing RBCs through ACK lysis buffer and passed through 40 µm filters. Cells were then resuspended in supplemented RPMI 1640 media (sPRMI) with 10% FBS, 1% L-Glutamine, 1% HEPES, 1% sodium pyruvate, 1% non-essential amino acids, 0.1% β-mercaptoethanol, and 100 U/ml of Penicillin.

2.3.2. *Ex Vivo* T Cell Stimulation

The lung and spleen cells were evenly distributed and plated in a U-bottom 96 well plate. Cells were stimulated with PMA/ionomycin which served as a positive control, culture filtrate and crude BCG (CFCB) and/or BCG (Pasteur strain), and an unstimulated well which served as a negative control (Concentrations are shown in *Table 2).* All samples were stimulated *ex vivo* with co-stimulatory 1 µg/ml of monoclonal anti-human CD28 (clone CD28.2; ThermoFisher, cat#: 16-0289-81) and anti-human CD49d antibodies (clone

9F10; ThermoFisher, cat#: 16-0499-81). They were then placed in the incubator at 37ºC with 5% CO_2 for 24 hours. Five hours prior to the end of incubation, 1:400 GolgiPlug (BD Biosciences, cat#: 555028) was added to each well to trap cytokines within the cells, and then placed back in the incubator for the remaining time. Once incubation was over, the cells were surface and intracellularly stained.

Table 2. **Antigen stimulation condition information for the experiments.**

Stimulation Condition	Concentration per well	Tissue	Source
PMA/Ionomycin	2μL/mL	Lung and Spleen	ThermoFisher, cat#: 00-4970-93
Culture Filtrate and Crude BCG (CFCB)	Culture filtrate = 2ul/well Crude BCG = 1ul/well	Lung and Spleen	Dr. Zhou Xing (McMaster University)
Live BCG (Pasteur strain)	MOI of 6	Spleen	Dr. Zhou Xing (McMaster University)

2.3.3. ART Preparation

For the combined antiretroviral therapy (ART) medications, two non-nucleoside reverse transcriptase inhibitors (NNRTIs), tenofovir disoproxil fumarate (TDF) and emtricitabine (FTC) and one integrase inhibitor, raltegravir (RAL) were used. For optimization of ART preparation, we followed the protocol created by Mu et al. with some small adjustments. We used prescription pills instead of using research-grade powder and since we were not able to get FTC and TDF as two separate pills in Canada, we used Truvada® which is a capsule-shaped tablet that contains 300mg of FTC and 200mg of TDF. We were able to get RAL under the brand name Isentress®, which is an oval shaped tablet that contains 400mg of RAL.

In the Mu et al. study they prepared 10 food cups with 250mg of FTC, 375mg of

TDF and 500mg of RAL total. To account for the filler in our pills, we used the entire pill which had similar concentrations of drug to the paper. The dry power was pushed through 100 μm pore size filters to help crush the larger chunks and the coating. For the crushed up Truvada pill, 2.5mL of DMSO was mixed with the powder, and for the Raltegravir pill, 1mL of DMSO was mixed with the powder. Since the Raltegravir didn't fully solubilize in the DMSO, 4mL of sterile tap water was added and mixed with the solution. The entire solution was aspirated through a 19-gage needle (BD, cat# 14-826-52) into a 10mL syringe (BD, cat# 309604), where it was sterilized through a 0.2 μm syringe filter (Acrodisc, cat# 4187) into a fresh tube. 250μL of the Truvada solution and 500μL of the Raltegravir solution was aliquoted into separate 1.5mL o-ring tubes and stored at -20ºC until needed. 350μL of DMSO was also aliquoted and stored with the ART medications to be used for the control mice. The ART/DMSO solutions were mixed with their DietGel Boost (Clear H_20, cat # 72-04-5022) and given to the mice every 2-3 days. This was in accordance with Amendment 22-118.

CHAPTER 2.4. READOUT AND ANALYSIS

2.4.1. HIV Plasma Viral Load by RT-qPCR

Approximately 150-200μL of whole blood was collected via retro-orbital bleed into EDTA-coated tubes. The whole blood was centrifuged at 14,000 revolutions per minute (rpm) for 5 minutes, and the plasma was aliquoted and kept in -80ºC. RNA was extracted from 50μL of the plasma using the QIAamp MinElute Virus Spin Kit (QIAGEN, cat# 57704) and quantification of viral load was performed using reverse transcription – quantitative polymerase chain reaction (RT-qPCR). RT-qPCR reactions were set up with

the SensiFAST Probe Hi-ROX One-Step Kit (FroggaBio, BIO-77005) mixed with HIV-1 specific primers (forward primer: 5′- GCC TCA ATA AAG CTT GCC TTG A-3’; reverse primer 5′- GGC GCC ACT GCT AGA GAT TTT -3’), and probes (reporter probe: 5′- /6-FAM/ AAG TAG TGT GTG CCC GTC TGT TRT KTG ACT/TAMRA/ -3’). Samples were run on the StepOnePlus Real Time PCR System (Applied biosystems). The samples were run with a standard curve, a negative control lacking RNA (no template), a negative control lacking reverse transcriptase, a positive control RNA from a successfully infected mouse’s plasma and a negative control from uninfected plasma. Results were generated on the StepOne Software (version 2.3). Final analysis of HIV-1 viral load was based on HIV RNA copies/mL derived from a standard curve of Ct values quantified by the Mount Sinai Department of Microbiology (Toronto, Ontario).

2.4.2. Flow Cytometry

Once cells were added to a U-bottom 96-well plate, the cells were washed with PBS containing 0.5% bovine serum albumin (FACS buffer) and human and mouse Fc block (eBiosciences, cat# 14-9161-73, and cat# 14-0161-82, respectively). The Fc block was added to block unwanted and non-specific binding of antibodies before being stained with a fluorochrome-labeled monoclonal antibody cocktail. The T cell panel consisted of: hCD45-Pacific Blue, mCD45-AlexaFluor 700, hCD3e-Qdot 605, hCD4-PerCP-Cy5.5 and hCD8a-PE-Cy7. For pre-experimental peripheral blood checks, hCD14-AlexaFluor647 and hCD19-PE was also added to the T cell panel. For the lung macrophage panel, the antibody cocktail consisted of: hCD45-Pacific Blue, hCD3e-Qdot 605, hCD11b PerCP-Cy5.5, hCD14-BV785, hCD16-FITC, hCD169-PE, hCD206-APC, and HLA-DR-PE-Cy7. After

ex vivo T cell stimulation, lung and spleen cells were surface stained for hCD45-Pacific Blue, hCD3e-Qdot 605, hCD4-PerCP-Cy5.5 and hCD8a-PE-Cy7, followed by intracellular staining for IFN-γ-PE, TNF-α-FITC, IL-2-AlexaFluor 700, and IL-17-APC. Cells were also stained with fixable viability dye (eFluor 780) then fixed with either 4% paraformaldehyde (PFA) solution in PBS or Cytofix/Cytoperm (BC, cat# 554722) and washed with 1x Perm/Wash (BD, cat# 554723) in MilliQ water. Once staining was complete, cells were run on the CytoFlex LX flow cytometer (Beckman Coulter) and data was analyzed using FlowJo software. All antibody concentrations are shown in *Table 3.*

Table 3. **Flow cytometry antibody markers used in the experiments.**

Marker	Indicator of	Clone	Fluorochrome	Quantity per well	Source
Dead cells	Viability	-	eFluor780	1:1000	eBiosciences cat# 65-0865-14
hCD45	Human leukocytes	H130	Pacific Blue	2.5µL	eBiosciences cat# MHCD4528
mCD45	Murine leukocytes	30-F11	Alexa Fluor 700	1µL	eBiosciences cat# 56-0451-28
hCD3e	T cells	UCHT1	Qdot 605	0.5µL	eBiosciences cat# Q10054
hCD4	Helper T cells	RPA-T4	PerCP-Cy5.5	2.5µL	eBiosciences cat# 45-0049-42
hCD8a	Killer T cells	RPA-T8	PE-Cy7	2.5µL	eBiosciences cat# 25-0088-42
hCD19	B cells	HIB19	PE	2.5µL	eBiosciences cat# 12-0199-42
hCD14	Monocytes/ macrophages	Tuk4	Alexa Fluor 647	2.5 µL	eBiosciences cat# A51013
		M5E2	BV785	2 µL	BioLegend cat# 301840
hCD16	NK cells/ macrophages	3G8	FITC	1.25 µL	BioLegend cat# 302006
hCD11b	Monocytes/ macrophages	CBRMI/5	PerCP-CY5.5	2.5 µL	BioLegend cat# 3011418
hCD169	Alveolar macrophages	7-239	PE	1 µL	BioLegend cat# 346004
hCD206	Monocytes/ macrophages	15-2	APC	5 µL	BioLegend cat# 321110

HLA-DR	HLA expression on APCs	LN3	PE-Cy7	2.5 µL	BioLegend cat# 327018
IFNγ	T cell associated cytokine	4S.B3	PE	2.5 µL	BioLegend cat# 502509
TNFα		Mab11	FITC	1 µL	BioLegend cat# 502906
IL-2		MQ1-17H12	Alexa Fluor 700	0.5 µL	BioLegend cat# 500320
IL-17A		eBio64DEC17	APC	10 µL	eBioscience cat# 17-7179-42

2.4.3. *M.tb* Bacterial Load by CFU Assay

The lung and spleen were mechanically homogenized in 2 mL of 10% glycerol (Fisher Scientific, cat# FLBP2291) and 0.1% Tween 80 (Fisher Scientific, cat# T164500) in PBS. The homogenates were plated in 10-fold serial dilutions on Middlebrook 7H10 agar plates containing Middlebrook oleic acid-albumin-dextrose-catalase (OADC) enrichment (Fisher Scientific, cat# B11886) and supplemented with 5µg/mL ampicillin (Sigma, cat#: A5354) and 50µg/mL cycloheximide (Sigma, cat#: C7698). The plates were incubated for 2.5 to 3 weeks at 37ºC and until the *M.tb* colonies were counted. The bacterial load in the respective tissues was quantified by multiplying the dilution factor, the average number of colonies, the tissue factor and amount of homogenization buffer (2mL) and dividing that value by the volume plated (100µL) to get the CFU.

2.4.4. Histopathology and Immunohistochemistry

The lung and spleen were placed in a falcon tube containing 10% formalin for a week, then sliced up, placed into a cassette and added to 70% ethanol where it was then sent to McMaster Histology Core Facility. The tissues were embedded in paraffin and stained with hematoxylin and eosin (H&E), acid-fast bacilli (AFB), CD4+ T cell and/or CD68+ macrophage immunohistochemistry. For H&E quantification, lung lesion and

granuloma structures were quantified using the ImageJ software developed by NIH by measuring the granulomatous tissue areas relative the total lung area. For each mouse, three lung slices were measured and averaged, with the histology figures showing the middle slice.

For immunohistochemistry, tissue sections were deparaffinized and boiled in Tris/EDTA for 20 minutes, following blocking with 5% bovine serum albumin (BSA). The sections were then incubated with 1:50 mouse anti-human CD4 monoclonal antibodies (clone 4B12, Leica Biosystems, cat#: PA0371) or mouse anti-human CD68 monoclonal antibodies (clone PG-M1, Dako, cat#: GA61361-2) for 1 hour at room temperature. The sections were visualized with the Bond Polymer Refine Red Detection kit (Leica BioSystems, cat# DS9390) on an automated Leica Bond RX autostainer (Leica Biosystems) and then quantified by mean grey intensity on Fiji ImageJ software.

2.4.5. Statistical Analysis

Groups were compared either using unpaired parametric T tests, or with a one-way or two-way ANOVA with Tukeys multiple comparison test in GraphPad Prism. Data was considered significant if p-values were <0.05. Significant differences were denoted as * $p < 0.05$, ** $p < 0.01$, *** $p < 0.001$, **** $p < 0.0001$. Data were expressed as mean +/- SEM.

CHAPTER 3. RESULTS

For all the experiments conducted, we aimed to use humanized mice that had greater than 10% hCD45 leukocytes or greater than 50,000 hCD45 cells/mL in their peripheral blood at 16 or 20 weeks post-stem cell engraftment. The type of humanized mouse (hu-

mouse) model and original n numbers chosen for each experiment relies mainly on the amount of well-engrafted mice available at the beginning of each experiment. The groups were randomized based on their hCD45 and hCD4 levels, sex and cord blood samples.

CHAPTER 3.1. AIM 1. EXAMINE THE IMMUNOGENECITY AND PROTECTIVE EFFICACY OF THE RESPIRATORY MUCOSAL ADMINISTRATION OF TRI:CHAD68 VACCINE AGAINIST PULMONARY *M.TB* INFECTION IN A HUMANIZED MOUSE MODEL

Aim 1.1. **Investigate the frequency and amount of *M.tb*-specific CD4+ and CD8+ T cells in the lung and spleen after intranasal administration of the Tri:ChAd68 vaccine in naïve humanized mice**

In this experiment, there were two vaccinated groups (VAC) with one of them consisting of n=3 hu-DRAGA2 and the other consisted of n=3 hu-NRG mice and an unvaccinated control group (UNVAC) which consisted of n=1 DRAGA2 and n=1 hu-NRG. On Day 0, the VAC mice were intranasally immunized with $1x10^7$ PFU Tri:ChAd68 vaccine while the UNVAC mice were not immunized to serve as a negative control. At experimental endpoint which was 4 weeks post-immunization, the mice were sacrificed, and their lungs and spleen were collected to undergo *ex vivo* T cell stimulation. To determine if our next-generation model of transgenic mice engrafted with HLA-matched HSCs for both HLA-A2 and -DRAG had any notable differences in cytokine production than that of our hu-NRG mice, both mouse models were used. The experimental outline and legend to indicate individual mice are shown in *Figure 1*. The reconstitution and initial

information about each mouse are shown in *Supplementary Table 1*.

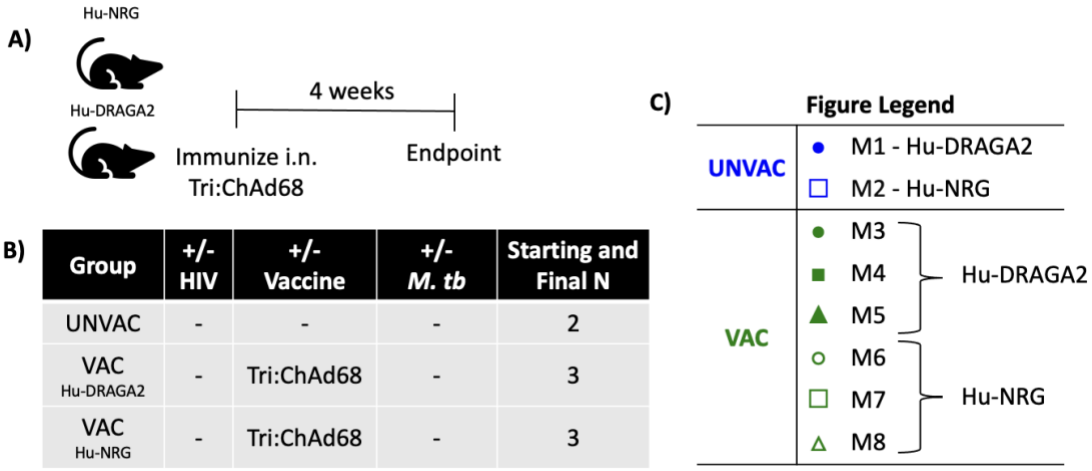

Group	+/- HIV	+/- Vaccine	+/- *M. tb*	Starting and Final N
UNVAC	-	-	-	2
VAC Hu-DRAGA2	-	Tri:ChAd68	-	3
VAC Hu-NRG	-	Tri:ChAd68	-	3

Figure 1. **Experiment for Aim 1.2.** (A) Experimental outline (B) Group information (C) Figure Legend

3.1.1. Investigate antigen specific T cells in the lungs after vaccination

At experimental endpoint, the mouse's entire lung and spleen was extracted, and the tissues were processed and digested. Roughly $5x10^5$ lung cells per well were plated for T cell stimulation or left unstimulated, followed by staining for surface T cells and intracellular pro-inflammatory cytokines. To assess for *M.tb*-specific T cell cytokine production, the unstimulated values were subtracted from their paired culture filtrate/crude BCG (CFCB) stimulated wells to remove non-specific background cytokine production. Mice that had a greater number or percentage of unstimulated cells than CFCB-stimulated cells were denoted as 0. Flow gating for the T cell stimulation can be found in *Supplementary Figure 1*, and values for unstimulated and stimulated conditions prior to adjustment can be seen in *Supplementary Figures 2 and 3.*

The VAC mice had an increased average trend in both the amount and frequency of

hCD4+ T cells producing IFNγ, TNFα and IL-2 in their lungs than the unvaccinated mice, with there being no significant difference in production between hu-NRG and hu-DRAGA2 mice (*Figure 2*). However, while there are a very low amount and percentage of IL-2 cells in *Figure 2C and F*, it seems as though the two out of the three hu-DRAGA2 mice produced more IL-2 than the rest of the mice. Between the hCD4+ T cells producing cytokines, TNFα had the highest number of cells among the other two cytokines with IFNγ following closest behind, and IL-2 production only accounting for less than 60 cells *(Figure 2D-F).*

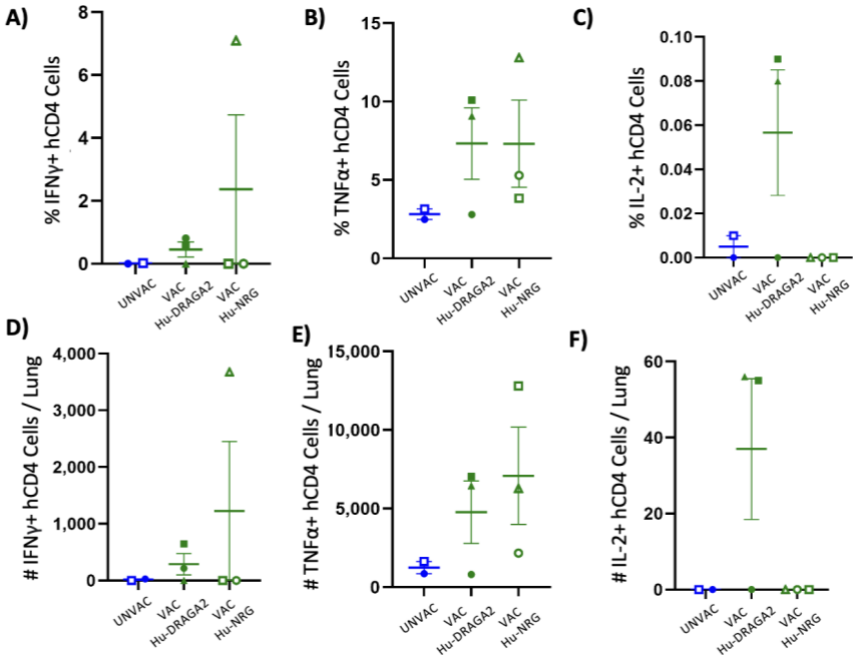

Figure 2. **Antigen-specific cytokine production by human CD4+ T cells in the lungs of hu-DRAGA2 and hu-NRG mice 4 weeks after vaccination.** Unstimulated values subtracted from CFCB cells after 24 hours of stimulation. Percentage of hCD4+ T cells producing (A) IFNγ (B) TNFα (C) IL-2. Absolute count of hCD4+ T cell producing (D) IFNγ (E) TNFα (F) IL-2 per lung. Data are expressed as +/- SEM. Statistical analysis was performed using a one-way ANOVA with Tukeys multiple comparison test. p values = * < 0.05, ** < 0.01, *** < 0.001, **** < 0.001.

It is important to note that the cytokine production amongst the mouse groups was averaged by only 2-3 mice, causing challenges showing significance. For hCD8+ T cells

analysis, there were minimal differences in percentage of cells producing cytokines between unstimulated and stimulated cells (*Figure 3A-C*). However, we can see the same trend with the number of hCD8+ T cells producing IFNγ and IL-2 in as we did with hCD4, and the average number of hCD8+ cells producing TNFα was only slightly greater in the VAC mice than the control mice (*Figure 3D-F*). While there is variability among the hu-mice as we would assume would be also in humans, we can see that the vaccine is producing more hCD4+ T cells responses in our mice than hCD8 responses.

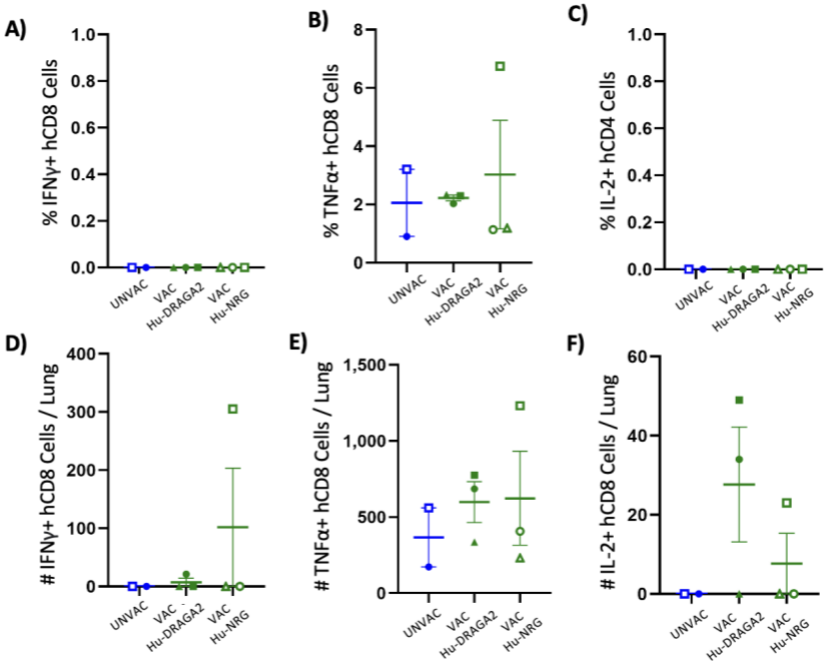

Figure 3. **Antigen-specific cytokine production by human CD8+ T cells in the lungs of Hu-DRAGA2 and hu-NRG mice 4 weeks after vaccination.** Unstimulated values subtracted from CFCB cells after 24 hours of stimulation. Percentage of hCD8+ T cells producing (A) IFNγ (B) TNFα (C) IL-2. Absolute count of hCD8+ T cell producing (D) IFNγ (E) TNFα (F) IL-2 per lung. Data are expressed as +/- SEM. Statistical analysis was performed using a one-way ANOVA with Tukeys multiple comparison test. p values = * < 0.05, ** < 0.01, *** < 0.001, **** < 0.001.

3.1.2. Investigate antigen specific T cells in the spleen after vaccination

For the spleen, $2x10^6$ spleen cells per well were plated for T cell stimulation,

followed by surface and intracellular staining. As mentioned, unstimulated values were subtracted by CFCB stimulated values to assess for *M.tb*-specific T cells. The spleen of the vaccinated mice had increased trends in frequency of hCD4+ T cells producing TNFα, IFNγ and IL-2 when compared to the unvaccinated mice, with the hu-DRAGA2 mice producing a greater percentage of IFNγ and TNFα than the hu-NRG mice *(Figure 4).* In the spleen, which contain many more cells than in the lungs, we can see that there are more than 10 times more cells producing TNFα cytokines than IFNγ, with IL-2 once again having very few cells, which is consistent with their percentages *(Figure 4).* Note that there is inconsistency with often one mouse producing much higher cytokine levels than others in our vaccinated groups.

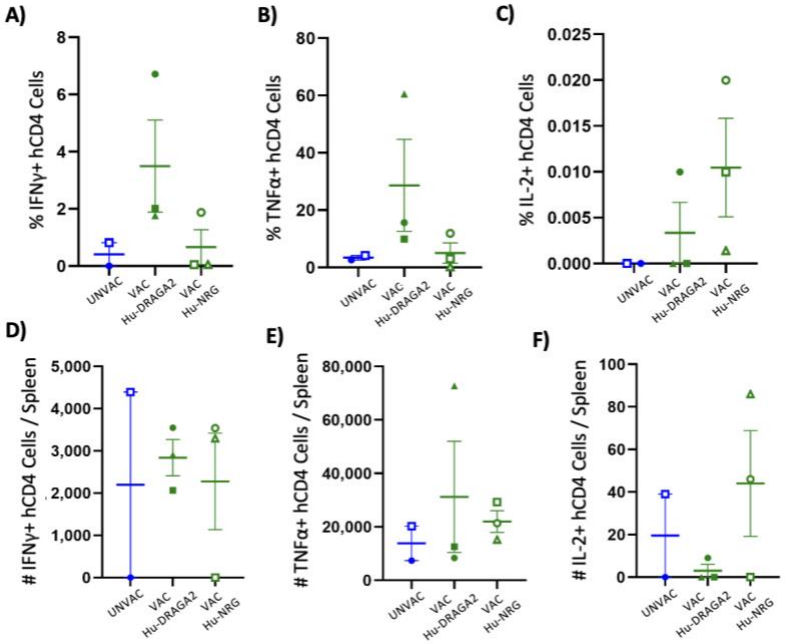

Figure 4. **Antigen-specific cytokine production by human CD4+ T cells in the spleen 4 weeks after vaccination.** Unstimulated values subtracted from CFCB cells after 24 hours of stimulation. Percentage of hCD4+ T cells producing (A) IFNγ (B) TNFα (C) IL-2. Absolute count of hCD4+ T cell producing (D) IFNγ (E) TNFα (F) IL-2. Data are expressed as +/- SEM. Statistical analysis was performed using a one-way ANOVA with Tukeys multiple comparison test. p values = * < 0.05, ** < 0.01, *** < 0.001, **** < 0.001.

In *Figure 5*, there is a greater trend for hCD8+ TNFα and IL-2 production in vaccinated mice compared to the unvaccinated mice. *Figure 5D-F* also show a greater number of hCD8+ cytokine producing cells in the spleen of immunized hu-NRG mice than in the hu-DRAGA2 mice. However, we do not see any antigen specific hCD8+ T cell IFNγ responses as our 2 unvaccinated mice appear to have significantly higher responses than our vaccinated mice.

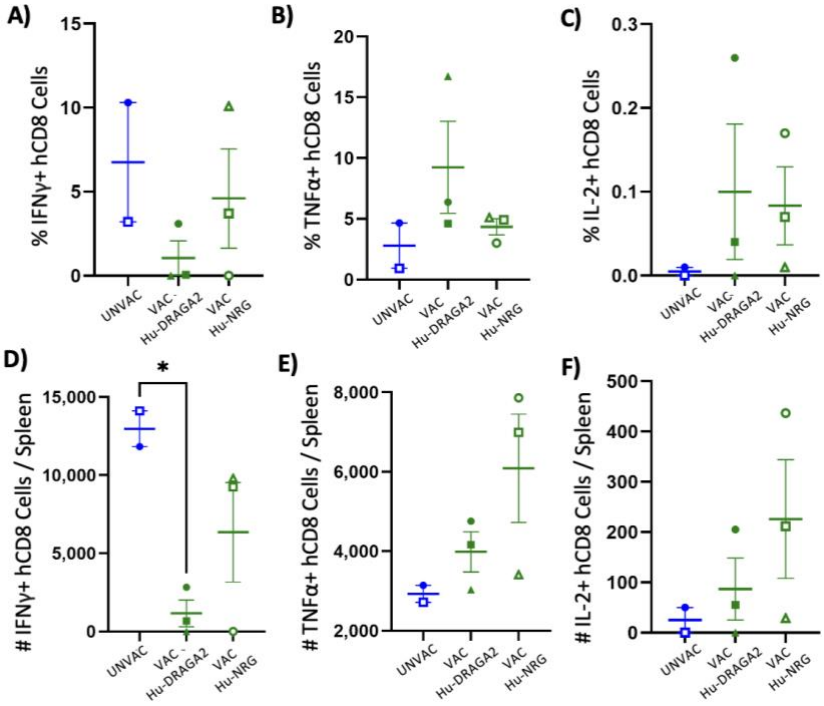

Figure 5. **Antigen-specific cytokine production by human CD8+ T cells in the spleen 4 weeks after vaccination.** Unstimulated values subtracted from CFCB cells after 24 hours of stimulation. Percentage of hCD8+ T cells producing (A) IFNγ (B) TNFα (C) IL-2. Absolute count of hCD8+ T cell producing (D) IFNγ (E) TNFα (F) IL-2. Data are expressed as +/- SEM. Statistical analysis was performed using a one-way ANOVA with Tukeys multiple comparison test. p values = * < 0.05, ** < 0.01, *** < 0.001, **** < 0.001.

Aim 1.2 - Determine if the intranasally delivered Tri:ChAd68 vaccine will confer protection against TB infection

In this next experiment, the vaccinated group (VAC) which first consisted of 4 hu-NRG mice was given $1x10^7$ PFU Tri:ChAd68 vaccine via the intranasal route on Day 0. The unvaccinated group (UNVAC) which consisted of 4 hu-NRG mice was not given any vaccine to serve as a negative control and to compare the protection levels when both groups were subsequently infected with *M.tb*. Four weeks post-immunization, all the mice were brought up to the Containment Level 3 (CL3) facility where they were all intranasally challenged with $1x10^4$ H37Rv *M.tb* lot #17. Four weeks after *M.tb* infection the mice reached experimental endpoint and were sacrificed, and their lungs and spleen was collected to assess for bacterial burden and pathology. The data from this experiment has been published by Afkhami et al. in *npj Vaccines.* The experimental outline and legend to indicate individual mice are shown in *Figure 6.* The reconstitution and initial information about each mouse are shown in *Supplementary Table 2.*

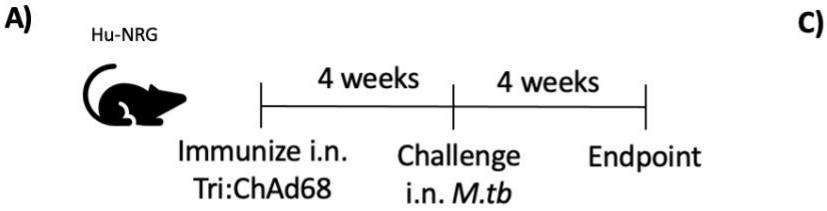

B)

Group	+/- HIV	+/- Vaccine	+/- *M. tb*	Starting N	Final N
UNVAC	-	-	H37Rv	4	4
VAC	-	Tri:ChAd68	H37Rv	4	3

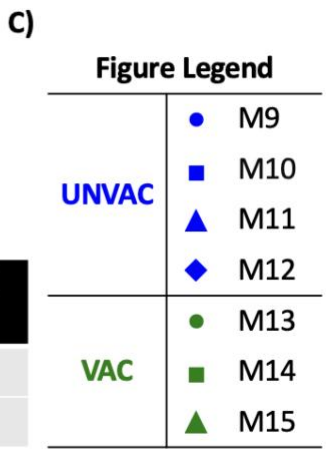

Figure 6. **Experiment for Aim 1.2.** (A) Experimental outline (B) Group information (C) Figure legend.

3.1.3. Examine mycobacterial burden in the lungs and spleen after vaccination and subsequent M.tb challenge

Throughout the experiment, all mice were monitored for weight loss as an indication of progressing TB disease, as 20% loss of original body weight would be considered endpoint and require euthanasia. As you can see in *Figure 7*, the UNVAC and VAC mice maintained consistent weights after *M.tb* challenge up until about Day 22, where the unvaccinated mice drastically dropped their body weight to an average of about 15% of their starting weight. Unfortunately, by the end of the experiment one mouse in the VAC group had extreme graft vs host disease (GvHD), which is when engrafted human immune cells attack the mouse cells. This mouse was removed from the experiment as this could greatly affect results, and the VAC group had a final n number of 3 hu-NRG mice.

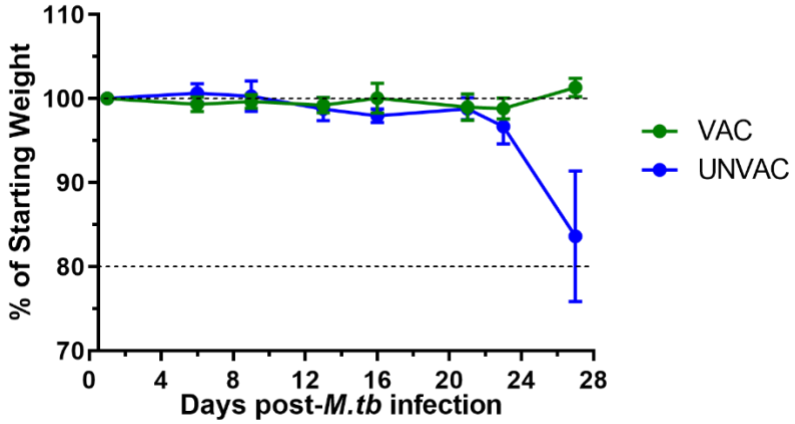

Figure 7. **Body weight changes as a percentage of starting body weight following mucosal challenge of *M.tb*.** VAC (n=3) and UNVAC group (n=4). Each mouse was weighed weekly or bi-weekly to assess for weight changes and averaged as a group. Data represented as +/- SEM.

To assess the mycobacterial load in the lung and spleen of the mice, the right lobe of the lung and ½ of the spleen was homogenized, diluted, and plated on agar plates. The

colony forming units (CFU) assay in the lung showed that the vaccinated mice had an averaged CFU log_{10} of 6.8, which was significantly less than the unvaccinated mice, which had a CFU log_{10} of 9.2 (*Figure 8A*). This was about a 2.4 log_{10} reduction in lung CFU, and while the difference isn't significant in the spleen, we can see a trend of an average 2.38 log_{10} reduction in the bacterial load in the spleen of the vaccinated mice (CFU log_{10} 4.2), compared to the unvaccinated mice (CFU log_{10} 6.6) *(Figure 8B).* This indicated that the vaccine significantly lowers mycobacterial burden in the lungs and potentially decreases tissue dissemination of mice infected with *M.tb* (CFU counts in *Supplementary Table 3).*

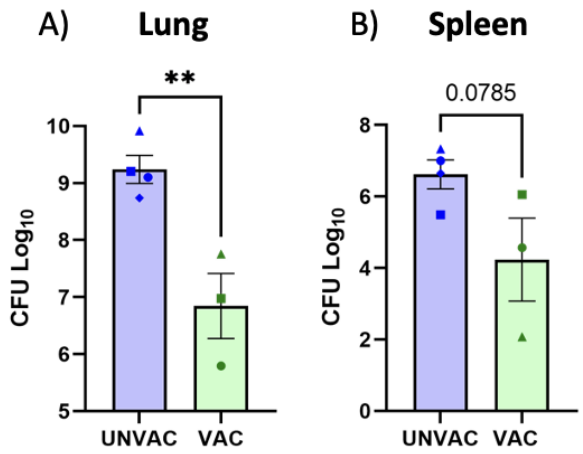

Figure 8. **Mycobacterial burden in tissues of VAC and UNVAC mice 4 weeks post-*M.tb* infection.** VAC (n=3) and UNVAC (n=4) log_{10} CFU of (A) Lung (B) Spleen. Data expressed as +/- SEM. Statistical analysis was performed using an unpaired parametric T test. p values = * < 0.05, ** < 0.01, *** < 0.001, **** < 0.001.

3.1.4. Examine pathology and granuloma formation in the lung and spleen after vaccination and subsequent M.tb challenge

To assess pathological differences in the tissues, the left lobe of the lung and other ½ of the spleen was fixed for histology and stained. To examine tissue granuloma structures, the tissues were stained with hematoxylin and eosin (H&E) and from the

representative image in *Figure 9A and B,* we can see the VAC mice contain less granuloma lesions in their lungs than the UNVAC mice. This was quantified to represent a percentage of granulomatous tissue within the lung section, and while not significant, we can see that there is an increased trend of granulomatous tissue in the UNVAC mice than the vaccinated mice, which is consistent with what we observe in the H&E stained image *(Figure 10A & B).* To visualize immune cells in the tissues, immunohistochemistry (IHC) of CD4+ T cell staining of the lung and spleen was conducted. In the representative image in *Figure 9C* and *D,* CD4+ cells stained in brown in the lung of the UNVAC and VAC mice did not show much difference visually between the groups. However, when the number of immune cells per section was quantified with imaging software and represented as mean grey intensity, the VAC group displayed slightly less CD4+ T cells in the spleen, but not in the lung, than the UNVAC group *(Figure 10C & D).* Lastly, in *Figure 9E and F*, the unvaccinated mice showed greater densities of acid-fast bacilli (AFB) inside their granuloma than in the lung of the vaccinated mice, indicating a protective aspect in containing *M.tb* growth and reducing dissemination. Histological images of each mouse are shown in *Supplementary Figure 4.*

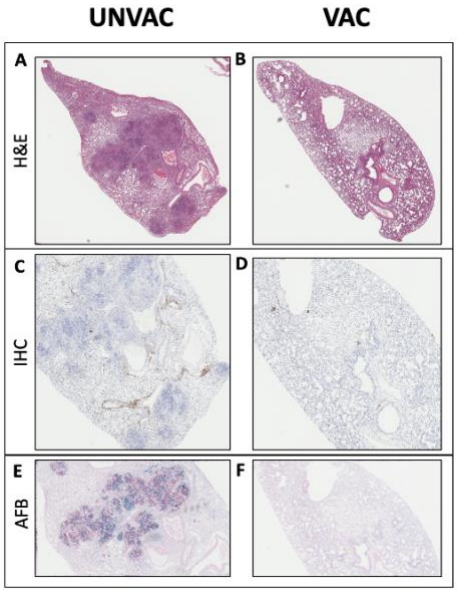

Figure 9. **Visualization of the lung pathology 4 weeks after *M.tb* infection in representative sections.** H&E staining of the middle lung segments in (A) UNVAC mice and (B) VAC mice. IHC CD4+ T cell staining of the middle lung segments in (C) UNVAC mice and (D) VAC mice. AFB staining of the middle lung segments in (E) UNVAC mice and (F) VAC mice. Representative as UNVAC group (n=4), VAC group (n=3).

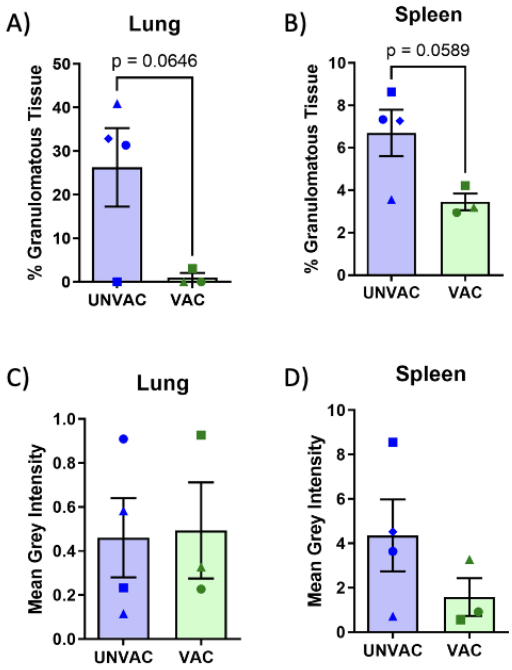

Figure 10. **Bar graph depicting quantified histopathology of H&E staining and IHC for CD4+.** Percentage of granulomatous tissue in the whole organ in the (A) lung and (B) spleen. Mean grey intensity of CD4 T cells in the (C) lung and (D) spleen. Statistical

analysis was performed using an unpaired parametric T test. p values = * < 0.05, ** < 0.01, *** < 0.001, **** < 0.001.

CHAPTER 3.2. AIM 2. EXAMINE THE IMMUNOGENECITY AND PROTECTIVE EFFICACY OF THE RESPIRATORY MUCOSAL ADMINISTRATION OF TRI:CHAD68 VACCINE AGAINIST PULMONARY *M.TB* INFECTION IN HIV-INFECTED HUMANIZED MICE

Aim 2.1 - Investigate the frequency of *M.tb*-specific CD4+ and CD8+ T cell T cells in the lung and spleen after intranasal administration of the Tri:ChAd68 vaccine in HIV-infected humanized mice

Experiment 1

In this experiment, the four experimental mouse groups were used consisted of a control group that received the empty-adenoviral vector vaccine (Control – Empty Ad), a vaccinated group (VAC), an HIV-infected group (HIV) and an HIV-infected group that subsequently was vaccinated (HIV+VAC). The HIV group (initially 4 hu-DRAG mice) and the HIV+VAC group (initially 4 hu-DRAG mice) received $1x10^5$ infectious units (IU) of HIV-1 (JRCSF) via the intraperitoneal (IP) route on Day 0. Five weeks post-infection, the VAC group that consisted of 4 hu-DRAG and the HIV+VAC group were intranasally immunized with $1x10^7$ PFU Tri:ChAd68 vaccine. The control (empty ad) group which first consisted of 4 hu-DRAG mice were intranasally immunized with the $1x10^7$ PFU of the empty adenoviral-vectored vaccine. Since the empty vector is able to provide non-specific protection, it is used to ensure the protection is from responses to the antigens and not just

from the vector itself, as the trivalent vaccine should induce *M.tb*-specific immune responses[78]. Unfortunately, many of the mice engrafted with a particular cord blood sample developed GvHD throughout the course of the experiment and had to be euthanized, thus changing the final n numbers. By the end of the experiment, the HIV+VAC group contained only 3 mice, the HIV group had only 2 mice left and there was only one control (empty ad) mouse left, thus the control mouse was removed from all data sets. The experimental outline and legend to indicate individual mice are shown in *Figure 11*. The reconstitution and initial information about each mouse are shown in *Supplementary Table 4.*

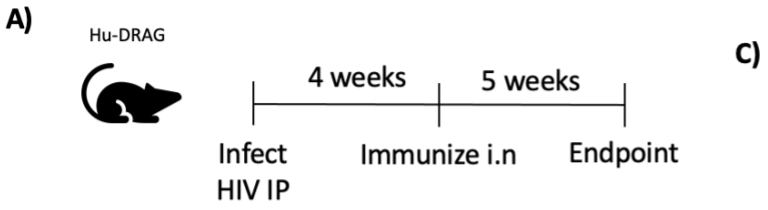

B)

Group	+/- HIV	+/- Vaccine	+/- *M. tb*	Starting N	Final N
Control	-	Empty Ad	-	4	1
HIV	JRCSF	-	-	4	2
VAC	-	Tri:ChAd68	-	4	4
HIV+VAC	JRCSF	Tri:ChAd68	-	4	3

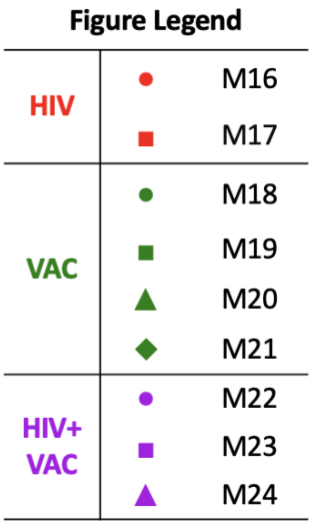

Figure 11. **Experiment 1 for Aim 2.1.** (A) Experimental outline (B) Group information (C) Figure legend.

3.2.1. Confirmation of primary HIV-1 infection prior to vaccination and throughout the experiment

To ensure the mice were successfully infected with HIV prior to immunization, at 3 weeks post-infection the viral load in their plasma was assessed through reverse-transcription quantitative polymerase chain reaction (RT-qPCR). Additionally, to confirm

the mice remained infected throughout the experiment and to determine if the vaccine had any effect on the viral load, mice were also bled at 6- and 9-weeks post-infection. Both groups started with similar average HIV viral load; however, the HIV+VAC group's viral load appeared to increase after vaccination. (*Figure 12*, individual RNA values in *Supplementary Table 5).* Consistent with what we see in literature and expect with HIV infection, as the HIV RNA copies/mL increased, the number of hCD4+ T cells/mL decreased shown in *Figure 13*.

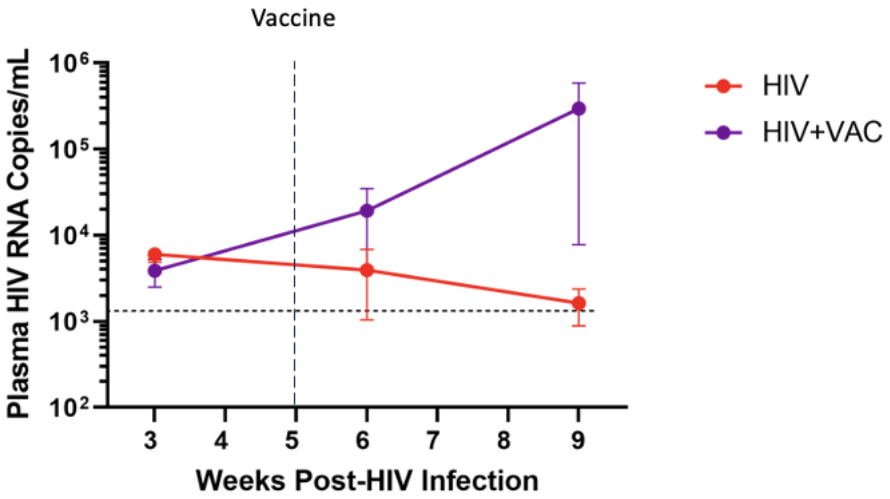

Figure 12. **HIV viral load in the plasma of HIV-infected mice.** Plasma HIV RNA copies/mL for the HIV only (n=3) and HIV+VAC (n=4) mice at 3-, 6- and 9- weeks post-infection. Horizontal dotted line indicates threshold level of ~1,500 RNA copies/mL, vertical dashed line indicated that the vaccine was administered 5 weeks post-infection.

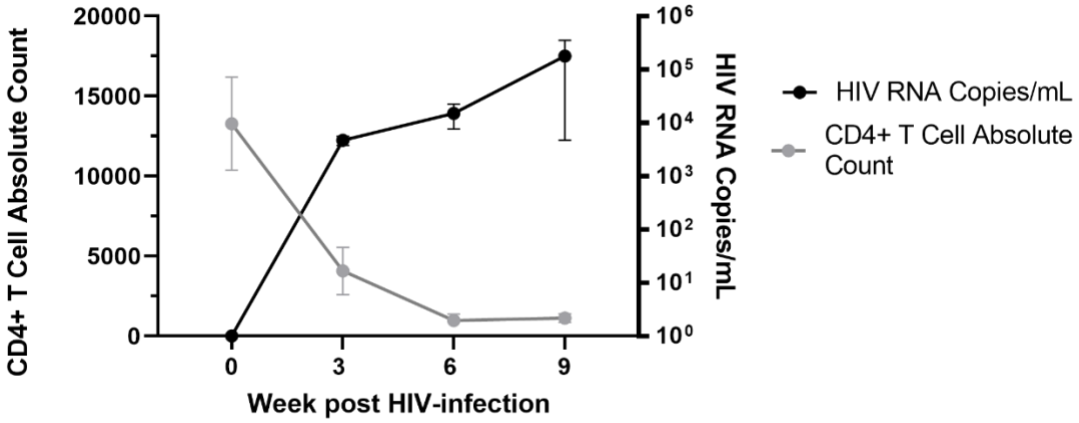

Figure 13. **Viral load in the plasma against number of CD4+ T cells in the blood.** The number of hCD4+ T cells and HIV RNA copies/mL at 0-, 3-, 6- and 9-weeks post-HIV infection of an average for all mice in the HIV only (n=2) and HIV+VAC (n=3) groups. Data represented at +/- SEM.

At experimental endpoint, which was 9 weeks post-HIV infection, the mice were sacrificed, and their lungs, spleen and blood was collected. To assess for the T cells present at endpoint and to determine if the HIV depleted their hCD4+ T cells, their peripheral blood was stained for hCD4+ and hCD8+ T cells and analyzed via flow cytometry. The mice in the HIV and HIV+VAC group had a lower percentage and absolute count of hCD4+ T cells in the blood than the VAC group, indicating that the HIV depleted their hCD4 levels, which is what was expected (*Figure 14A, B*). It is of interest to note that while there is significance between the decreased percentage of hCD4 in the HIV+VAC group compared to the VAC only group, the HIV+VAC group have similar average number of hCD4 T cells as the HIV-only group (*Figure 14B*). However, this analysis is hampered due to only 2 surviving mice in the HIV alone group. Unfortunately, due to a technical error many of the CD8+ T cells potentially died; thus, the percentage and absolute count is much lower than expected and this data is not conclusive. The trend still remains as the VAC group have slightly less

percentage and amount of hCD8+ T cells than the two HIV groups, which is reversed to what we saw with hCD4 (*Figure 14C, D).*

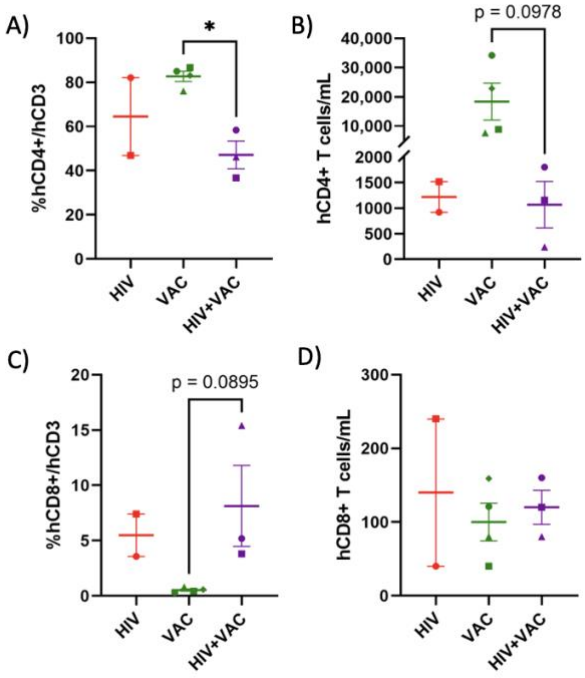

Figure 14. **Flow cytometry of CD4+ and CD8+ T cells in the peripheral blood of all groups 9 weeks post-HIV infection.** (A) Percentage and (B) Absolute count of hCD4+ T cells. (C) Percentage and (D) Absolute count of hCD8+ T cells in the blood at endpoint. HIV group (n=2), VAC group (n=4) and HIV+VAC group (n=3). Data is represented as +/- SEM. Statistical analysis was performed using a one-way ANOVA with Tukeys multiple comparison test. p values = * < 0.05, ** < 0.01, *** < 0.001, **** < 0.001.

3.2.2. Investigate macrophages in the lung and TII after vaccination

Macrophages are known to be the main target of *M.tb* and serve as the major host cell for the its growth and survival[156]. Macrophages, along with dendritic cells (DCs), are responsible for the initiation and activation of both innate and adaptive cellular and humoral immune responses, which are necessary to control or eliminate the infection[156]. Macrophages also play a crucial role in different phases of HIV-1 infection, as they help to

establish the infection at the mucosa, disseminate the virus to different organs and tissues and act as a viral reservoir[157]. Since macrophages are reservoirs for both HIV and *M.tb*, HIV-associated TB infections can negatively impact the ability of macrophages to respond to infection with *M.tb*[158]. Human leukocyte antigen-DR (HLA-DR), a major histocompatibility complex II (MHC II) cell surface receptor found on antigen presenting cells (APCs) such as monocytes, macrophages and DCs, can be used to study macrophage activation[80]. Increased expression of HLA-DR in alveolar and interstitial macrophages not only induces the adaptive immune system by presenting *M.tb*-specific antigen peptides to CD4+ T cells, but is also a measure of trained innate immunity (TII) phenotypic long-term memory in these cells caused by respiratory mucosal (RM) immunization[80]. On the other hand, a low expression of HLA-DR is linked to increased immunosuppression, disease pathogenesis, sepsis and even death[159]. Therefore, our aim is to determine if the vaccine is able to induce TII in our naïve and HIV-infected mice, which could aid in the protection against TB.

To assess for TII induced by the intranasal vaccine, about 1/3 of the lung cells were stained and analyzed. The cells were stained with hCD45 to isolate human leucocytes and were also stained with hCD206, a mannose receptor marker, to identify the total macrophages[160]. The $hCD45^+$ $hCD206^+$ cells were then examined by hCD14 versus hCD169 staining. The $hCD45^+$ $hCD206^+$ cells that were $hCD14^-$ $hCD169^+$ were alveolar macrophages (AMØs), and the $hCD45^+$ $hCD206^+$ cells that were $hCD14^+$ $hCD169^-$ were interstitial macrophages (IMØs)[160]. The $hCD45^+$ $hCD206^-$ cells represented granulocytes such as neutrophils, mast cells and eosinophils which we did not investigate further. The

sample flow gating strategy for this panel can be found in *Supplementary Figure 5*.

Figure 15 shows a trend of increased percentage of total macrophages, IMØs and AMØs in the VAC group compared to the other groups. Unfortunately for the IMØs, the percentage of cells in the fluorescence minus one (FMO) control was higher than expected, providing some potential auto-fluorescence interference *(Supplementary Figure 6)*. Due to the abnormally high FMO level, this data cannot be considered as strong since usually FMO levels are less than 1%, while in this data set the FMO for IMØs was 14.5%. Furthermore, the VAC group has significantly more AMØs than the HIV group, with the HIV+VAC group having only a slightly greater percentage of AMØs than the HIV group.

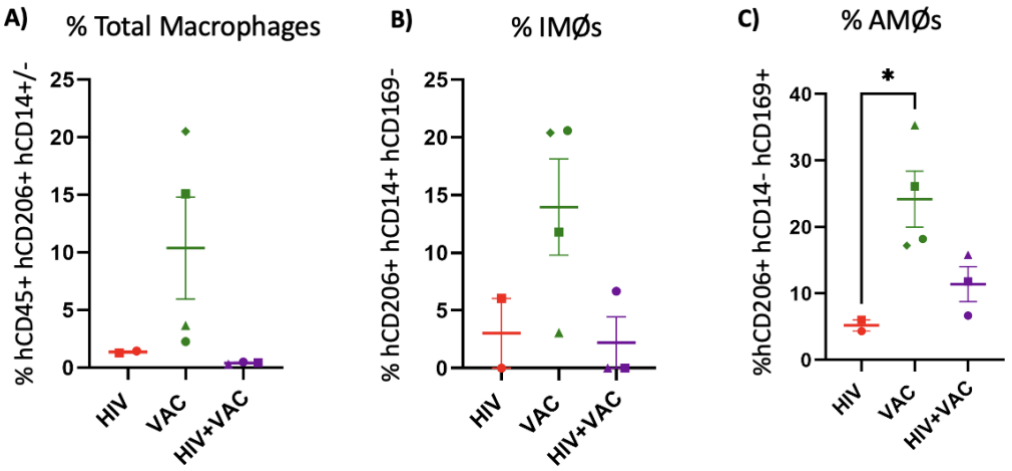

Figure 15. **Macrophage cells in the lungs at 9 weeks post-HIV infection.** (A) Percentage of total macrophage cells (B) Percentage of interstitial macrophage cells (C) Percentage of alveolar macrophage cells. HIV group (n=2), VAC group (n=4) and HIV+VAC group (n=3). Data is represented as +/- SEM. Statistical analysis was performed using a one-way ANOVA with Tukeys multiple comparison test. p values = * < 0.05, ** < 0.01, *** < 0.001, **** < 0.001. IMØs, interstitial macrophages; AMØs, alveolar macrophages.

The expression of HLA-DR on these macrophages was measured by the frequency and median fluorescent index (MFI) on their parent cell. For HLA-DR expression on their total macrophages, the VAC only mice have almost all their macrophages expressing HLA-

DR, with a significantly greater percentage and MFI HLA-DR than the HIV-infected groups (*Figure 16A, D).* The HIV+VAC group have roughly half their total macrophages expressing HLA-DR, with a significantly greater percentage than the HIV group. Once again, the HLA-DR is expressed on most IMØs in the VAC only group, with there being no expression of HLA-DR on IMØs in the HIV only and HIV+VAC group *(Figure 16B & E).* Next, for the AMØs, most of the mice in each group showed expression of HLA-DR when looking at the percentage, but the vaccine group still had greater MFI than the HIV only group, with the HIV+VAC group having a larger spread *(Figure 16C & F).*

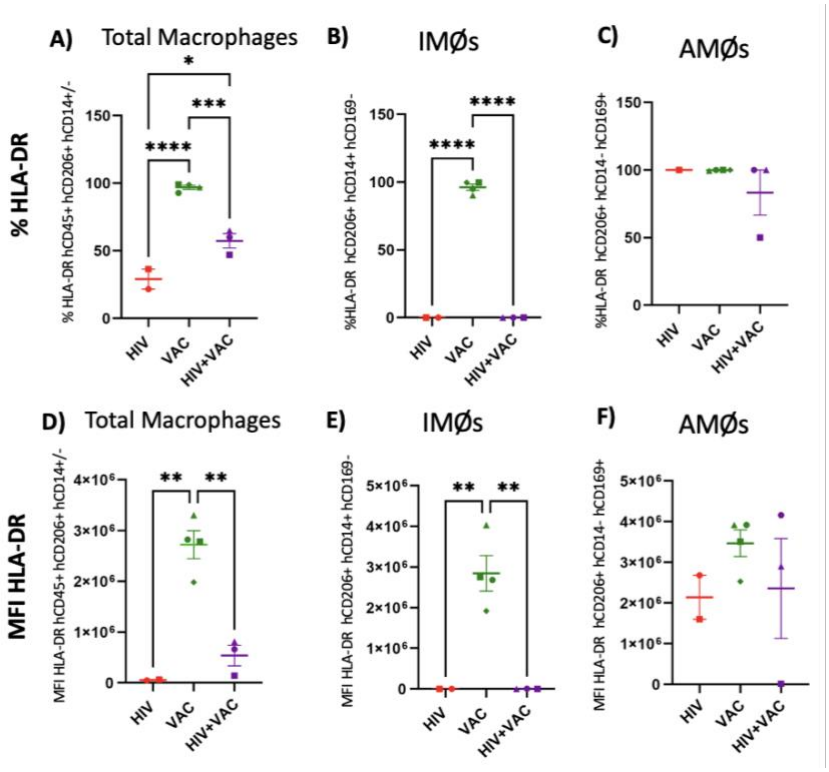

Figure 16. **HLA-DR on macrophage cells in the lungs at 9 weeks post-HIV infection.** Percentage of HLA-DR on (A) total macrophages (B) IMØs (C) AMØs. MFI of HLA-DR receptors on (D) total macrophages (E) IMØs (F) AMØs. HIV (n=2), VAC (n=4) and HIV+VAC (n=3). Statistical analysis was performed using a one-way ANOVA with Tukeys multiple comparison test. p values = * < 0.05, ** < 0.01, *** < 0.001, **** < 0.001. MFI, mean fluorescent index; IMØs, interstitial macrophages; AMØs, alveolar macrophages.

3.2.3. Investigate antigen specific T cells in the lung and spleen after vaccination

To investigate the immunogenicity of the Tri:ChAd68 vaccine in naïve and HIV-infected hu-mice, the other 2/3 of the lung cells as well as all the spleen cells were plated for *ex vivo* T cell stimulation, with 1/3 of the lung cells plated for stimulation, and the other 1/3 unstimulated. PMA/ionomycin was used as a positive control on the pooled mouse cells, as well as for all the FMOs and each sample's cells had an unstimulated well used as a negative control. For the lung, the cells were stimulated with CFCB and for the spleen, the cells were stimulated with CFCB in one well and BCG ($1.5x10^5$ CFU) in another well. Unstimulated values were subtracted from the cells produced from the CFCB condition to account for cells that non-specifically produced cytokines. Sample flow gating strategy for the T cell stimulation can be found in *Supplementary Figure 7*, and values for unstimulated and stimulated conditions prior to adjustment can be seen in *Supplementary Figures 8-10.*

While there are no statistically significant differences in hCD4+ and hCD8+ T cells producing cytokines in the lung, there is an increased averaged trend of hCD4+ IFNγ, TNFα and IL-17 as well as hCD8+ IFNγ in the HIV+VAC group compared to the other groups *(Figure 17A-E).* For TNFα+ hCD8 cells, there were none to very limited cells in both the CFCB and unstimulated well, and once subtracted all the values became zero *(Figure 17F).* For hCD8+ IL-2 and IL-17, there was only one mouse that had cells after being subtracted, however that value is very small *(Figure 17G, H).*

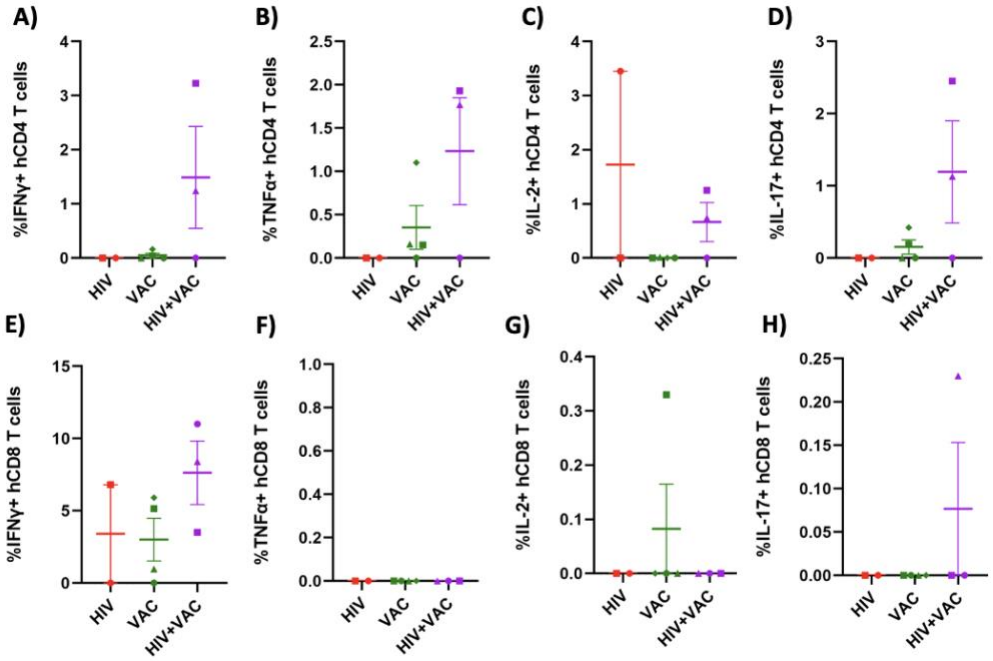

Figure 17. **Frequency of CFCB minus unstimulated Ag-specific T cell cytokine production in the lung at 9 weeks post-HIV infection.** Percentage of hCD4+ T cells producing (A) IFNγ (B) TNFα (C) IL-2 (D) IL-17. Percentage of hCD8+ T cells producing (E) IFNγ (F) IL-2 (G) IL-17. Data is represented as +/- SEM. Statistical analysis was performed using a one-way ANOVA with Tukeys multiple comparison test. p values = * < 0.05, ** < 0.01, *** < 0.001, **** < 0.001.

In the spleen, we can see that the HIV+VAC group have the greatest averaged trend of hCD4+ TNFα, IL-2, IL-17 as well as hCD8+ IL-2 (*Figure 18B-D, G).* HIV+VAC also shows a similar average to the HIV group for IFNγ in the T cells, with both groups being greater than the VAC group *(Figure 18A, E).* Once again, there were zero hCD8+ TNFα once CFCB was subtracted from unstimulated cells *(Figure 18F).* Interestingly, the HIV group has the greatest average for hCD8+ IL-17, but it is important to note that out of the 2 mice only one mouse showed production *(Figure 18H).*

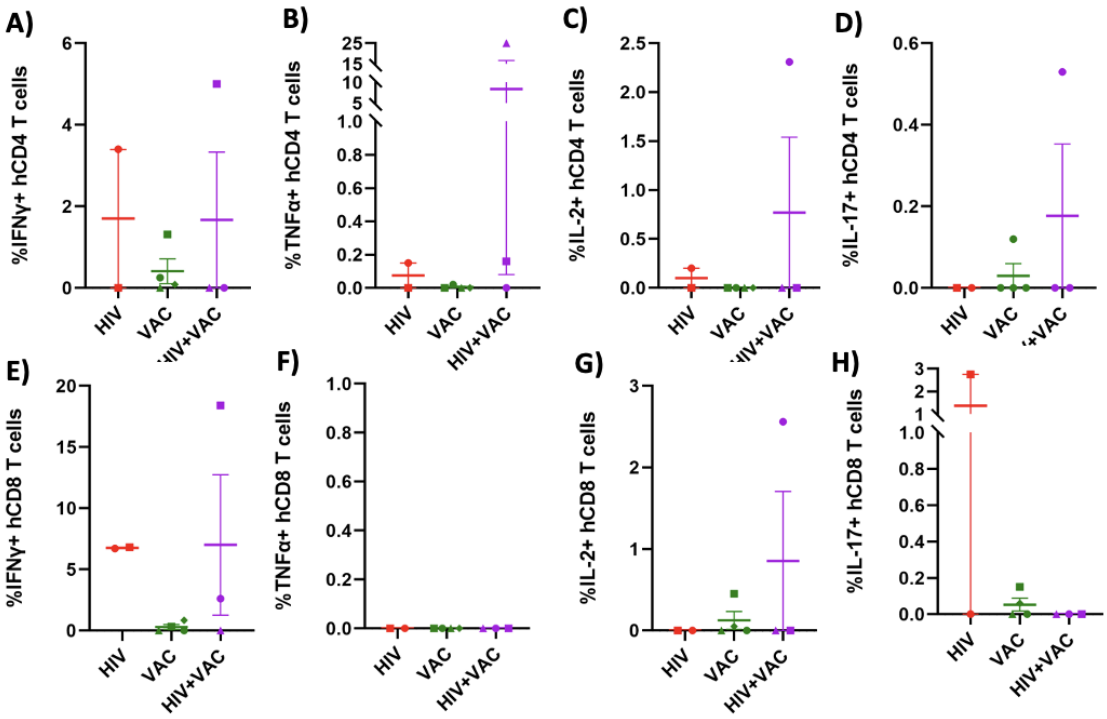

Figure 18. **Frequency of CFCB minus unstimulated Ag-specific T cell cytokine production in the spleen at 9 weeks post-HIV infection.** Percentage of hCD4+ T cells producing (A) IFNγ (B) TNFα (C) IL-2 (D) IL-17. Percentage of hCD8+ T cells producing (E) IFNγ (F) IL-2 (G) IL-17. Data is represented as +/- SEM. Statistical analysis was performed using a one-way ANOVA with Tukeys multiple comparison test. p values = * < 0.05, ** < 0.01, *** < 0.001, **** < 0.001.

When stimulated with BCG, we can see slightly greater production of cytokines compared to the CFCB stimulation in the spleen. The HIV+VAC group once again have the greatest averaged trend in IFNγ, TNFα, IL-17 production from hCD4 T cells, with it having similar percentage to the VAC group for IL-2 (*Figure 19A-D)*. For hCD8+ T cells, the VAC and HIV+VAC group also have similar averages to IFNγ production, with the HIV group having the highest trend in TNFα, the HIV+VAC group in IL-2 and the VAC group in IL-17 production *(Figure 19E-H).*

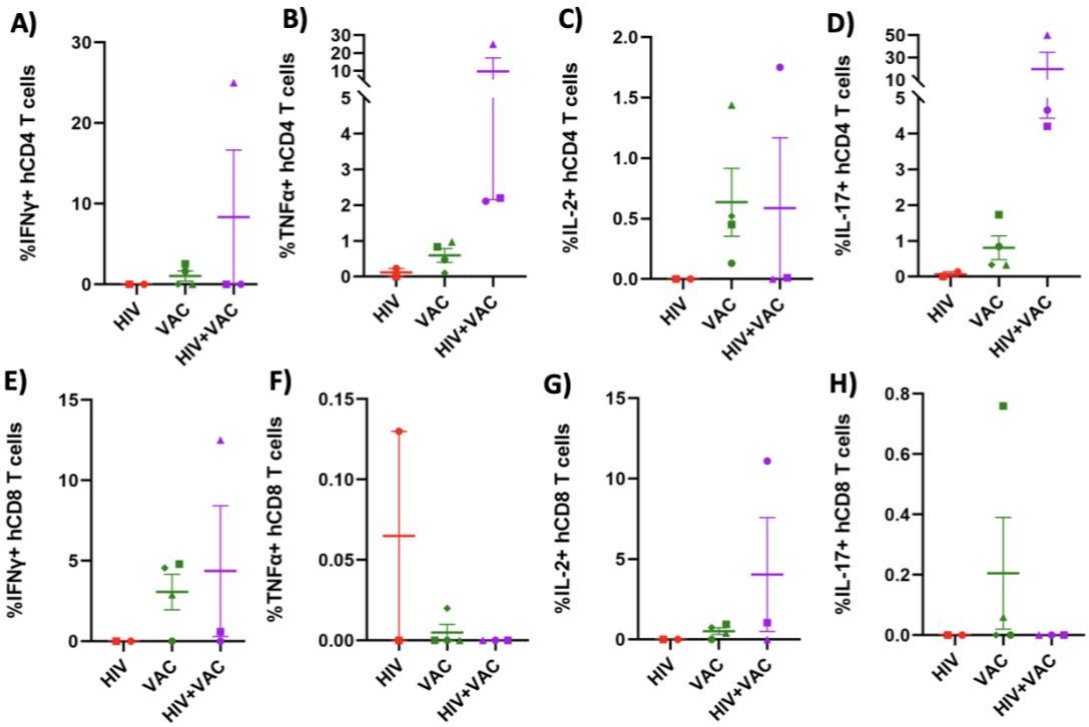

Figure 19. **Frequency of BCG minus unstimulated Ag-specific T cell cytokine production in the spleen at 9 weeks post-HIV infection.** Percentage of hCD4+ T cells producing (A) IFNγ (B) TNFα (C) IL-2 (D) IL-17. Percentage of hCD8+ T cells producing (E) IFNγ (F) TNFα (G) IL-2 (H) IL-17. Data is represented as +/- SEM. Statistical analysis was performed using a one-way ANOVA with Tukeys multiple comparison test. p values = * < 0.05, ** < 0.01, *** < 0.001, **** < 0.001.

Experiment 2

This experiment also aimed to investigate the immunogenicity of the vaccine, as well as increasing its final n numbers. In contrast to the previous experiment, this one uses hu-NRG mice and another group was added to look at *M.tb*-specific cells when given the vaccine before HIV infection. Firstly, the unvaccinated group (UNVAC) which initially consisted of 5 hu-NRG mice and were not given any vaccine nor HIV to serve as a negative control. On Day 0, the HIV group (5 hu-NRG mice) and the HIV+VAC group (6 hu-NRG mice) received $1x10^5$ IU of HIV (JRCSF). The newly included group initially consisted of

5 hu-NRG mice and were given $1x10^7$ PFU Tri:ChAd68 vaccine on Day 0 and were subsequently infected with $1x10^5$ IU of HIV 4 weeks later. At that timepoint, the HIV+VAC group and the VAC group (5 hu-NRG mice) received $1x10^7$ PFU Tri:ChAd68 vaccine, and four weeks after that all mice reached experimental endpoint and were sacrificed. The experimental outline and legend to indicate individual mice are shown in *Figure 20*. The reconstitution and initial information about each mouse are shown in *Supplementary Table 6.*

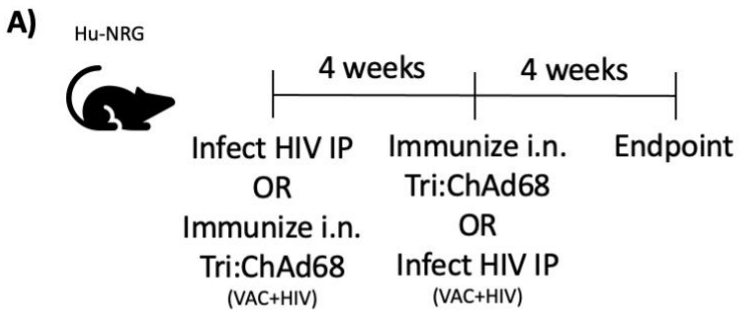

B)

Group	+/- HIV	+/- Vaccine	+/- *M. tb*	Starting N	Final N
UNVAC	-	-	-	5	3
HIV	JRCSF	-	-	5	5
VAC	-	Tri:ChAd68	-	5	5
HIV+ VAC	JRCSF	Tri:ChAd68	-	6	6
VAC+ HIV	JRCSF	Tri:ChAd68	-	5	4

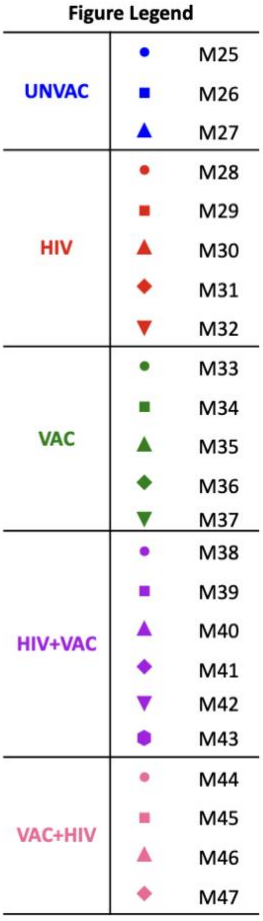

Figure 20. **Experiment 2 for Aim 2.1.** (A) Experimental outline (B) Group information (C) Figure legend.

3.2.4. Confirmation of primary HIV-1 infection prior to vaccination and throughout the experiment

Once again, to ensure the mice were successfully infected with HIV prior to immunization and thereafter, at 3-, 6- and 8- weeks post-infection the viral load in their plasma was assessed through RT-qPCR. In *Figure 21,* we can see that both HIV and HIV+VAC groups maintained their averaged viral load, with a slight increase after 6 weeks. On the other hand, the VAC+HIV group, which was infected with HIV 4 weeks after the other two groups, slightly decreased their averaged viral load after 2 weeks of HIV-infection, but overall not much change amongst the groups. Individual RNA values can be found in *Supplementary Table 7.*

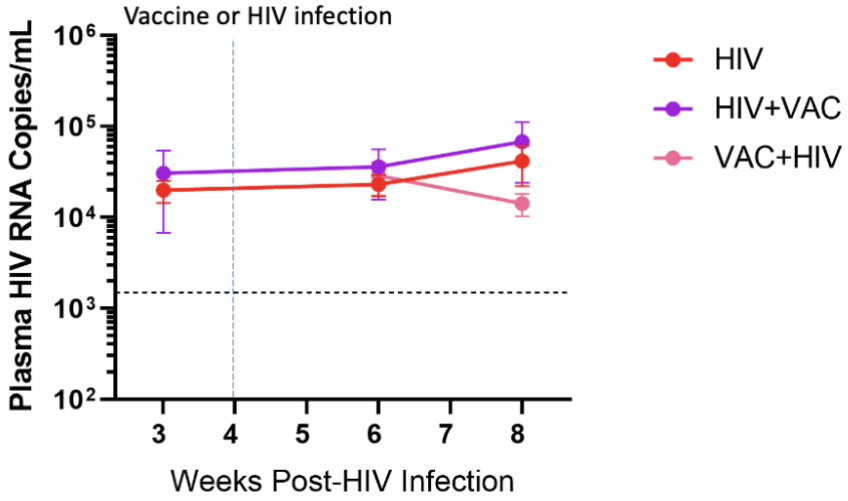

Figure 21. **HIV viral load in the plasma of HIV-infected mice.** Plasma HIV RNA copies/mL for the HIV (n=5), HIV+VAC (n=6,) and VAC+HIV (n=4) mice at 3-, 6- and 8- weeks post-infection. Horizontal dotted line indicates threshold level of ~1,500 RNA copies/mL, vertical dashed line indicated that the vaccine or HIV was administered 4 weeks post-initial infection. Data represented as +/- SEM.

Once sacrificed at 8 weeks post-infection, the mice's lungs, spleen and blood were collected for analysis. For the blood, both the HIV and HIV+VAC group have a

significantly lower percentage of hCD4+ T cells than the VAC group, with the HIV+VAC group also having significantly less than the UNVAC group (*Figure 22A).* Also, in *Figure 22A*, the VAC+HIV had a decreased frequency of hCD4 cells, similar to that of the HIV group even though the VAC+HIV group was infected only 4 weeks prior to endpoint. The number of hCD4+ T cells in the blood of all three HIV groups was significantly less than the VAC and UNVAC group, which is what we expected *(Figure 22B*). The HIV groups have a slightly greater frequency of hCD8 T cells than the non-HIV groups, with HIV+VAC having a significantly greater percentage of hCD8 T cells than the VAC group *(Figure 22C).* While there was no significant difference in the amount of hCD8 cells, the VAC and UNVAC groups appear to have a greater average number of cells than the HIV groups *(Figure 22D).*

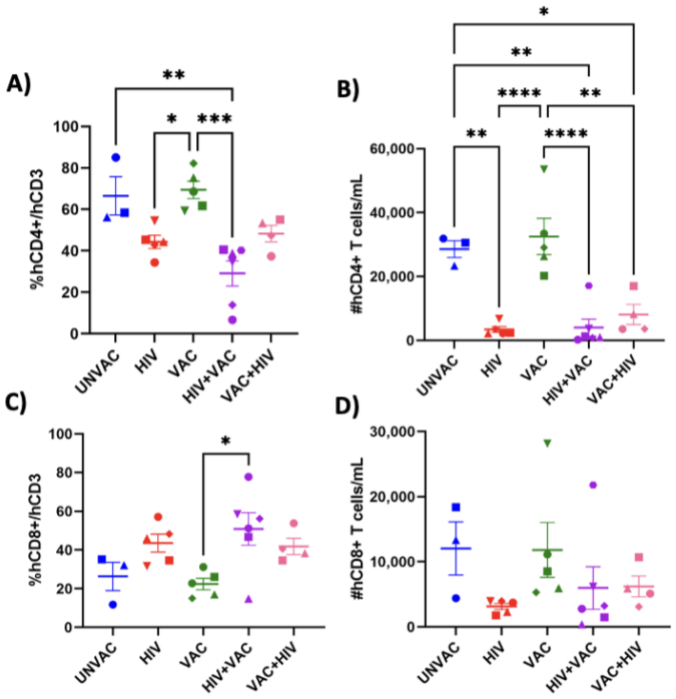

Figure 22. **Flow cytometry of CD4+ and CD8+ T cells in the peripheral blood of all groups 8 weeks post-HIV infection.** (A) Percentage and (B) Absolute count of hCD4+ T

cells. (C) Percentage and (D) Absolute count of hCD8+ T cells in the blood at endpoint. Data is represented as +/- SEM. Statistical analysis was performed using a one-way ANOVA with Tukeys multiple comparison test. p values = * < 0.05, ** < 0.01, *** < 0.001, **** < 0.001.

3.2.5. Investigate T cells and macrophages in the lung and TII after vaccination

TII was assessed via HLA-DR expression on the macrophages in the lung, by looking at the percentage of cells expressing HLA-DR and their MFI. In *Figure 23A*, while not significant, the VAC group had the greatest trend of total macrophages. In *Figure 23B & C,* the VAC group had significantly more IMØs than the three HIV-infected groups, while the HIV-infected groups had a greater trend of AMØs. While not significant, the percentage of HLA-DR on the total macrophages was greatest in the UNVAC and VAC groups (*Figure 23D*). In *Figure 23E,* both the UNVAC and VAC group had a significantly greater percentage of HLA-DR on their IMØs than the HIV and HIV+VAC group. For the percentage of HLA-DR on AMØs, most of the groups were similar with the non-HIV infected groups slightly greater. When looking at the MFI HLA-DR on total macrophages, we see a similar trend to the percentage of HLA-DR but for MFI the difference between the UNVAC group and the HIV and HIV+VAC group was significant *(Figure 23G*). We can also see that the UNVAC group had a significantly higher MFI HLA-DR on IMØs than all three of the HIV-infected groups, with no significant trends on the MFI HLA-DR on AMØs (*Figure 23 H, I*). The flow gating strategy can be found in *Supplementary Figure 11.*

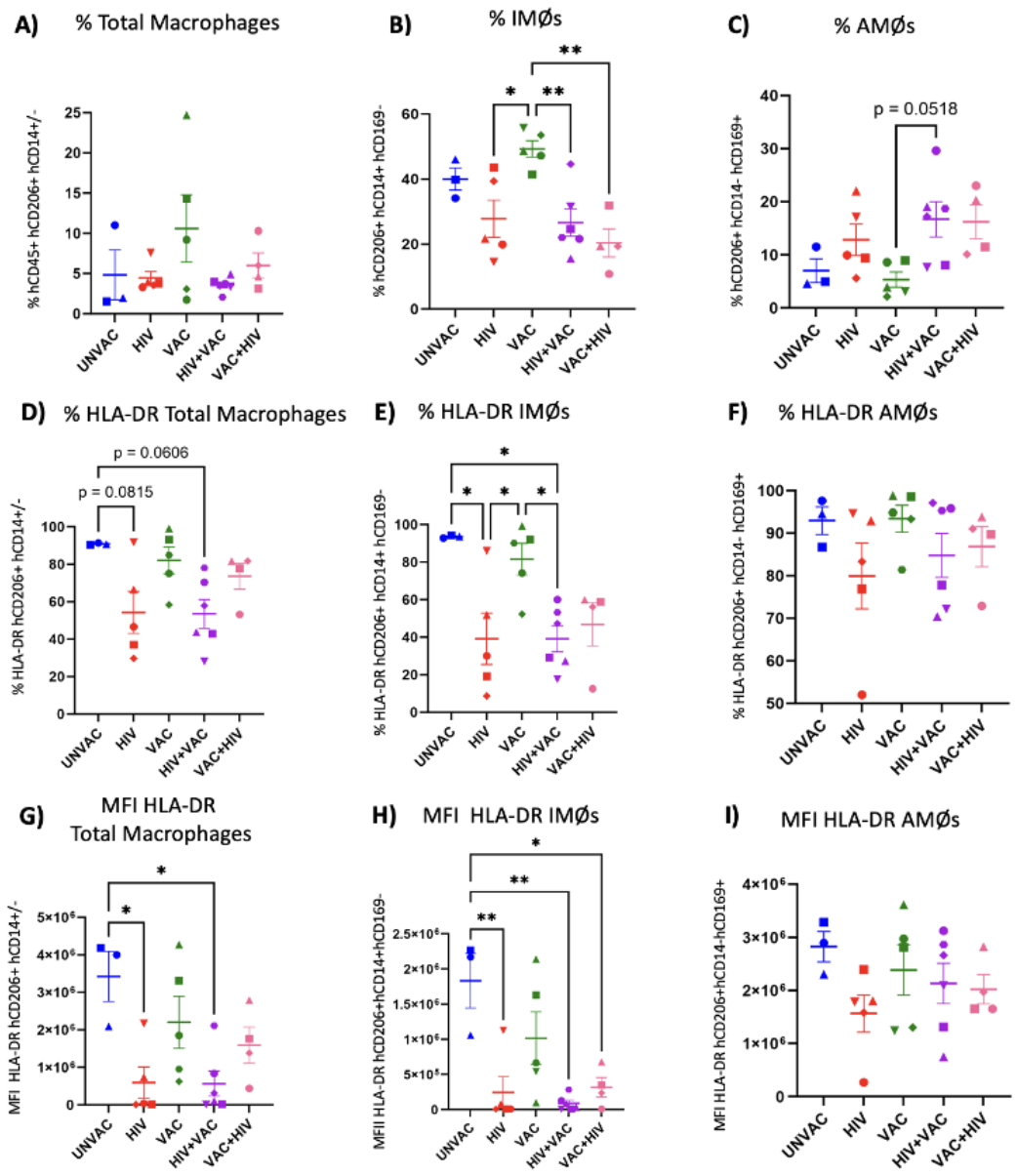

Figure 23. **Macrophage cells and HLA-DR activation in the lungs at 8 weeks post-HIV infection.** Percentage of (A) total macrophages (B) IMØs (C) AMØs. Percentage of HLA-DR on (D) total macrophages (E) IMØs (F) AMØs. MFI of HLA-DR on (G) total macrophages (H) IMØs (I) AMØs. Data is represented as +/- SEM. Statistical analysis was performed using a one-way ANOVA with Tukeys multiple comparison test. p values = * < 0.05, ** < 0.01, *** < 0.001, **** < 0.001. IMØs, interstitial macrophages; AMØs, alveolar macrophages.

When looking at the T cells in the lungs of the mice, we can see in *Figure 24A* that

all the groups have fairly the same percentage of hCD3+T cells. Alternatively, for the percentage of hCD4+ T cells in the lungs, the UNVAC and VAC group have significantly more hCD4 cells than the HIV and HIV+VAC group, which is to be expected *(Figure 24B).* Since the VAC+HIV group got infected with HIV four weeks after the other HIV groups, their hCD4+ T cell levels are similar showing that they haven't been depleted to the same extent as the other HIV-infected groups yet.

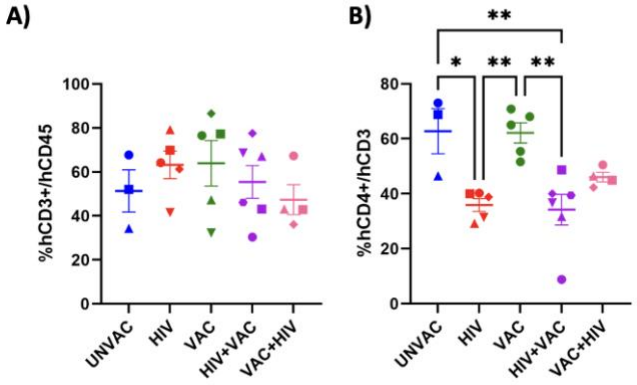

Figure 24. **T cells in the lungs at 8 weeks post-HIV infection.** (A) Percentage of hCD3+ T cells (B) hCD4+ T cells. Data is represented as +/- SEM. Statistical analysis was performed using a one-way ANOVA with Tukeys multiple comparison test. p values = * < 0.05, ** < 0.01, *** < 0.001, **** < 0.001.

3.2.6. Investigate antigen specific T cells in the lung and spleen after vaccination

The immunogenicity of the vaccine was assessed through an *ex vivo* T cell stimulation experiment, where 2/3 of the lung cells and all of the spleen cells were plated and incubated for 24 hours. Once again, the CFCB was subtracted from the unstimulated values to take out any background and non-specific cytokines. Unfortunately, due to a technical error we weren't able to confidently analyze IL-2 production, thus it was taken out of the data set. While there were no statistical differences, all the groups except for

UNVAC had some *M.tb*-specific hCD4+ T cells producing IFNγ, TNFα and IL-17 in their lungs, with the highest cell percentages seen in the TNFα group *(Figure 25A-C*). In most cases though, the values for the HIV alone group were similar to vaccinated groups, thus indicating these were not vaccine specific responses. For hCD8+ T cells, all the groups produced IFNγ and TNFα, with very little production of IL-17 *(Figure 25D-F).* The flow gating strategy for the T cell stimulation can be found in *Supplementary Figure 12*, and values for unstimulated and stimulated conditions prior to adjustment can be seen in *Supplementary Figures 13 and 14.*

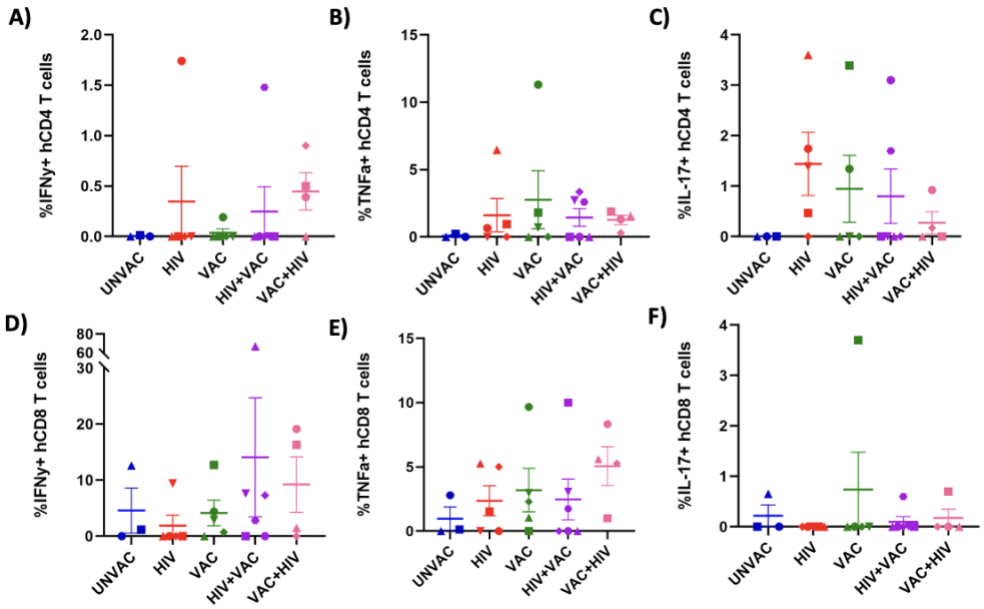

Figure 25. **Frequency of CFCB minus unstimulated Ag-specific T cell cytokine production in the lung at 8 weeks post-HIV infection.** Percentage of hCD4+ T cells producing (A) IFNγ (B) TNFα (C) IL-17. Percentage of hCD8+ T cells producing (D) IFNγ (E) TNFα (F) IL-17. Data is represented as +/- SEM. Statistical analysis was performed using a one-way ANOVA with Tukeys multiple comparison test. p values = * < 0.05, ** < 0.01, *** < 0.001, **** < 0.001.

For the spleen, the vaccinated groups had the greatest trend of hCD4+ and hCD8+ producing IFNγ and TNFα, with the VAC+HIV group have the highest average trend. The

VAC group had the greatest trend of hCD4+ IL-17 and once again, there was not much production from hCD8+ IL-17 *(Figure 26).*

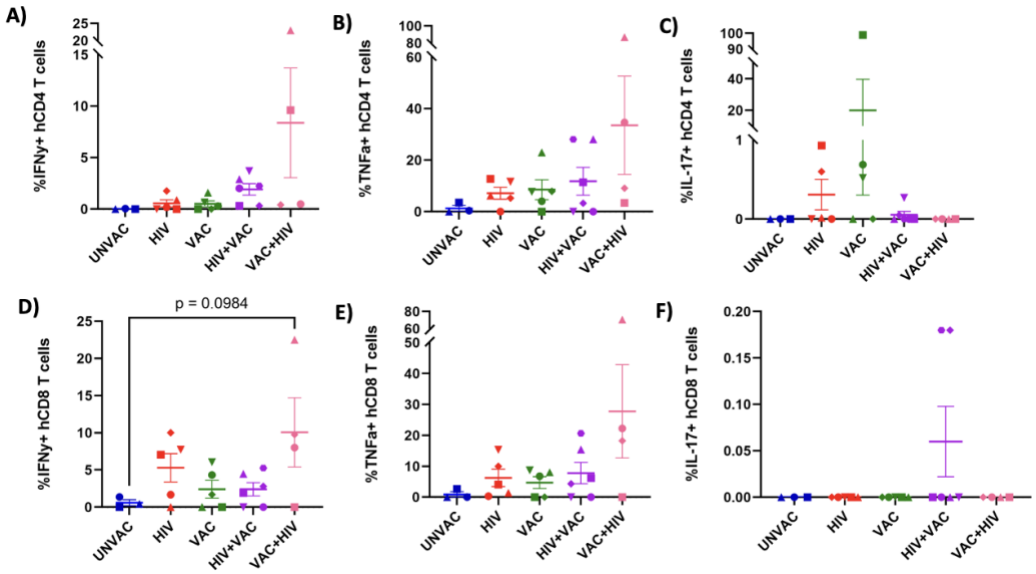

Figure 26. **Frequency of CFCB minus unstimulated Ag-specific T cell cytokine production in the spleen at 8 weeks post-HIV infection.** Percentage of hCD4+ T cells producing (A) IFNγ (B) TNFα (C) IL-17. Percentage of hCD8+ T cells producing (D) IFNγ (E) TNFα (F) IL-17. Data is represented as +/- SEM. Statistical analysis was performed using a one-way ANOVA with Tukeys multiple comparison test. p values = * < 0.05, ** < 0.01, *** < 0.001, **** < 0.001.

Aim 2.2 - Examine the Tri:ChAd68 vaccine's protective efficacy and effect on disease progression of immunized HIV-infected humanized mice when subsequently challenged with TB infection

Experiment 1

This experiment consisted of four different groups; each being challenged with *M.tb.* At Day 0, the HIV+TB group (initially 4 hu-DRAG mice) and the HIV+VAC+TB group (4 hu-DRAG mice) received $1x10^5$ IU of HIV via the IP route. Four weeks after that the VAC+TB group (initially 4 hu-DRAG mice) and the HIV+VAC+TB group were intranasally immunized with $1x10^7$ PFU Tri:ChAd68 vaccine, and the TB only group

(initially 4 hu-DRAG mice) was not infected with HIV nor immunized to serve as a negative control. Four weeks later, all the mice were brought up to CL3 and challenged intranasally with $1x10^3$ CFU of H37RV *M.tb* lot #18 and four weeks after that for a total of 12 weeks since the start of the experiment, the mice reached endpoint and were sacrificed. The experimental outline and legend to indicate individual mice are shown in *Figure 27.* The reconstitution and initial information about each mouse are shown in *Supplementary Table 8.*

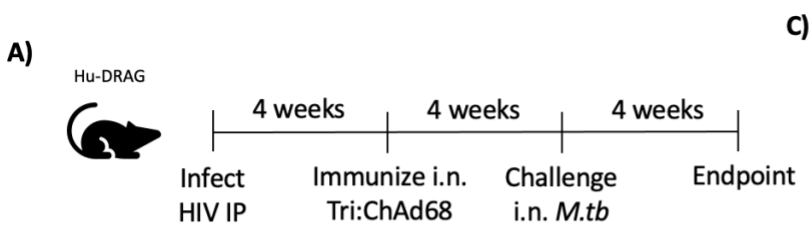

B)

Group	+/- HIV	+/- Vaccine	+/- *M. tb*	Starting N	Final N
TB Only	-	-	H37Rv	4	3
HIV+TB	JRCSF	-	H37Rv	4	3
VAC+TB	-	Tri:ChAd68	H37Rv	4	2
HIV+VAC +TB	JRCSF	Tri:ChAd68	H37Rv	4	4

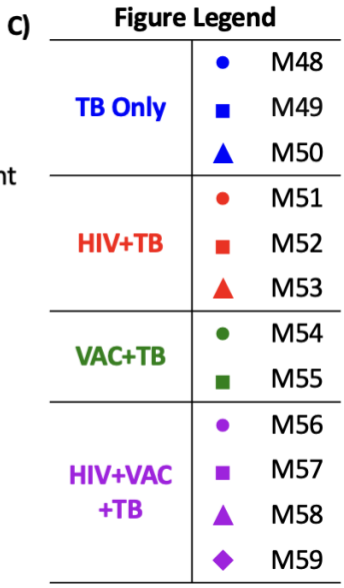

Figure 27. **Experiment 1 for Aim 2.1.** (A) Experimental outline (B) Group information (C) Figure Legend.

3.2.1. Confirmation of primary HIV-1 infection prior to vaccination and throughout the experiment.

Once again, to ensure the mice were successfully infected with HIV prior to immunization and subsequent *M.tb* challenge, at 3 weeks post-infection the viral load in their plasma was assessed through RT-qPCR. Additionally, to monitor their viral load after

vaccination and *M.tb* infection, the mice were also bled at 7-, 10- and 12-weeks post-infection. In *Figure 28,* we can see that both groups decreased their viral load after initial assessment at 3 weeks, then increased slightly after 10 weeks (Individual RNA values in *Supplementary Table 7).*

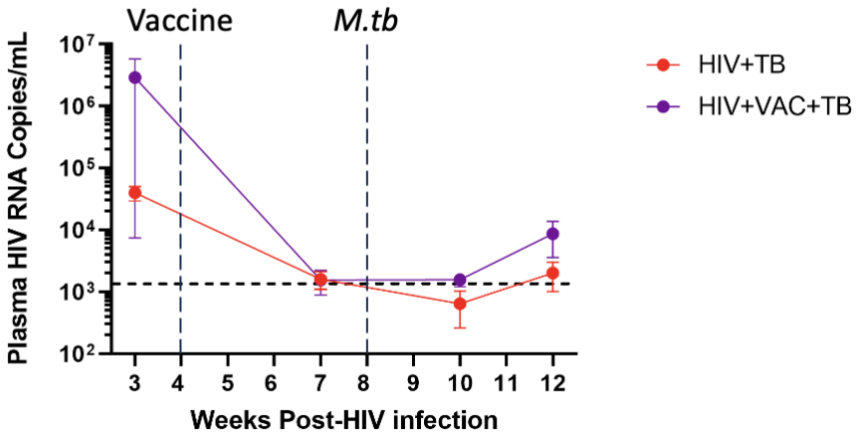

Figure 28. **HIV viral load in the plasma of HIV-infected mice.** Plasma HIV RNA copies/mL for the HIV only (n=3) and HIV+VAC (n=4) mice at 3-, 7-, 10-, and 12- weeks post-HIV infection. Horizontal dotted line indicates threshold level of ~1,500 RNA copies/mL, vertical dashed line indicated that when the vaccine or *M.tb* was administered. Data represented as +/- SEM.

At 12 weeks post HIV-infection, the mice were sacrificed, and their blood was collected to assess for T cell levels, as well as their lung and spleen for CFU and histological analysis. Unfortunately, when their blood was collected, one mouse in the HIV+VAC+TB group and one mouse in the VAC+TB group had clotted blood, causing the T cell levels of those two mice to be zero or close to zero, thus it was excluded from the blood data set. Another VAC mouse was also excluded from the data for reasons explained in the next paragraph, therefore there was only one VAC mouse left to compare T cell levels in the blood with. In *Figure 29A & B,* while there are no obvious trends, we can see that there is

a slightly greater average of hCD4+ T cells in the TB only mice compared to the HIV groups, which may correlate to their low viral load shown in *Figure 28.* Moreover, the two HIV groups do have a slightly higher trend of the percentage of hCD8+ T cells; however, their averaged number of hCD8 cells is lower than the non-HIV groups *(Figure 29C, D).*

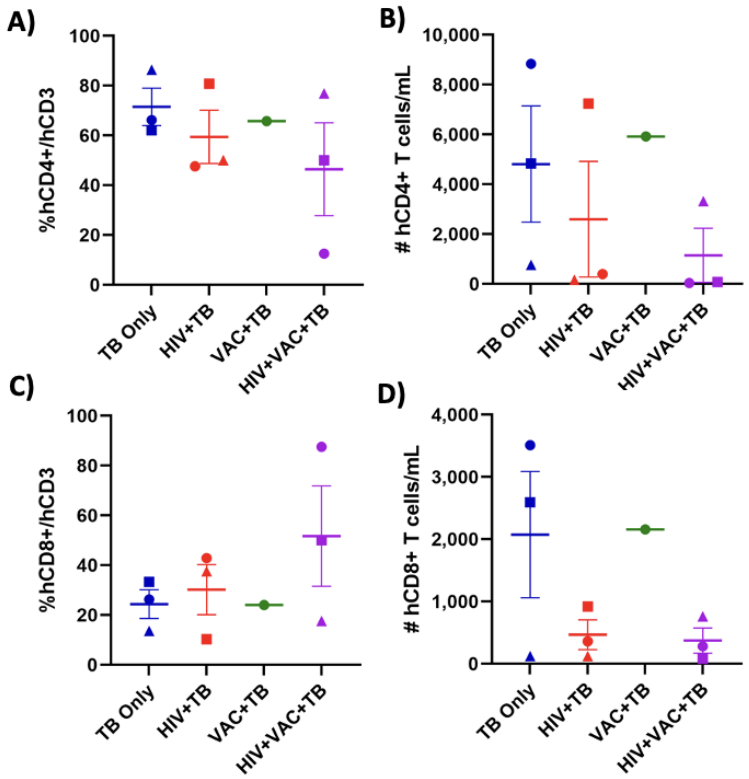

Figure 29. **Flow cytometry of CD4+ and CD8+ T cells in the peripheral blood of all groups 12 weeks post-HIV infection.** (A) Percentage and (B) Absolute count of hCD4+ T cells. (C) Percentage and (D) Absolute count of hCD8+ T cells in the blood at endpoint. Data is represented as +/- SEM. Statistical analysis was performed using a one-way ANOVA with Tukeys multiple comparison test. p values = * < 0.05, ** < 0.01, *** < 0.001, **** < 0.001.

3.2.2. Determine mycobacterial load in the lungs and spleen and amount of granulomatous tissue in the lungs

When the mice were challenged with *M.tb*, it was noted that at the time of intranasal administration there were technical issues in two mice, one from the VAC+TB group and

one from the TB group. It was unlikely the dose of the *M.tb* got into their respiratory tract as it correlated with extremely low/absent CFU for these two mice. Thus, these mice were excluded from the final data set, making their final numbers n=2 for VAC+TB and n=3 for the TB group.

For CFU analysis, the right lobe of the lung and ½ of the spleen was homogenized, diluted and plated on agar plates before being counted. While there was no significance difference in the lung and spleen CFU, likely due to the low n numbers, the average bacterial load in the lung of the mice in the vaccinated groups was slightly lower than the unvaccinated groups, while the spleen didn't display any trends *(Figure 30)*. The two vaccinated groups, VAC+TB and HIV+VAC+TB, had a lung CFU $\log_{10}$ of 7.4 and 7.6 respectively, while the two unvaccinated groups, TB only and HIV+TB, had a lung CFU $\log_{10}$ of 8.7 and 8.2 respectively. There was an averaged 1.26 $\log_{10}$ difference between the VAC+TB and the TB group, and an averaged 0.61 $\log_{10}$ difference between the HIV+VAC+TB group and the HIV+TB group in the lung. CFU counts are in *Supplementary Table 10.*

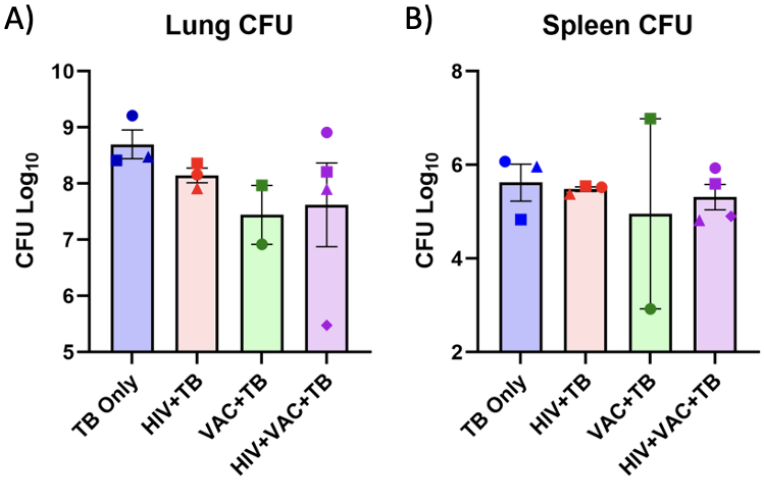

Figure 30. **Mycobacterial burden in tissues of mice 4 weeks post-*M.tb* infection.** Log_{10} CFU of (A) Lung and (B) Spleen. Data expressed as +/- SEM. Statistical analysis was performed using a one-way ANOVA with Tukeys multiple comparison test. p values = * < 0.05, ** < 0.01, *** < 0.001, **** < 0.001.

For pathological analysis, the left lobe of the lung and the other ½ of the spleen was fixed and sent for H&E staining to assess granuloma structures. There were no clear consistent tissue patterns between each mouse in the same group, thus *Figure 31A* shows the mouse' lung that displayed the closest average amount of granulomas, except for the VAC+TB group which only had two mice. Their histopathology was quantified to represent a percentage of granulomatous tissue within the lung section, and as we can see in *Figure 31B*, there is a considerable amount of spread between mice in each group. Nevertheless, there is a decreased average trend in granulomatous lesions in the VAC+TB and HIV+VAC+TB group than the unvaccinated groups and combined with the CFU data, this suggests potential protection of the TB vaccine in the context of HIV infection. Each individual mouse lung histology can be found in *Supplementary Figure 15.*

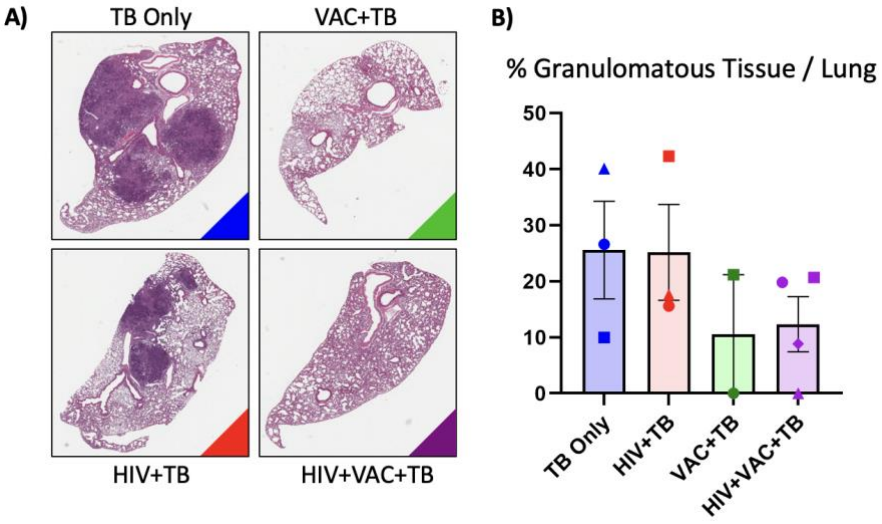

Figure 31. **Lung histopathology 4 weeks after *M.tb* infection.** (A) H&E staining of the middle lung segment of individual mice in each group. (B) Percentage of granulomatous

tissue in the whole lung of each mouse. TB only (n=3), HIV+TB (n=3), VAC+TB (n=2), HIV+VAC+TB (n=4). Data is represented as +/- SEM. Statistical analysis was performed using a one-way ANOVA with Tukeys multiple comparison test. p values = * < 0.05, ** < 0.01, *** < 0.001, **** < 0.001.

Experiment 2

This experiment also aimed to investigate the protection that the trivalent vaccine conferred, as well as increasing final n numbers. In contrast to the previous experiment, this one uses hu-NRG mice instead of hu-DRAG mice. Each group was also vaccinated, some with the trivalent vaccine and some with the empty ad-vectored vaccine to determine the degree of protection that the three TB antigens in the trivalent vaccine delivered. On Day 0, the HIV+EA+TB group (4 hu-NRG mice) and the HIV+VAC+TB group (4 hu-NRG mice) received $1x10^5$ IU of HIV via the IP route. Four weeks after that, two groups were intranasally immunized with $1x10^7$ PFU of the empty adenoviral (EA) vectored vaccine, the first group being EA+TB (4 hu-NRG mice) and the second group being HIV+EA+TB. The other two groups were vaccinated with $1x10^7$ PFU of the Tri:ChAd68 vaccine, with one of the groups being the VAC+TB group (4 hu-NRG) and the HIV+VAC+TB group. Four weeks later all the mice were brought up to CL3 and were intranasally challenged with $1x10^3$ CFU H37Rv *M.tb* lot #19, and four weeks after that for a total of 12 weeks the mice were sacrificed. The experimental outline and legend to indicate individual mice are shown in *Figure 32*. The reconstitution and initial information about each mouse are shown in *Supplementary Table 11*.

A)

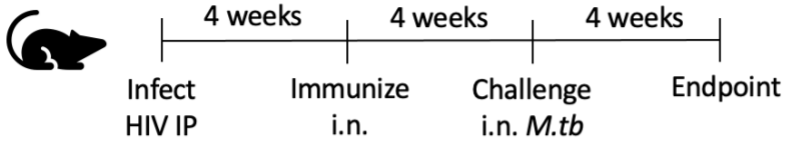

B)

Group	+/- HIV	+/- Vaccine	+/- *M. tb*	Starting N	Final N
EA+TB	-	Empty Ad	H37Rv	4	4
VAC+TB	-	Tri:ChAd68	H37Rv	4	4
HIV+EA +TB	JRCSF	Empty Ad	H37Rv	4	4
HIV+VAC +TB	JRCSF	Tri:ChAd68	H37Rv	4	4

C)

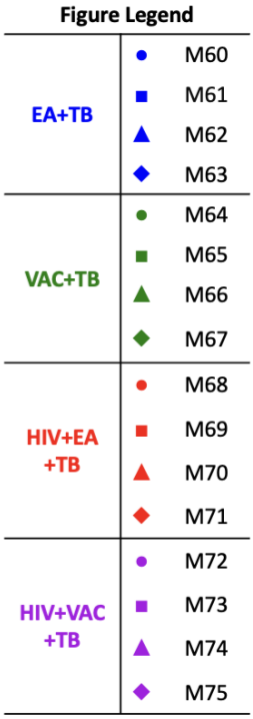

Figure 32. **Experiment 2 for Aim 2.2.** (A) Experimental outline (B) Group information (C) Figure Legend.

3.2.3. Confirmation of primary HIV-1 infection prior to vaccination and throughout the experiment.

At 3 weeks post-HIV infection, the mice were bled and their viral load was assessed through RT-qPCR in order to confirm successful HIV infection before immunization the following week. The mice were also bled at 6- and 12- weeks post-infection to monitor any changes in their viral load *(Figure 33).* As a negative control, the mice in the two non-HIV infected groups were bled and analyzed as well to ensure that they did not have any HIV and that the RT-qPCR readout was accurate. Both HIV groups' average viral load decreased slightly after 3 weeks to just below the detection limit, then increased slightly after 6 weeks to above the detection limit again. The two non-HIV infected groups

remained below the threshold level during the entire experiment. Individual RNA values are in *Supplementary Table 12.*

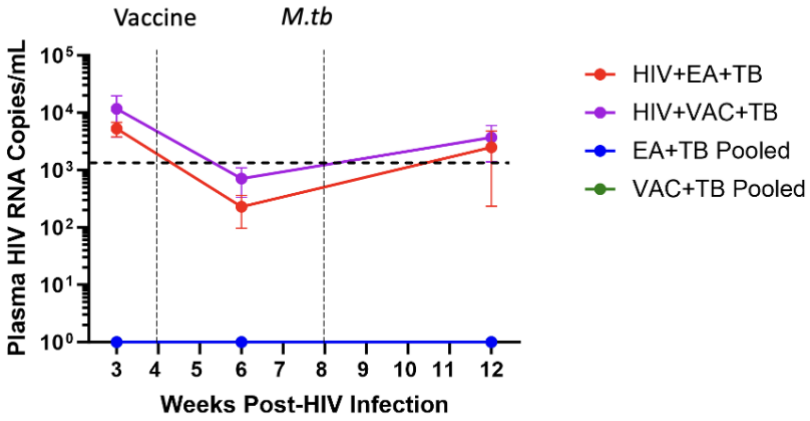

Figure 33. **HIV viral load in the plasma of HIV-infected mice.** Plasma HIV RNA copies/mL for the HIV+EA+TB (n=4) and HIV+VAC+TB (n=4) mice at 3-, 6-, and 12-weeks post-HIV infection. Horizontal dotted line indicates threshold level of ~1,500 RNA copies/mL, vertical dashed line indicated that when the vaccine or *M.tb* was administered. Data represented as +/- SEM.

In *Figure 34A,* the percentage of hCD4+ T cells in the peripheral blood at the time of endpoint was significantly reduced in the two HIV groups compared to the other groups, which is what we expect and helps confirm successful HIV infection. This is contrasted in *Figure 34C,* where the percentage of hCD8+ T cells is higher in the two HIV groups than the non-HIV groups, with it being significantly higher in the HIV+EA group than the EA+TB group. The absolute number of both hCD4 and hCD8 follow the same trend, with the two HIV groups having a lower number than the other two groups *(Figure 34B, D).*

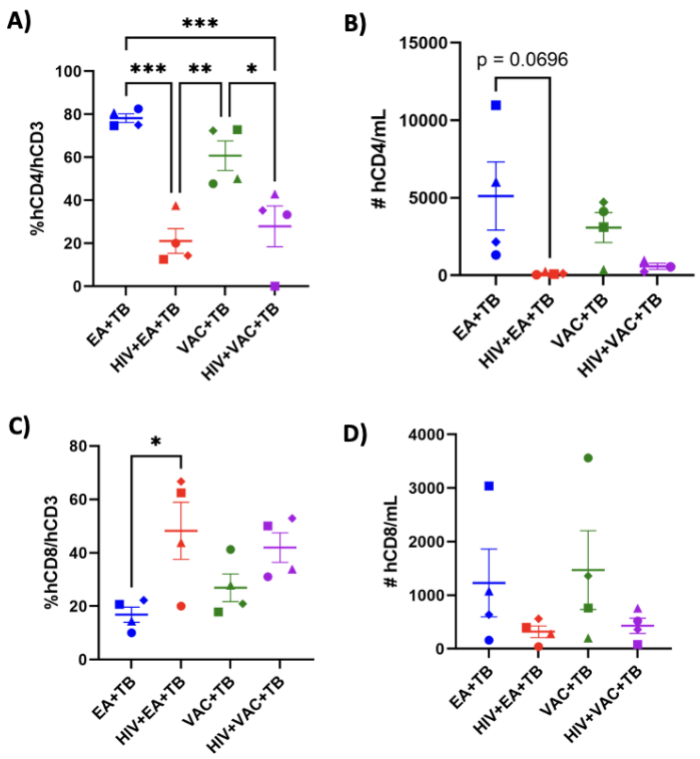

Figure 34. **CD4+ and CD8+ T cells in the peripheral blood of all groups 12 weeks post-HIV infection.** (A) Percentage and (B) Absolute count of hCD4+ T cells. (C) Percentage and (D) Absolute count of hCD8+ T cells in the blood at endpoint. Data is represented as +/- SEM. Statistical analysis was performed using a one-way ANOVA with Tukeys multiple comparison test. p values = * < 0.05, ** < 0.01, *** < 0.001, **** < 0.001.

Moreover, *Figure 35* shows the starting and final blood T cell levels, and while they all start at about the same percentage, the HIV+EA+TB and HIV+VAC+TB groups' hCD4+ T cells decreases while their hCD8+ T cells increases, compared to EA+TB and VAC+TB, where their hCD4 increases and their hCD8 decreases, which is consistent to what we saw in the figure above.

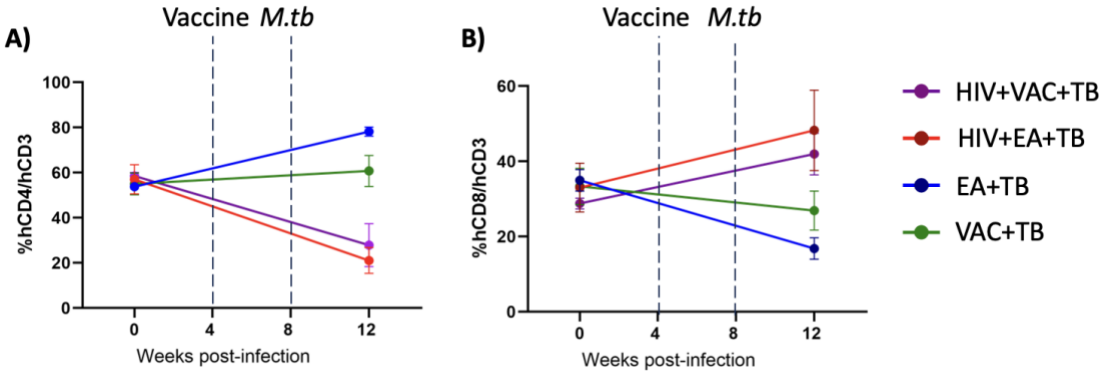

Figure 35. **Percentage of CD4+ and CD8+ T cells in the peripheral blood throughout the experiment.** Percentage of (A) hCD4+ (B) hCD8+ T cells at 0- and 12- weeks post-HIV infection. Vertical dashed lines represent vaccination at 4 weeks and *M.tb* challenge at 8 weeks post-infection. All groups have n=4 mice. Data is represented as +/- SEM.

3.2.4. Determine mycobacterial load in the lungs and spleen and amount of granulomatous tissue in the lungs

Unfortunately, for the *M.tb* load in the lung and spleen, there wasn't a clear or significant difference between the groups, perhaps because every group still conferred a variable degree of protection against TB. In *Figure 36* it appears that the VAC+TB group had the lowest average CFU in both the lung and spleen compared to the other groups, which all had very similar CFU to one another. The black symbols in the graphs denotes the mice that had very few countable colonies on the lowest dilution, thus making the actual CFU not completely accurate. These homogenates will be re-plated in the future to ensure we have accurate numbers. Since there is such a large spread in each of the groups, we cannot make any conclusions on if the trivalent vaccine provides greater protection against TB than the empty-ad vector vaccine. Individual CFU counts can be found in *Supplementary Table 13.*

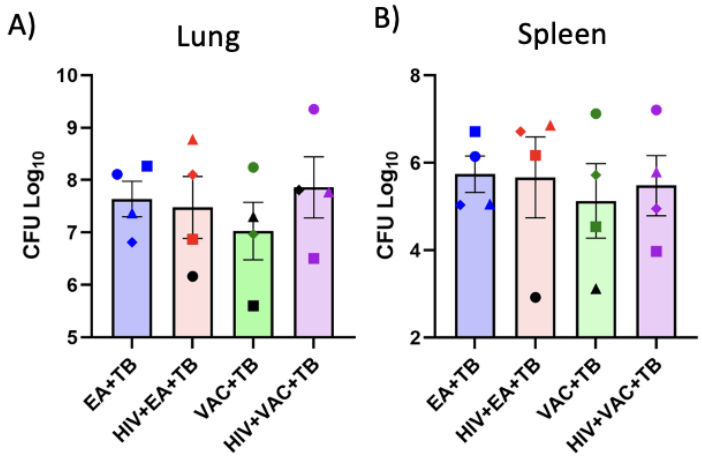

Figure 36. **Mycobacterial burden in tissues of mice 4 weeks post-*M.tb* infection.** Log_{10} CFU of (A) Lung and (B) Spleen for all groups. Data expressed as +/- SEM. Statistical analysis was performed using a one-way ANOVA with Tukeys multiple comparison test. p values = * < 0.05, ** < 0.01, *** < 0.001, **** < 0.001.

To analyze the histopathology of the tissues, the left lobe of the lung and ½ of the spleen were fixed and stained with H&E to assess granuloma structures. Once again, the mice displayed varying amount of lung granulomas within each group, causing there to be no significant visible difference *(Figure 37A).* This was then quantified to represent a percentage of granulomatous tissue in the whole lung, and in *Figure 37B* we can see that while there is some spread among the mice in each group, the EA+TB group had the highest averaged percentage of granulomatous tissue with 3 out of 4 mice having granulomas. In the VAC group only 1 of the 4 mice had granulomas in their lungs, and in the HIV group 2 out of 4 mice had granulomas. While in the HIV+VAC+TB group 2 mice also had granulomas, the percentage was lower than the others thus they had the lowest averaged percentage of granulomatous tissues (*Figure 37B).* Each individual mouse lung histology can be found in *Supplementary Figure 16.*

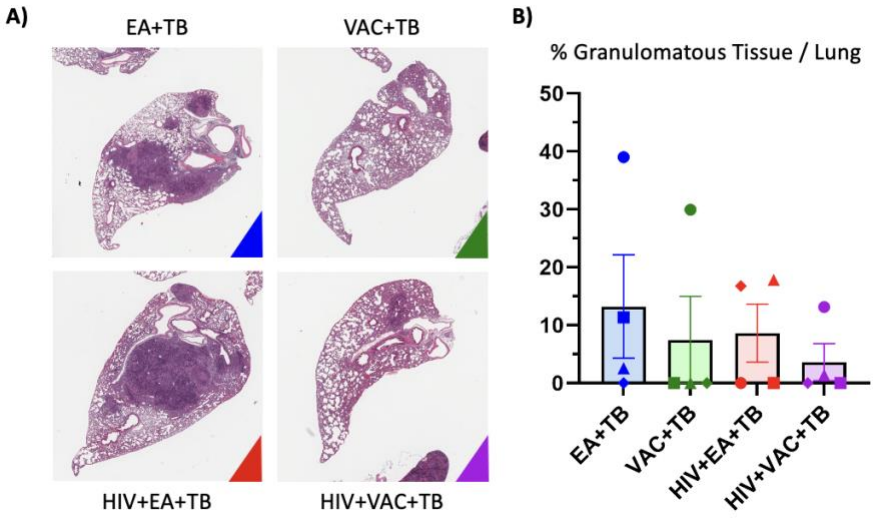

Figure 37. **Lung histopathology 4 weeks after *M.tb* infection.** (A) H&E staining of the middle lung segment of individual mice in each group. (B) Percentage of granulomatous tissue in the whole lung of each mouse. EA+TB (n=4), VAC+TB (n=4), HIV+EA+TB (n=4), HIV+VAC+TB (n=4). Data is represented as +/- SEM. Statistical analysis was performed using a one-way ANOVA with Tukeys multiple comparison test. p values = * < 0.05, ** < 0.01, *** < 0.001, **** < 0.001.

3.2.5. Investigate the T cells and macrophages in the lung

Next, the T cells and macrophages in the auxiliary lobe of the lung were measured to determine the different immune cells expressions between each of the groups. In *Figure 38A*, the EA+TB group had the highest percentage of hCD3+ T cells while HIV+EA had the lowest. Consistent with what was seen in the blood, *Figure 38B* shows that the two HIV groups displayed lower percentage of hCD4+ T cells than the other two groups, at about the same level. Interestingly in *Figure 38C*, the HIV+VAC+TB group had the highest average trend of percentage of hCD8+ T cells while the EA+TB group had the lowest trend. It is important to note that since only the auxiliary lobe was used, there are not as many cells as would be expected in the whole lung, thus the data is not as strong. Flow count of

the CD3+, CD4+ and CD8+ T cells for each group can be found in *Supplementary Figure 16*.

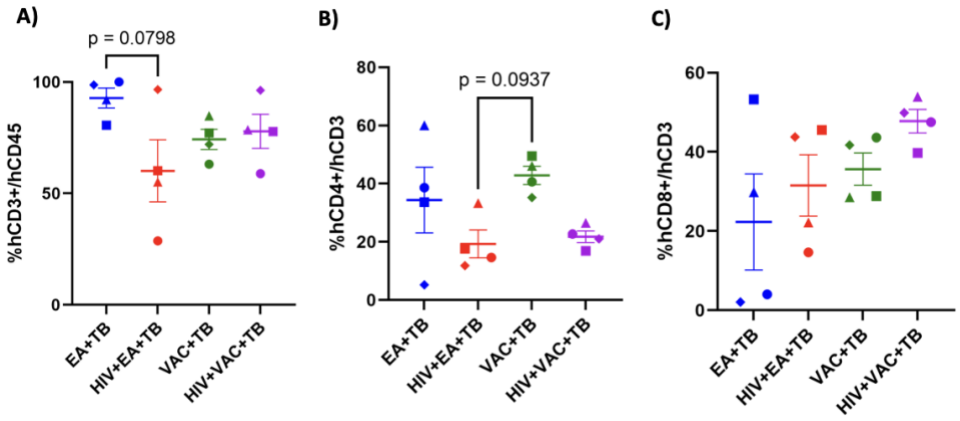

Figure 38. **Percentage and number of T cells in the lung at 12 weeks post-HIV infection.** Percentage of (A) hCD3+ (B) hCD4+ (C) hCD8+ T cells in the auxiliary lobes of the lungs at endpoint. Data expressed as +/- SEM. Statistical analysis was performed using a one-way ANOVA with Tukeys multiple comparison test. p values = * < 0.05, ** < 0.01, *** < 0.001, **** < 0.001.

For the macrophages in the auxiliary lobes, 4 weeks after TB infection we observed the total macrophages, interstitial and alveolar macrophages. In *Figure 39A*, the VAC+TB group have the highest average trend of macrophages in the lung. In *Figure 39B*, while there is a small spread between the mice there the VAC+TB group also have the greatest average trend of IMØs, with the EA+TB group having the lowest percentage. For AMØs shown in *Figure 39C*, we have a different trend than the other two sub-figures. The HIV+EA group have the highest overall average percentage of AMØs, being significantly higher than the VAC+TB group, which has the lowest percentage. The HIV+VAC+TB group has slightly higher percentage than the VAC+TB group, but lower than the average of the EA+TB group. Once again, the data is based upon very low cell numbers and should

be interpreted as such. Flow count of the total macrophage, IMØ and AMØ cells for each group can be found in *Supplementary Figure 17*.

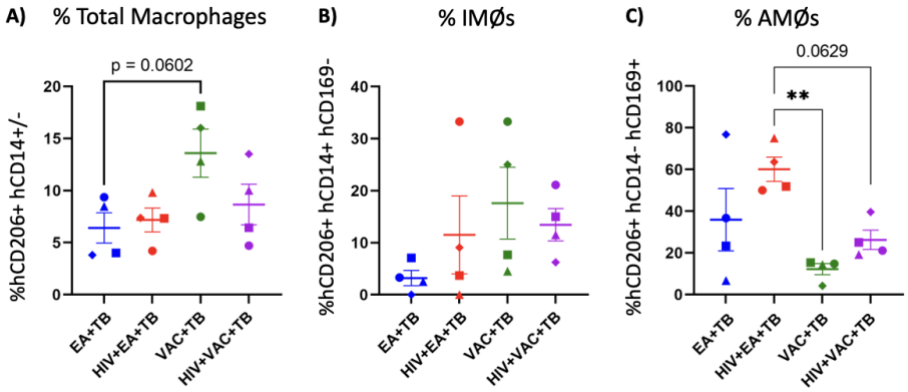

Figure 39. **Percentage and number of macrophage cells in the lung at 12 weeks post-HIV infection.** Percentage of (A) total macrophages (B) IMØs (C) AMØs in the auxiliary lobes of the lungs at endpoint. Data expressed as +/- SEM. Statistical analysis was performed using a one-way ANOVA with Tukeys multiple comparison test. p values = * < 0.05, ** < 0.01, *** < 0.001, **** < 0.001.

CHAPTER 3.3. AIM 3. ESTABLISH AND OPTIMIZE AN EFFICIENT METHOD FOR DELIVERING ART TO HUMANIZED MICE TO USE FOR FUTURE EXPERIMENTS

For this experiment, all the mice were received $1x10^5$ IU of HIV via the IP route on Day 0. Four weeks after that, the ART group, consisting of 3 hu-NRG mice, were given the two ART medications while the control group, also consisting of 3 hu-NRG mice, were not given any ART but the same volume of DMSO to serve as a negative control. Four weeks after the initiation of ART the medication was ceased to look at viral rebound, and four weeks after that the mice reached experimental endpoint.

The combination of ART medications we decided to use are widely used in literature for both humans and humanized mice and consist of two non-nucleoside reverse

transcriptase inhibitor (NNRTIs), tenofovir disoproxil fumarate (TDF) and emtricitabine (FTC) and one integrase inhibitor, raltegravir (RAL). The experimental outline and legend to indicate individual mice are shown in *Figure 40*. The reconstitution and initial information about each mouse are shown in *Supplementary Table 14.*

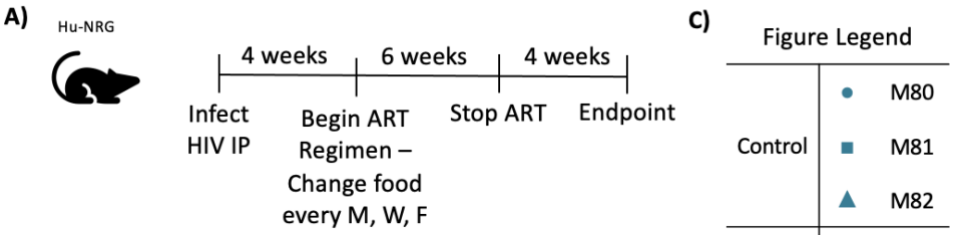

B)

Group	+/- HIV	+/- ART	Starting and Final N
CTRL	JRCSF	DSMO	3
ART	JRCSF	FTC+TDF+RAL	3

Figure 40. **Experiment for Aim 3.** (A) Experimental outline (B) Initial group information (C) Figure Legend. M, Monday; W, Wednesday; F, Friday; FTC, Emtricitabine; TDF, Tenofovir Disoproxil Fumarate; RAL, Raltegravir.

Aim 3.1. Establish a regimen to process and safely administer ART in DietGel Boost

At 3 weeks post-HIV infection, the mice's pellet food was switched out for DietGel Boost. To allow time for the mice to adjust to their new food, we gave the mice gel without any ART or DMSO. On Day 7, we thawed tubes of the solubilized crushed up ART pills and mixed it with the ART groups' gel and added the same volume of DMSO to the Control group's gel. Their food was discarded and replaced with the medications every Monday, Wednesday and Friday. The leftover gel in the cup, new gel given and the new gel with added water (mixed with the ART and/or DMSO) was weighed at every change. The leftover gel was subtracted from the new gel (with and without added liquid) from the

previous week to determine how much the mice consumed. The ART or DMSO was given for 6 weeks (up to 10 weeks post-HIV infection) and then only mixed with water for another 4 weeks (up to 14 weeks post-HIV infection) before reaching experimental endpoint.

In *Figure 41*, we can see that the mice consumed the gel at a constant rate regardless of the medication or DMSO added. The high peaks denote their consumption over 3 days (from Friday to Monday), as the lower peaks show their consumption over 2 days (from Monday to Wednesday and from Wednesday to Friday). In the ART group, each mouse ate an average of 3.1-3.7g of food a day, and the Control group each mouse ate an average of 2.8-3.4g of food a day.

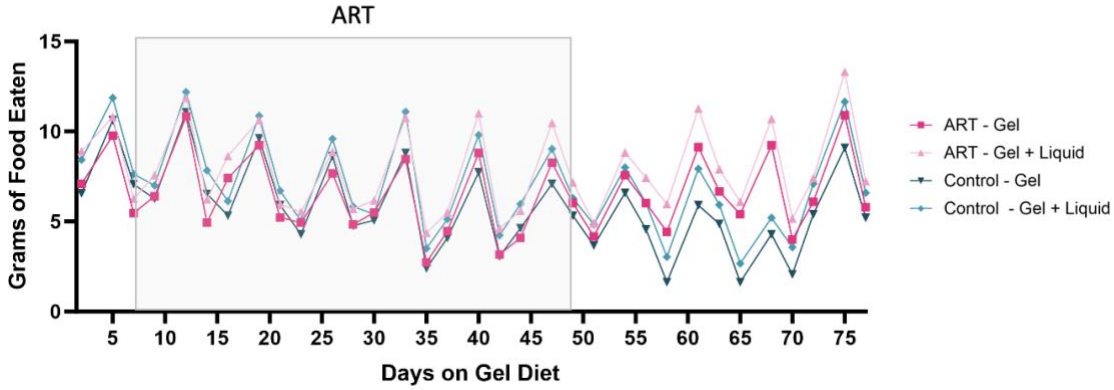

Figure 41. **Grams of DietGel Boost eaten by the mice throughout the experiment.** Light grey box denotes when the ART or DMSO was mixed with the gel. The leftover gel was subtracted from the originally added gel, with and without the added liquid.

Overall, each mouse's body condition and activity appeared normal; however, one mouse from the Control group started losing weight after Day 42 and had to be euthanized. The rest of the mice continued to increase their weight from the starting weight, as the DietGel boost contains a high amount of fat which likely contributed to the weight gain *(Figure 42).* However, the other two mice in the control group appear to have lost weight

after Day 56, slowly getting back to their original weight.

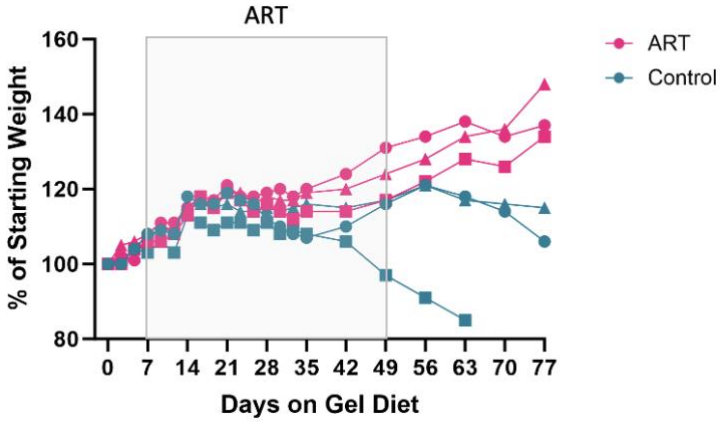

Figure 42. **Body weight changes as a percentage of starting body weight while on gel diet.** Each mouse was weighed every Monday, Wednesday, and Friday until Day 35, where they were weighed weekly. Light grey box denotes when the ART or DMSO was mixed with the gel.

Aim 3.2. Investigate the efficacy of the ART regimen

To determine if the ART will restore hCD4+ T cell levels in the blood, the T cell levels were measured before, during and after ART administration. *Figure 43A* shows the percentage of CD4+ T from the start of the experiment and we can see that while both groups start at the same level, the control group steadily decreases as the weeks go on. On the other hand, the ART groups' CD4+ T cells decreases slightly after HIV-infection, then remain at a consistent level while on the ART medications from weeks 4 to 10 and start to decrease again once taken off the medication after week 10. In *Figure 43B,* both groups steadily increase their percentage of CD8+ T cells from the start; however, the ART group had slightly more variation between the weeks.

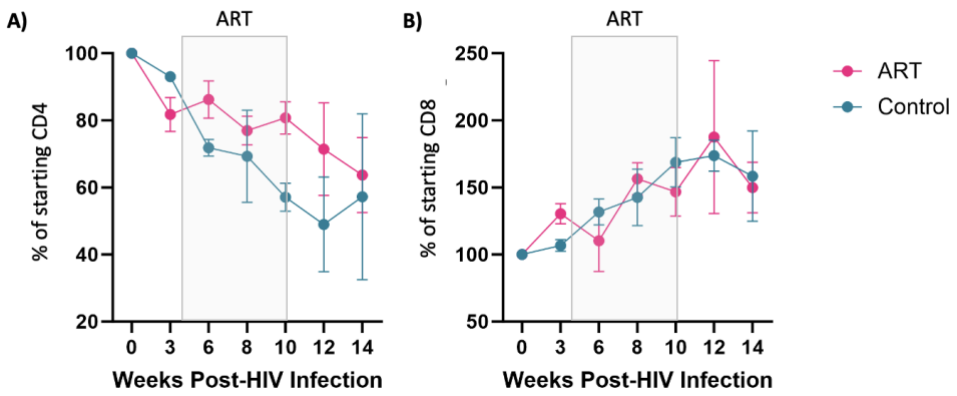

Figure 43. **Percentage of CD4+ and CD8+ T cells in their peripheral blood from the start of the experiment.** (A) CD4+ T cells (B) CD8+ T cells. ART (n=3) and Control (n=3). Light grey box denotes when the ART was mixed with the gel. Data expressed as +/- SEM. Statistical analysis was performed using an unpaired parametric T test. p values = * < 0.05, ** < 0.01, *** < 0.001, **** < 0.001.

To determine if the ART is able to decrease the mice's viral load to below the detection limit, their plasma was extracted and their viral load was assessed via RT-qPCR. While both groups started at similar HIV RNA levels, the ART group decreased their viral load to undetectable levels 2, 4 and 6 weeks on ART treatment *(Figure 44*). Once taken off the ART medications, we can see that after week 10 the ART groups' viral load increases above the limit of detection. Meanwhile, the Control group had consistently high HIV RNA plasma copies throughout the experiment, thus we can conclude that the ART medications were able to decrease their viral load, and show viral rebound. Individual RNA values are in *Supplementary Table 15.*

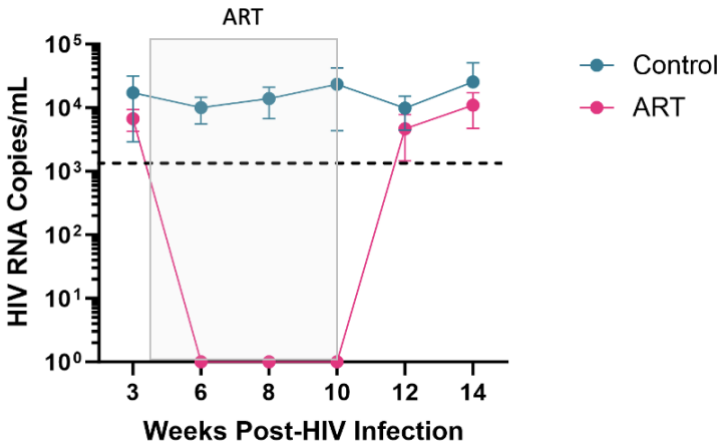

Figure 44. **HIV viral load in the plasma of the mice.** Plasma HIV RNA Copies/mL for the ART (n=3) and Control – DMSO (n=3) mice at 3-, 6-, 8-, 10-, and 12-weeks post-HIV infection. Light grey box denotes when the ART or DMSO was mixed with the gel. Horizontal dotted line indicated threshold level of ~1,500 RNA copies/mL. Data expressed as +/- SEM. Statistical analysis was performed using an unpaired parametric T test. p values = * < 0.05, ** < 0.01, *** < 0.001, **** < 0.001.

CHAPTER 4. DISCUSSION AND CONCLUSION

Chapter 4.1. Discussion

HIV and TB infections are among the top 10 causes of death in the world, as each potentially life-threatening disease is endemic in overlapping regions, thus increasing the risk of co-infection[161]. The only available TB vaccine, BCG, has been used for many decades to combat and prevent TB; however, it only provides variable protection against pulmonary TB in adults, thus not contributing to reducing the spread of the disease[162]. For one of the most high-risk populations of developing active TB being people living with HIV (PLWH), the only vaccine licensed for use is not recommended as the live attenuated nature of the BCG vaccine can cause adverse effects in PLWH[69]. While there are many TB vaccines being currently developed, very few are administered directly to the site of *M.tb*

exposure, the lung mucosa. Past evidence has suggested that respiratory mucosal (RM) vaccination confers greater immune protection by inducing tissue-resident polyfunctional T cells and pro-inflammatory cytokines in the lung[152]. Moreover, RM vaccination contributes to trained innate immunity (TII) by causing transcriptional and epigenetic changes in airway macrophages, allowing them to persist as memory macrophages and enhance host defense responses upon *M.tb* exposure[79].

The Xing Lab at McMaster University in Hamilton, Ontario has made significant advancements in the development of adenoviral-vectored vaccines for TB. A phase 1b clinical trial of their novel recombinant replication-deficient human serotype 5 adenoviral-vector vaccine (AdHu5) expressing Ag85A (AdHu5Ag85A) successfully exhibited both safety and strong immunogenicity when used as a primary vaccination and as a booster to combat *M.tb* infection[72]. Furthermore, the AdHuAg85A vaccine was administered in humanized mice and was able to enhance T cell responses and show protection against TB[152]. The next generation trivalent chimpanzee serotype 68 adenoviral-vectored TB vaccine (Tri:ChAd68) not only takes advantage of RM administration to induce robust protection, but also targets three main *M.tb* antigens: Ag85A, TB10.4 and RpfB. These antigens are active during the acute, chronic or dormant stages of infection, allowing the vaccine to target both actively replicating bacilli and dormant, non-replicating bacilli that reside in the majority of TB-infected individuals. In normal mouse models, this vaccine is able to have broadly protective immunity against the different stages of the *M.tb* life cycle, in contrast to monovalent (Ag85A) vaccines whose expression profile is significantly reduced following the acute stage of infection[163].

This next generation RM Tri:ChAd68 vaccine's ability to induce TII within the airway macrophages and the adaptive immunity through *M.tb*-specific CD4+ and CD8+ producing IFNγ, TNFα, IL-2 and IL-17 are important in regards to PLWH. While it is believed that HIV targets and depletes the CD4+ T cells that the vaccine would act on, we hypothesized that the vaccine would offer enough immune defensive responses from the available T cells to confer protection from TB infection in PLWH. HIV also targets macrophages which play crucial roles in the transmission, acute and chronic phases of HIV as well as serve as HIV reservoirs in tissues[164]. Through TII, we hypothesized that inducing memory in innate macrophages important for HIV progression would help re-program these cells to increase host defenses. Thus, the aim of this project was to determine the immunogenicity and protective efficacy of the respiratory mucosal administration of the Tri:ChAd68 vaccine in hu-mice with and without HIV.

4.1.1. Challenges With the Hu-Mouse Model

While our humanized mouse (hu-mouse) model offers translatability by recapitulating the human immune system and replicating disease pathology similar to humans, we are often limited in the production of abundantly high engrafted mice. Hu-mice can be more challenging to produce than conventional murine models as they require a supply of enriched HSCs available for whenever there is a new litter, as they must be engrafted 24-72 hours after birth. We are thus limited by the number and quality of the umbilical cord blood (UCB) samples we receive, their HLA-type, and the number and quality of living HSCs we extract from the blood. Additionally, due to the COVID-19 pandemic, the amount of UCB samples drastically decreased, causing us difficulties in

humanizing our mice.

Efficient engraftment of mice is also sample dependent and can be between 40-80% of mice, which we can only determine at 12 weeks of age. The number of mice chosen for experimental groups depends on the amount of well engrafted mice of the same strain, often resulting in 3-5 mice per group at the beginning of the experiment. Therefore, some experiments were done in NRG mice whereas others were done in DRAG. By the time our experiments start, the mice need to be over 16 weeks old to have sufficient T cell engraftment, and our experiments can run anywhere from 4 to 12 weeks long, causing the mice to be as old as 7-8 months by the end of the experiment. As they age, hu-mice are susceptible to developing Graft versus Host Disease (GvHD), often characterized by hair loss, weight loss, increased respiration, decreased body movement and often death, which can decrease our group numbers[165]. In our lab, we see roughly 10% of our hu-mice develop GvHD.

Due to the low numbers at the end of many of the experiments, this impedes statistical analysis and significant findings. In the context of HIV/TB co-infections, there are often two plausible clinical scenarios. An individual can be initially infected with HIV, subsequently followed by TB infection. Alternatively, they could establish a primary TB infection first, followed by HIV. This project focused on the first scenario in which we infected our humanized mice prior to TB infection. Previously published studies in the lab have been able to successfully infect our hu-mouse model with HIV and TB alone, as well as HIV/TB co-infection[143].

4.1.2. Immunogenicity of the Vaccine

In *Aim 1.1*., we investigated the immunogenicity of the Tri:ChAd68 vaccine by measuring their *M.tb*-specific T cell cytokine production in lung and spleen. We also sought out to determine if our next-generation hu-DRAGA2 mice were better at producing antigen specific T cells after vaccination than our non-transgenic hu-NRG mice. According to the literature, using hu-DRAGA2 mice that are HLA-matched for HLA-A2 and HLA-DR should produce more functionally mature CD4+ and CD8+ T cells and improved secretion of T cell-associated cytokines such as IFNγ , TNFα and IL-2 than the hu-NRG mice[166]. In *Figures 2-5*, we saw no consistent differences between the cytokine production levels between the two models. This could be due to the low n numbers used in this experiment, and with mice that display an abundance of variability similar to that seen in humans, low n numbers made it particularly difficult to make a conclusion.

Furthermore, our hu-mouse models have a relatively low human myeloid population, including highly efficient antigen presenting cells (APCs) such as dendritic cells (DCs). When performing *ex vivo* T cell stimulation as a readout, APCs are necessary for T cell stimulation as they process and present the *M.tb* antigens to the CD4+ and CD8+ T cells. However, the number of APCs may be insufficient or differ enough between individual mice, making it challenging to generate robust T cell responses and show significant differences between the two models. The use of artificial APCs may be a viable solution, as artificial APCs are able to expand sufficient numbers of T cells *in vitro* with improved responses to specific antigens[167]. Another solution could be the use of MHC tetramer technology, conjugating them to fluorochromes on our antibodies for flow

cytometry which will allow accurate enumeration and immunomagnetic sorting of antigen-specific T cells[168].

In *Aim 1.1.*, we were able see a trend of increased *M.tb*-specific T cells producing TNFα, IFNγ and IL-2 in the vaccinated mice compared to the unvaccinated mice, meaning the vaccine was able to provide some specific production of immune cells. While there was variability among the hu-mice, in *Figures 2-5* we can see that the vaccine produced more hCD4+ T cells responses in our mice than hCD8 responses. Although the unstimulated values essentially should have contained close to zero *M.tb*-specific cytokines, we can see in *Supplementary Figures 3-4,* cytokines were still produced. This may have been due to the CD28 and CD49d co-stimulatory molecules that are added to all the wells, including the unstimulatory wells. The need for these additional molecules was previously worked out in hu-mice vaccine studies in the Xing Lab[152]. Like mentioned previously, our hu-mouse model does not produce highly functional APCs, thus co-stimulatory molecules are needed to help with the stimulation of T cells to produce cytokines. These co-stimulatory molecules, however, may increase overall cytokine production in the unstimulated conditions.

In *Aim 2.1. Experiment 1.,* we investigated the immunogenicity of the vaccine in our HIV-infected humanized mice, and if their *M.tb*-specific T cell cytokine production was altered due to the preferential depletion of CD4+ T cells. This experiment initially aimed to also examine the specific immunogenicity conferred by the three TB antigens by including a control group that was immunized with an empty-adenoviral vaccine; however, by the end of the experiment many of the mice developed GvHD and had to be euthanized.

This caused low n numbers in all the groups and only one mouse left in the control (empty ad) group, thus this group was excluded from the data. While hu-DRAG should have lower rates of GvHD due to the HLA-matching of the HSCs to their transgenes, the mice that developed GvHD were all engrafted with either cord blood (CB) sample 38 or 48. While we don't have flow cytometry data on those samples' CD3+ T cell count, it is likely that these samples had high CD3 contamination leading to the onset of GvHD.

In *Figure 12*, we can see that as time progressed, the viral load of the HIV+VAC group appears to increase after vaccination. This potentially occurs due to the vaccine inducing CD4+ T cell responses, which in turn gives the virus more CD4+ T cells to infect and thus increase their HIV RNA in the plasma. This is similar to what was observed in the Step Study, where they tested a replication deficient Ad5 HIV vaccine and determined that increased risk of HIV infection was associated with vaccination[169]. It is important to note that this was the only time that we observed this trend, as in the other experiments the HIV+VAC groups' viral load followed a similar pattern to the HIV only group.

TII is important for protection as it is able to overcome *M.tb*-induced innate immune suppression and restricts bacterial growth. One characteristic of TII is the expression of HLA-DR on airway macrophages such as alveolar macrophages (AMØs) and interstitial macrophages (IMØs). Therefore, to determine the RM Tri:ChAd68's ability to induce TII, we looked at both the percentage and median fluorescent index (MFI) of HLA-DR on these macrophages. In *Figure 16*, it appeared that both the percentage and MFI of HLA-DR on the total lung macrophages and the IMØs was significantly greater in the VAC mice than the HIV and HIV+VAC mice, indicating that while the RM vaccination potentially elicited

long-lasting memory in airway macrophages, this may have been reduced when infected by HIV as macrophages are main targets of HIV. We do see that for total macrophages *(Figure 16A*), the HIV + VAC group had a higher percentage of HLA-DR expressing cells, thus even with prior HIV infection the vaccine appears to be able to induce some TII in lung macrophages which is promising. Interestingly, while the percentage of AMØs was lower in the HIV-infected groups than the VAC group (*Figure 15C*), their percentage and MFI of HLA-DR was similar amongst the groups (*Figure 16C & F).* It would be beneficial to investigate the transcriptomics of the macrophages to determine the differentially expressed genes in vaccinated compared to unvaccinated mice, as well as the reprogrammed metabolism of the airway macrophages to determine their glycolic capacity in mediating protection[170]. It would also be interesting to knock out CD4+ and CD8+ T cells to determine if the vaccine can confer protection in a human T-cell-dependent manner and to further examine the role that TII plays.

In *Aim 2.1. Experiment 1,* to investigate if the vaccine is able to induce immune responses specific to *M.tb*, *ex vivo* T cell stimulation was conducted to look at the immune cytokines produced within the mice's lungs and spleen. A study by Yao et al. 2017 stimulated their cells with live BCG (Pasteur strain) which was able to produce antigen-specific cytokine responses in the hu-mice bronchoalveolar lavage (BAL), lung and spleen cells[152]. While our previous investigations indicated CFCB induced higher responses, we included a BCG stimulated group in the spleen, but not the lung due to lower cell numbers. Thus, while the lung cells were still stimulated with CFCB, the spleen cells were stimulated with both CFCB and BCG to compare the cytokine production for the different stimulation

conditions. Just like in *Aim 1.1.*, there were no significant trends between the groups, as there were low n numbers and variability among the mice. While the percentage of cells producing cytokines was low overall, it appeared that in the lung hCD4+ T cells produced a greater percentage of TNFα, IL-2 and IL-17 while hCD8+ cells produced more IFNγ in the lungs *(Figure 17).* In addition, surprisingly the HIV+VAC group often produced the highest levels of cytokines, even above the VAC group.

For the spleen, when comparing the CFCB versus the BCG stimulated cells, it does appear that there was a slightly greater production of cytokines in the BCG stimulation, but this appearance could be skewed by one mouse producing a much greater amount than the other mice *(Figure 18-19).* In the stimulation experiment by Yao et al., they found that the majority of their BCG-stimulated spleen hCD4+ T cells were bifunctional for IFNγ and TNFα[152]. When looking at our BCG-stimulated spleen, the hCD4+ T cells in the VAC and HIV+VAC groups were able to produce IFNγ, TNFα, very low IL-2 and IL-17, making them potentially polyfunctional; however, we would need to further analyze it to be certain.

In *Aim 2.1. Experiment 2*, we once again looked at the immunogenicity of the vaccine but started with greater n numbers and included a new group (VAC+HIV) to look at *M.tb*-specific cell production when given the vaccine before HIV infection. It is important to note that the VAC+HIV group received HIV 4 weeks after the other HIV groups, thus at endpoint the VAC+HIV group had HIV for only 4 weeks while the other HIV groups were infected for 8 weeks. Therefore, we would expect to see differences in CD4+ and CD8+ T cells levels. In *Figure 22A & B*, we can see that the VAC+HIV group had almost 20% more hCD4+ T cells in the blood than the HIV+VAC group, and roughly

5,000 more hCD4+ T cells/mL. We can see the same trend in the hCD4+ T cell levels in the lung, with the VAC+HIV group having about 10-20% more hCD4+ T cells than both the HIV and HIV+VAC group, which is as expected *(Figure 24B).*

Moreover, in contrast to *Experiment 1*, this experiment uses hu-NRG mice solely due to the availability of well engrafted mice. However, we saw very similar trends in the expression of HLA-DR on their airway macrophages. In *Figure 23D, E,* the UNVAC and VAC group had the greatest percentage of HLA-DR on their total macrophages and IMØs, with it being significantly greater than the HIV and HIV+VAC group for their IMØs. The percentage of HLA-DR on AMØs followed a similar pattern, but with no significant differences *(Figure 23F).* For the MFI HLA-DR on total macrophages and IMØs, the UNVAC group was significantly greater than some of the HIV-infected groups, with AMØs not showing any large differences *(Figure 23G-I).* This is interesting as the UNVAC group was not given any vaccination, not even the empty ad-vectored vaccine. Like seen in Experiment *1 Figure 16,* the HIV-infected groups had the lowest percentage and MFI HLA-DR on their total macrophages and IMØs but had consistent levels of AMØs as the non-HIV infected groups. It is postulated that at this time point (8-9 weeks post-HIV infection) the HIV infected AMØs haven't undergone apoptosis and are still able to express HLA-DR.

Once again, the *ex vivo* T cell stimulation did not show significant differences between the groups. While the UNVAC group did not have any *M.tb*-specific hCD4+ T cells in the lung and no *M.tb*-specific T cells in the spleen, we did see that the values for the HIV group (that received no vaccination) were similar to that of the

vaccinated groups, thus indicating these were not vaccine specific responses (*Figure 25-26*). It is inferred that the inflammatory responses caused by HIV may have caused an increase in non-specific T cell responses, thus altering the data. This has been seen in HIV-infected hu-BLT mice where they saw an increase in T cell turnover and activation, as well as upregulated HLA-DR expression in CD8+ T cells[171]. In the spleen, the highest averages for IFNγ and TNFα in hCD4+ and hCD8+ T cells are seen in the vaccinated groups *(Figure 26 A-B, D-E).* Moreover, in Yao et al.'s study, their *M.tb*-specific hCD4+ T cell responses in the lung and spleen for TNFα was about 1.8% (+/-0.7) and 0.1% (+/-0.1), respectively. Whereas we observed an average of 1.3-2.8% hCD4+ TNFα in our vaccinated groups for the lung, and an average of 8.5-33.5% in the spleen (*Figure 25-26).* The difference in production may be due to our model, as we used hu-DRAG mice while Yao et al. used hu-NRG mice. It could also be due to the vaccine used, since the paper used the monovalent AdHu5Ag85A, thus potentially indicating that the trivalent vaccine induces hCD4+ T cells capable of producing multiple cytokines in response to TB antigens.

The production of robust hCD8+ IFNγ in the lung follows the same trend as in *Experiment 1*, and in a study conducted by Jeyanathan et al. 2015, they also observed increased responses of hCD8+ IFNγ in the lung upon stimulation with an immunodominant Ag85A peptide when intranasally immunized with AdCh68Ag85A[76]. Interestingly, the VAC+HIV group has the highest average trend of hCD4+ and hCD8+ IFNγ and TNFα in the spleen; however, this data may be skewed by Mouse #46 (M46) which produced much higher amounts of cytokines than the rest of the mice in that group (*Figure 25).* As mentioned, hu-mice have fewer cells than conventional mice, and it is often challenging to

see specific cytokines in samples with few cells. Overall, between all the T stimulation experiments, it appears that the average of the vaccinated mice groups had the highest percentage of *M.tb*-specific CD4+ T cells, with TNFα being the highest and most consistent trend seen.

While the T cell stimulations were shown in only *Aim 1.1* and *2.1*, they were conducted in some of the other challenge experiments as well. However, those were not shown since when infected with *M.tb*, the bacilli present in the lung and spleen caused *M.tb*-specific immune responses that could not be solely attributed to the vaccine. While we subtracted non-specific unstimulated background cytokines from specific stimulated ones, when infected with *M.tb* we often saw a greater number and percentage of unstimulated cells compared to stimulated cells, thus was not included in the final data set since we could not claim the vaccine's ability to induce specific antigen responses.

Unfortunately, for *Aim 2.1. Experiment 1* there were technical difficulties with IL-2, thus could not be shown in the figure *(Figure 25-26).* When running the compensation controls on the Cytoflex machine, the antibody used for IL-2 was not being picked up by the machine. It was later discovered that it was due to the bead not matching the antibody, as a different bead should have been used. Therefore, the IL-2 compensation control was not properly conducted and the samples were run without it. Due to this error, the other compensation controls may have been skewed, thus we cannot conclude that the T cell stimulation was accurate. A new IL-2 compensation was run with the samples again, and while this may have shown a more accurate representation of the T stimulation, it was still not completely accurate. When comparing the two data sets, some of the graphs look

similar while others do not, potentially altering our findings (data not shown). The graphs in *Figures 25-26* will thus just be used as a reference and this experiment may have to be fully repeated in the future.

4.1.3. Protection of the Vaccine

In *Aim 1.2.*, we wanted to determine if the Tri:ChAd68 vaccine will confer effective protection against TB infection. The results of this experiment demonstrated that the Tri:ChAd68 vaccine is able to significantly reduce the lung mycobacterial load by 2.4 $\log_{10}$, as well as potentially decrease the dissemination to the spleen (*Figure 8).* Moreover, enhanced bacterial control in vaccinated mice was further supported by remarkably reduced granulomatous lesions and density of acid fast-bacilli (AFB) *(Figure 9-10).* The data from this experiment is published by Afkhami et al. 2023 in *npj Vaccines.*

After concluding that the vaccine conferred protection in naïve hu-mice, we wanted to investigate the degree of protection it would confer when co-infected with HIV. In *Aim 2.2. Experiment 1,* the mice were immunized then challenged with a lower dose of *M.tb* at $1x10^3$ CFU *M.tb* H37Rv, since it is predicted that the HIV infection may exacerbate the TB and progress to endpoint quicker. Previous experiments in our lab have conducted co-infection experiments with $1x10^3$ CFU *M.tb* H37Rv and have concluded that this dosage is sufficient to enable productive infection in the lower respiratory tract without inducing rapid disease progression. When the blood was collected and assessed for T cell levels at endpoint, and it was noted that two of the mice's (n=1 HIV+VAC+TB group, n=1 VAC+TB group) blood clotted and since majority of the blood cells were in the blood clot, their T cells levels were close to zero. Therefore, those two mice were excluded from the

blood data set. In *Figure 29*, the T cell pattern of decreased hCD4 and increased hCD8 is consistent with the previous experiments, but the difference in percentages is not as drastic as seen previously. This could be due to the low viral load in the HIV-infected groups, shown in *Figure 28*. Since their averaged viral load hovers around the threshold viral load at ~1,500 HIV RNA copies/mL from 7-12 weeks post HIV-infection, this could mean that some of the mice harbour very low HIV levels and thus didn't have as severe hCD4+ T cell depletion.

When intranasally immunized and/or infected, hu-mice were sensitive to anesthesia and often had difficulty with intranasal fluid intake, thus could have affected the dose of vaccine/*M.tb* received in the lung. Based on our observations, hu-mice appear to have weaker respiration compared to non-humanized mice, as BALB/c mice are capable of intaking larger volumes of fluid with continued respiration. We hypothesize that this is an outcome from the irradiation during the humanization process, leading to structural or cellular lung damage and fibrosis[172]. The mice that had issues with intranasal administration were noted and taken into account when analyzing the final data. For this experiment, there were technical issues in two of the mice (n=1 VAC+TB group, n=1 TB only group) when intranasally challenged with *M.tb*. It was unlikely the dose of the *M.tb* got into their respiratory tract as it correlated with extremely low/absent CFU for these two mice. Thus, they were excluded from the entire data set. In *Figure 30*, while not significant, we can see there was about a 1.26 $\log_{10}$ reduction between the TB only group and the vaccinated TB group, and a 0.61 $\log_{10}$ reduction between the HIV+TB group and the vaccinated HIV+TB group in the lung. This is also evident when looking at the percentage of granulomatous

tissues in the lung, and while there is a spread between mice in the same group, the vaccinated groups have a lower average amount by about 15% than the unvaccinated groups (*Figure 31).*

Interestingly, the unvaccinated co-infected group has a slightly lower average CFU than the TB-only group in the lung, and similar CFU in the spleen. This could be due to the previously mentioned low viral load in the HIV+TB group. This experiment used a different *M.tb* lot than in *Aim 1.2*, and at the time of experiment it had a predicted titer of 30,000 CFU/μL (actual titer = 41,750 CFU/μL) with an aimed dosage of $1x10^4$ CFU/mouse whereas this experiment had a lower predicted titer of 20,000 CFU/μL (actual titer = 19,783 CFU/μL) with an aimed dosage of $1x10^3$ CFU/mouse. In the CFU levels exhibited in the lung of the mice, the unvaccinated TB-only group in *Aim 1.2.* had averaged CFU of 9.24 and the same control group in *Aim 2.2. Experiment 1* had an averaged CFU of 8.70, 0.5 of a log difference.

This experiment also used hu-DRAG mice instead of hu-NRG mice, and a previous vaccination study using tetanus toxoid immunized hu-DRAG mice and was able to determine that they were capable of eliciting anti-tetanus toxin IgG antibodies produced by their human B cells, unlike the hu-mouse control lacking HLA[166]. This study was also able to show that the B cells developed by the hu-DRAG mice were functional and able to reconstitute serum levels of human IgM, which was comparable to those in human serum[166]. The human B cells were also able to undergo immunoglobulin class switching and to secrete IgG, IgA and IgE unlike the hu-BLT mice[166]. This shows that hu-DRAG mice are ideal for vaccination studies in their ability to production functional human T and

B cells and undergo class-switching to generate human antibodies. All in all, there are many variables that could have altered the CFU data, as the *M.tb* lot, titer and infectious dose was different among the two experiments. Moreover, the hu-DRAG mice have more mechanisms to reduce TB load and induce specific immunity given from the vaccine, thus may make it more difficult to see differences among the groups.

In *Aim 2.2. Experiment 2,* we wanted to investigate the degree of protection that the three TB antigens conferred against TB. Thus, each group was vaccinated, some with the trivalent vaccine (VAC) and some with the empty ad-vectored (EA) vaccine. The T cell levels in the blood at endpoint (12 weeks post-HIV infection) were consistent with what we expected, with the percentage of hCD4+ T cells in the HIV-infected mice decreasing while their hCD8+ T cells increased *(Figure 34-35).* On the other hand, their mycobacterial burden was not as expected. Due to the experiments conducted in conventional mice by the Xing Lab, we would expect the trivalent vaccine would provide better protection than then empty-ad vector. It has been shown that by expressing Ag85A, TB10.4 and RpfB, animals who received the Tri:ChAd68 vaccine exhibited a significant reduction in their pulmonary mycobacterial load[78]. This reduction correlated with notable diminished immunopathology in the lungs compared to animals immunized with vaccines that lacked the same range of antigens or failed to cover the spectrum of the *M.tb* life cycle[78]. In *Figure 38 & 37,* we can see that the mycobacterial load in the lung and spleen as well as the percentage of lung granulomatous tissues in all groups do not have statistical significant differences; however, the VAC+TB group does have the lowest average CFU in lung and spleen. *Aim 2.2. Experiment 1,* the mice in TB-only and HIV+TB control groups were not given any

protection, thus displayed more granulomas and a higher averaged CFU, unlike the same control groups in this experiment that were given the empty-ad vaccine (TB+EA and HIV+EA+TB). Like the other *M.tb* challenge experiments, this one uses a different vial, H37Rv *M.tb* lot#19 but has an even lower predicted titer of 15,000 CFU/μL (actual titer = 10,750 CFU/μL). Overall, there have been challenges with production of *M.tb* stocks leading to extremely low stock concentration in comparison to prior preparations. Since we give a low dose of TB in this experiment, this may be creating variable results. A recent paper has shown that infecting murine models (C57BL/6 mice) with ultra-low doses (ULD) of aerosol *M.tb* of between 1-3 CFU produces heterogenous bacterial burdens. It is believed that ULD aerosol model may resemble human pulmonary tuberculosis disease and is advantageous for pre-clinical vaccine and immunotherapy testing[173]. In this paper, mice exposed to ULD aerosols had greater within-group CFU variability compared to low dosage, which is what we saw in this experiment[174]. The increased variability from the low *M.tb* CFU stock may have caused us to miss the lower dilutions when plating.

Since the empty-ad control mice and the trivalent vaccinated mice don't have significant differences in their protection against TB, it can be postulated that the involvement of TII contributed to protection in every group. Although we didn't specifically test for TII in this experiment due to the already low cell numbers in the auxiliary lobes of the lungs, we did see a greater trend of AMØs in the EA groups than the VAC groups *(Figure 39).* Furthermore, when counting the colonies to determine their CFU in in the lung and spleen, we noted that some of the mice had very few countable colonies on the lowest dilution we plated, thus not making the final count accurate. The leftover lung

and spleen homogenates will thus have to be re-plated on lower dilutions to be certain of conclusions.

4.1.4. Efficiency of ART

In *Aim 3*, we established and optimized an efficient method for delivering antiretroviral therapy (ART) to our hu-mice. With the optimal dose, we can begin to investigate the immunogenicity and protective efficacy the Tri:ChAd68 confers against TB when on ART. This would allow for clinical relevance, since 75% of PLWH were accessing ART globally by the end of 2022[175]. The combination of ART medications we decided to use are widely used in the literature in humanized mice[145–149] and are available for humans in Canada[176]. It consists of two non-nucleoside reverse transcriptase inhibitor (NNRTIs), tenofovir disoproxil fumarate (TDF) and emtricitabine (FTC), and one integrase inhibitor, raltegravir (RAL). The protocol we followed for administration of the drugs was created by Mu et al., however they use sterile research-grade powdered ART directly from Gilead, and since this is extremely costly, we used an alternative method in which we grinded up the prescription medication with a mortar and pestle. The filler that was included in the pills is not ideal, as it caused difficulties in mixing it with DMSO, and potentially caused some of the filler and/or medication to be stuck in the filter of the 0.2μm pore syringe filter, making it difficult to accurately determine the concentration of ART they received.

For the mice's CD4+ T cell levels, the ART mice displayed a decrease before and after to ART administration, and while on ART their CD4+ T cells remained consistent *(Figure 43A)*. When looking at their viral load, we saw that all of the mice's HIV RNA copies/mL were below the detection limit when on ART from week 2 to 6 *(Figure 44)*.

Once the ART group was taken off the medication, their viral load increased to about the same HIV RNA copies as the control mice. The control mice that received no ART had high viral plasma levels throughout the duration of the experiment (*Figure 44).* Overall, the ART medication was able to lower viral load and circumvent the CD4+ T cell levels from depleting, and cause viral rebound when taken off the medication.

Chapter 4.2. Conclusion and Future Directions

In this research project, we have demonstrated that in both our naïve and HIV-infected hu-mice, this next generation RM administered Tri:ChAd68 vaccine was able to induce *M.tb*-specific immune responses, especially in hCD4+ TNFα, and confer protection against *M.tb* infection by decreasing their mycobacterial load and granulomatous tissue. For HLA-DR expression on airway macrophages to determine TII, vaccinated mice had increased expression in their total macrophages and IMØs, whereas the expression on the AMØs of each group was similar. It was also shown that HIV-infected groups reduced HLA-DR on lung macrophages, but vaccination prior to or after HIV infection may improve this. Furthermore, we have optimized and efficient method of delivering combined ART medications to HIV-infected hu-mice's food and have determined that the ART administration is able to decrease their viral load and restore hCD4+ T cell levels. In the future, it would be beneficial to investigate how the ART treated HIV-infected mice's immune response changes when immunized and/or subsequently infected with TB. It would also be beneficial to infect the mice with HIV via the intravaginal route rather than the interperitoneally route, as this would be more clinically relevant since the majority of HIV cases are transmitted through mucosal surfaces.

CHAPTER 5: SUPPLEMENTARY MATERIALS

Supplementary Table 1. **Engraftment information for each mouse.** * = engrafted via tail vein injection.

Group	Strain	Mouse Symbol	Mouse #	Sex	CB Sample	Approx. Age (wks)	%hCD45	hCD45/mL	%hCD3	hCD3/mL	%hCD4	hCD4/mL	%hCD8	hCD8/mL
UNVAC (n=2)	Hu-DRAGA2	●	M1*	F	37	36	3.1	20,240	83.0	16,800	79.0	13,280	13.8	2,320
	Hu-NRG	□	M2	F	66	19	34.0	191,360	29.7	56,800	79.4	45,120	17.3	9,840
VAC (n=6)	Hu-DRAGA2	●	M3*	F	37	35	15.2	54,960	40.0	22,000	77.5	17,040	17.5	3,840
		■	M4*	F	37	36	5.1	40,480	47.4	19,200	70.8	13,600	23.8	4,560
		▲	M5*	F	37	36	6.3	24,480	22.2	5,440	64.7	3,520	23.5	1,280
	Hu-NRG	○	M6	F	35	34	40.5	91,700	36.4	33,400	54.8	18,300	41.6	13,900
		□	M7	F	66	19	18.5	87,429	32.7	28,571	66.8	19,086	29.2	8,343
		△	M8	M	66	19	5.1	27,600	30.1	8,320	75.0	6,240	12.5	1,040

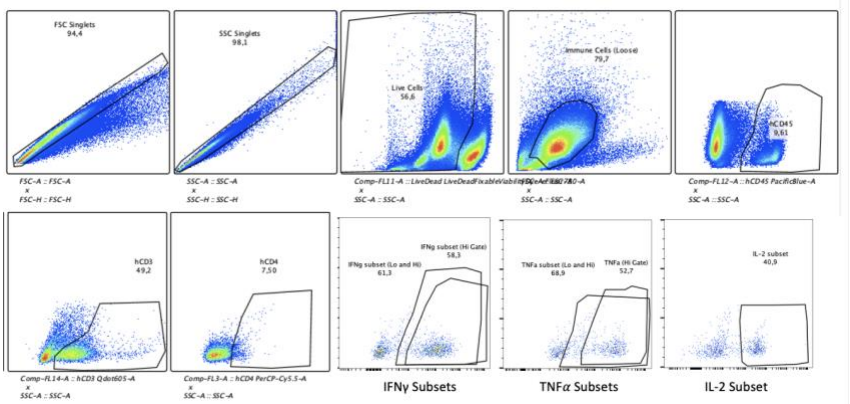

Supplementary Figure 1. **T Cell Stimulation Flow Gating Strategy in the Lung.** Gating done by Yang, J. IFNγ and TNFα Lo and Hi gate used for analysis.

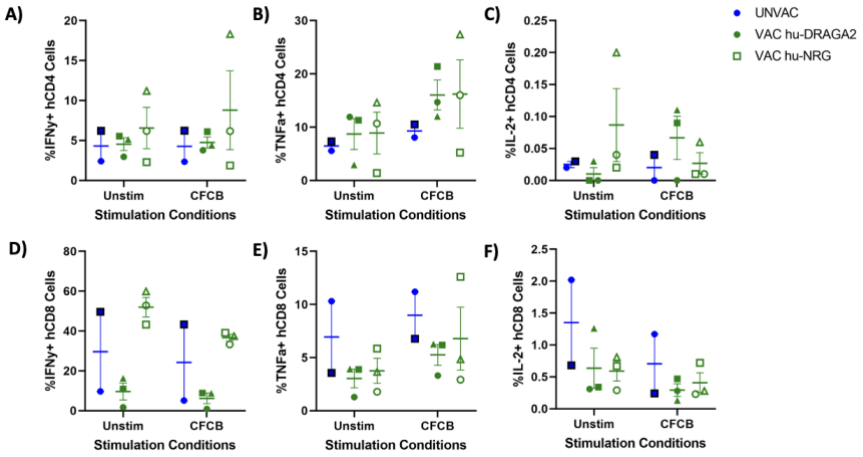

Supplementary Figure 2. **Unstimulated and CFCB stimulated values for the lung.** Percentage of hCD4+ T cells producing (A) IFNγ (B) TNFα (C) IL-2. Percentage of hCD8+

T cells producing (D) IFNγ (E) TNFα (F) IL-2 per lung. Data are expressed as +/- SEM. Statistical analysis was performed using a two-way ANOVA with Tukeys multiple comparison test. p values = * < 0.05, ** < 0.01, *** < 0.001, **** < 0.001.

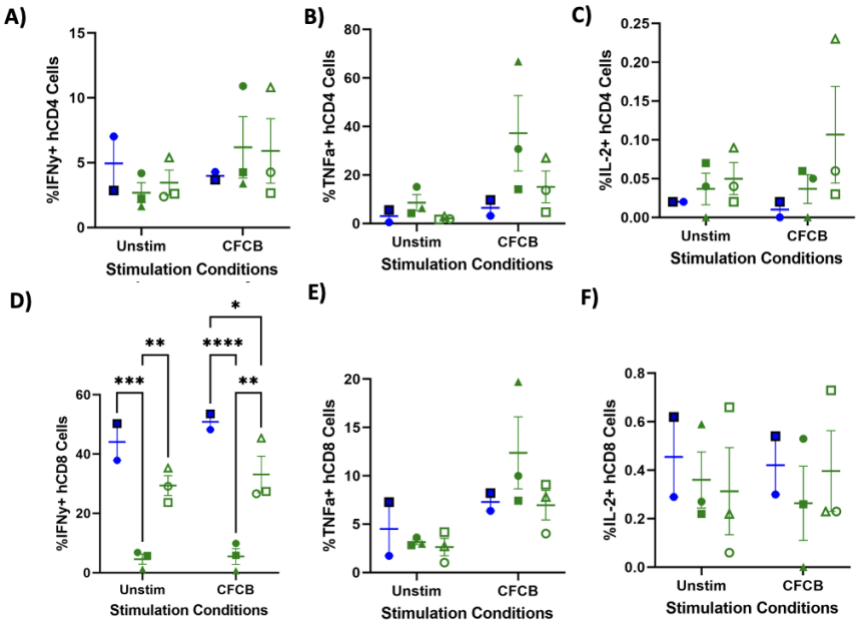

Supplementary Figure 3. **Unstimulated and CFCB stimulated values for the spleen.** Percentage of hCD4+ T cells producing (A) IFNγ (B) TNFα (C) IL-2. Percentage of hCD8+ T cells producing (D) IFNγ (E) TNFα (F) IL-2 per lung. Data are expressed as +/- SEM. Statistical analysis was performed using two-way ANOVA with Tukeys multiple comparison test. p values = * < 0.05, ** < 0.01, *** < 0.001, **** < 0.001.

Supplementary Table 2. **Engraftment information for each mouse.**

Group	Mouse Symbol	Mouse #	Sex	CB Sample	Approx. Age (wks)	%hCD45	hCD45/mL	%hCD3	hCD3/mL	%hCD4	hCD4/mL	%hCD8	hCD8/mL
UNVAC (n=4 NRG)	●	M9	F	33	26	23.9	118,000	73.7	31,500	48.8	14,100	36.4	12,300
	■	M10	F	33	26	16.4	58,667	61.1	35,867	62.8	22,533	21.6	7,733
	▲	M11	M	66	19	23.9	85,600	73.7	63,120	48.8	30,800	36.4	22,960
	◆	M12	F	35	34	4.9	31,600	58.2	18,400	34.3	6,320	46.5	8,560
VAC (n=3 NRG)	●	M13	M	66	19	31.8	80,080	79.1	63,360	54.4	34,480	34.0	21,520
	■	M14	F	33	26	52.4	206,560	26.6	54,880	57.9	31,760	31.5	17,280
	▲	M15	M	33	26	9.6	42,080	54.2	22,800	53.3	12,160	29.8	6,800

Supplementary Table 3. **CFU Log_{10} in the lung and spleen of the individual mice at 4 weeks post-*M.tb* infection.**

Group	Mouse #	CFU Log_{10} Lung	CFU Log_{10} Spleen	Lung Average	Spleen Average
UNVAC	M9	9.10	7.00	9.24	6.62
	M10	9.21	5.49		

	M11	9.91	7.33		
	M12	8.74	6.65		
VAC	M13	5.79	4.57	6.84	4.24
	M14	6.98	6.06		
	M15	7.76	2.08		

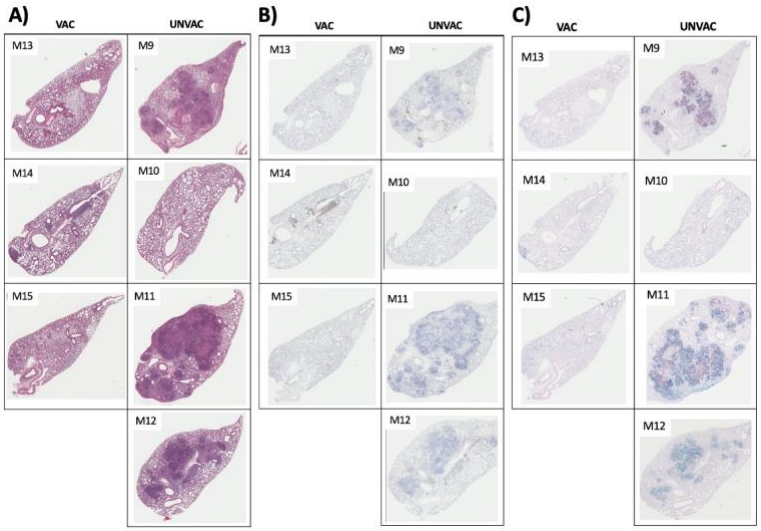

Supplementary Figure 4. **Visualization of the histology of each mouse 4 weeks post-*M.tb* infection.** (A) H&E staining (B) CD4+ IHC staining (C) AFB staining of the middle lung segments.

Supplementary Table 4. **Engraftment information for each mouse.**

Group	Mouse Symbol	Mouse #	Sex	CB Sample	Approx. Age	%hCD45	hCD45/mL	%hCD3	hCD3/mL	%hCD4	hCD4/mL	%hCD8	hCD8/mL
HIV (n=2 Hu-DRAG)	●	M16	M	34	26. wks	9.5	18,200	31.9	5,806	56.9	3,304	27.6	1,602
	■	M17	M	34	26. wks	15.9	26,080	41.1	10,719	71.6	7,675	16.4	1,758
VAC (n=4 Hu-DRAG)	●	M18	M	38	26. wks	10.7	15,200	64.7	9,834	62.6	6,156	27.6	2,714
	■	M19	M	34	26. wks	11.6	26,640	56.5	15,052	68.6	10,325	23.4	3,522
	▲	M20	F	34	26. wks	20.2	57,829	41.7	24,115	73.9	17,821	19.0	4,582
	◆	M21	F	38	26. wks	17.2	58,880	53.5	31,501	67.5	21,263	14.7	4,631
HIV+VAC (n=3 Hu-DRAG)	●	M22	M	34	26. wks	3.0	23,733	94.0	22,309	78.9	17,602	15.1	3,369
	■	M23	F	34	26. wks	24.3	98,160	40.7	39,951	58.5	23,371	26.1	10,427
	▲	M24	F	48	20. wks	55.3	42,400	42.1	17,850	65.9	11,763	21.1	3,766

Supplementary Table 5. **RNA Copies/mL for individual mice at 3-, 6- and 9-weeks post-HIV infection.**

		RNA Copies/mL at Weeks Post HIV-Infection		
Group	**Mouse #**	**3 Weeks**	**6 Weeks**	**9 Weeks**
HIV	M16	7,144	1,041	890
	M17	4,893	6,843	2,366
HIV+VAC	M22	2,204	2,277	0

	M23	6,596	5,539	15,704
	M24	2,821	50,082	875,569

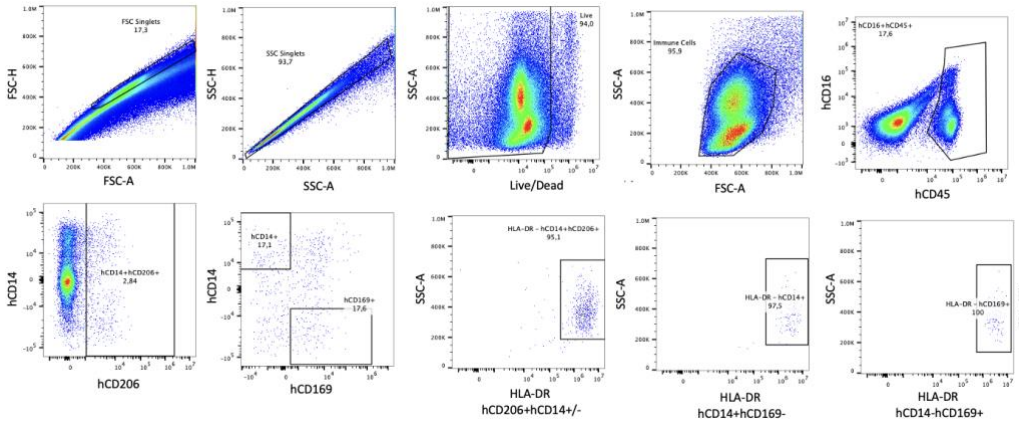

Supplementary Figure 5. **Sample macrophage flow gating strategy in the lung.**

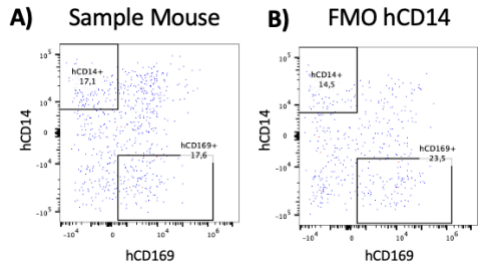

Supplementary Figure 6. **Flow gating strategy for hCD14+ and hCD169+ cells.** (A) Flow gates on a randomized sample mouse (B) Flow gates on FMO CD14.

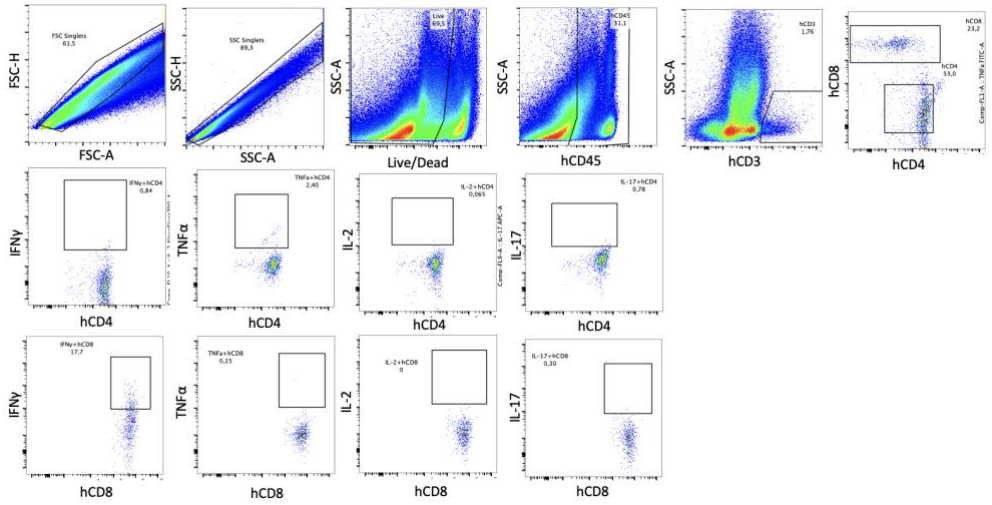

Supplementary Figure 7. **Sample T stimulation flow gating for the lung and spleen.**

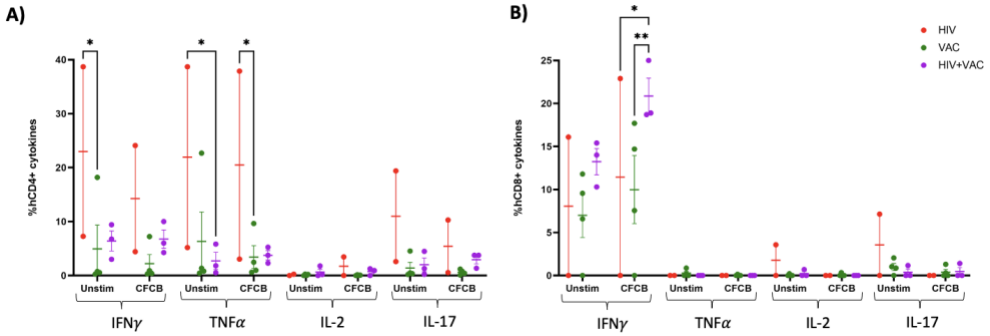

Supplementary Figure 8. **Unstimulated and CFCB stimulated values for the lung.** Percentage of (A) hCD4+ cytokines and (B) hCD8+ cytokines. Data are expressed as +/- SEM. Statistical analysis was performed using a two-way ANOVA with Tukeys multiple comparison test. p values = * < 0.05, ** < 0.01, *** < 0.001, **** < 0.001.

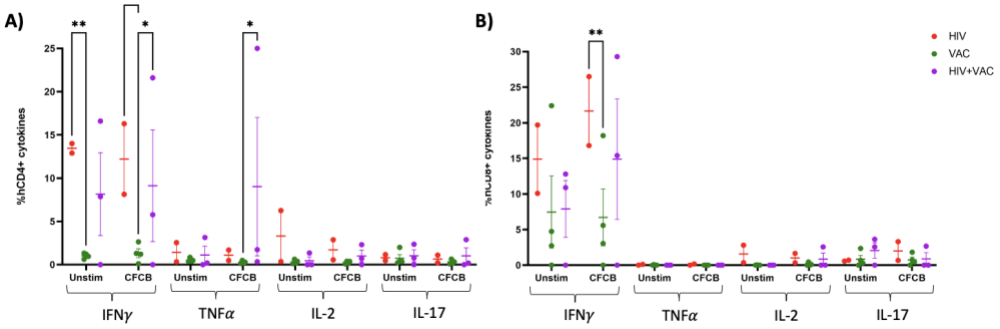

Supplementary Figure 9. **Unstimulated and CFCB stimulated values for the spleen.** Percentage of (A) hCD4+ cytokines and (B) hCD8+ cytokines. Data are expressed as +/- SEM. Statistical analysis was performed using a two-way ANOVA with Tukeys multiple comparison test. p values = * < 0.05, ** < 0.01, *** < 0.001, **** < 0.001.

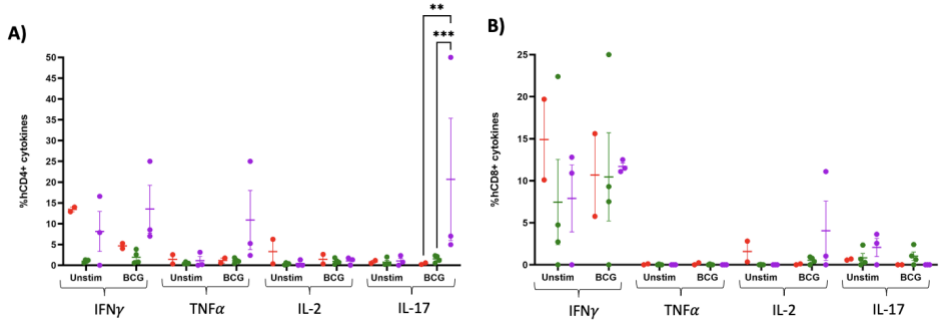

Supplementary Figure 10. **Unstimulated and BCG stimulated values for the spleen.** Percentage of (A) hCD4+ cytokines and (B) hCD8+ cytokines. Data are expressed as +/- SEM. Statistical analysis was performed using a two-way ANOVA with Tukeys multiple comparison test. p values = * < 0.05, ** < 0.01, *** < 0.001, **** < 0.001.

Supplementary Table 6. **Engraftment information for each mouse.**

Group	Mouse Symbol	Mouse #	Sex	CB Sample	%hCD45	hCD45/mL	%hCD3	hCD3/mL	%hCD4	hCD4/mL	%hCD8	hCD8/mL
UNVAC (n=3 hu-NRG)	●	M25	F	75	35.6	153,840	61.3	94,304	69.7	65,730	27.1	25,556
	■	M26	F	82	52.1	85,840	44.1	37,855	41.9	15,861	47.1	17,830
	▲	M27	F	82	70.0	287,920	43.5	125,245	49.1	61,495	37.1	46,466
HIV (n=5 hu-NRG)	●	M28	F	75	48.8	99,680	58.8	58,612	64.5	37,805	29.3	17,173
	■	M29	M	81	65.1	134,300	45.2	60,704	71.5	43,403	22.9	13,901
	▲	M30	F	81	75.9	74,560	42	31,315	49.1	15,376	44.5	13,935
	◆	M31	F	81	76.9	120,240	34.7	41,723	45.1	18,817	45.7	19,068
	▼	M32	M	82	74.6	425,520	40.3	171,485	63.4	108,721	29.9	51,274
VAC (n=5 hu-NRG)	●	M33	F	71	24.0	40,480	59.9	24,248	71.9	17,434	23.4	5,674
	■	M34	F	75	20.2	88,720	34.4	30,520	58	17,701	34.6	10,560
	▲	M35	M	81	34.2	142,880	23.7	33,863	57.9	19,606	33.3	11,276
	◆	M36	F	81	83.4	96,560	42.8	41,328	60.9	25,169	32.4	13,390
	▼	M37	M	82	83.6	505,520	31.4	158,733	62.4	99,050	29.7	47,144
HIV+VAC (n=6 hu-NRG)	●	M38	F	71	16.5	52,320	31.7	16,585	11.6	1,924	13.5	2,239
	■	M39	F	75	9.7	42,400	69.1	29,298	62.6	18,341	34.2	10,020
	▲	M40	M	82	74.6	339,120	35.8	121,405	65.3	79,277	27.1	32,901
	◆	M41	F	82	91.1	156,480	38.1	59,619	58.3	34,758	33.2	19,793
	▼	M42	F	81	62.9	138,480	36.2	50,130	56.9	28,524	34.8	17,445
	⬢	M43	F	82	62.7	193,280	41.1	79,438	53.5	42,499	39	30,981
VAC+HIV (n=4 hu-NRG)	●	M44	F	75	26.1	121,520	76.6	93,084	54.6	50,824	40.2	37,420
	■	M45	M	82	47.8	193,680	52.6	101,876	57.5	58,579	36.6	37,286
	▲	M46	M	82	53.8	234,160	43.5	101,860	55.4	56,430	36.8	37,484
	◆	M47	F	82	75.2	233,360	41.5	96,844	59.8	57,913	34	32,927

Supplementary Table 7. **RNA Copies/mL for individual mice at 3-, 6- and 9-weeks post-HIV infection.**

		RNA Copies/mL at Weeks Post HIV-Infection		
Group	**Mouse #**	**3 Weeks**	**6 Weeks**	**8 Weeks**
HIV	M28	16,612	8,059	3,373
	M29	20,206	28,430	97,733
	M30	15,532	9,325	5,536
	M31	39,835	34,287	23,256
	M32	6,962	35,246	77,205
HIV+VAC	M38	1,337	0	859
	M39	2,903	1,247	1,025
	M40	13,044	82,050	258,242
	M41	149,366	113,980	136,247
	M42	9,533	9,103	3,645
	M43	7,266	8,514	7,916
VAC+HIV	M44	0	57,767	4,966
	M45		24,496	14,332
	M46		3,541	24,260
	M47		28,807	13,189

VAC Pooled	-	2,125	487	891
UNVAC Pooled	-	0	0	0

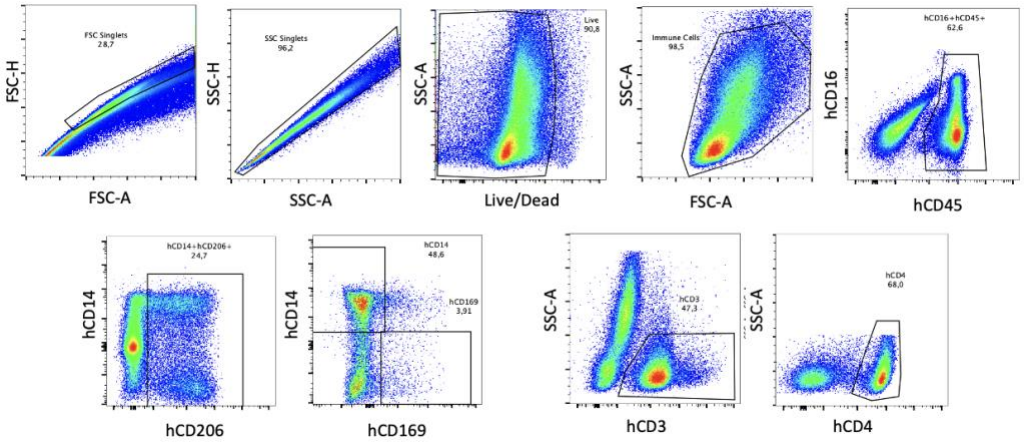

Supplementary Figure 11. **Sample macrophage flow gating strategy in the lung.**

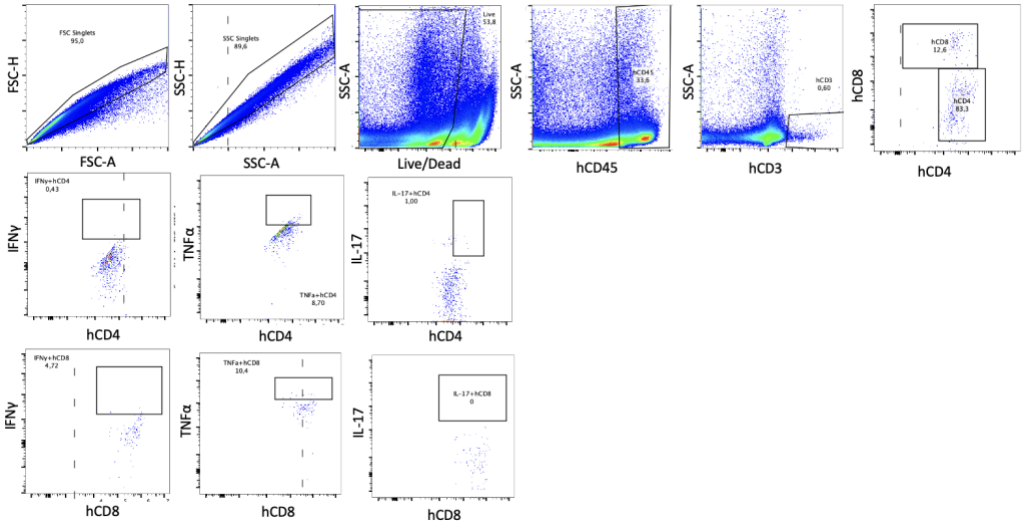

Supplementary Figure 12. **Sample T stimulation flow gating for the lung and spleen.**

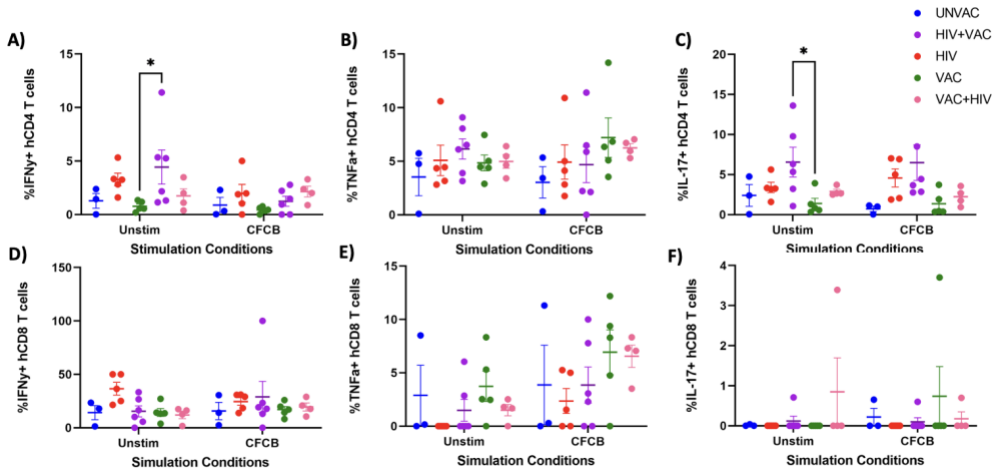

Supplementary Figure 13. **Unstimulated and CFCB stimulated values in the lung.** Percentage of hCD4+ (A) IFNγ (B) TNFα (C) IL-17. Percentage of hCD8+ (A) IFNγ (B) TNFα (C) IL-17. Data are expressed as +/- SEM. Statistical analysis was performed using a two-way ANOVA with Tukeys multiple comparison test. p values = * < 0.05, ** < 0.01, *** < 0.001, **** < 0.001.

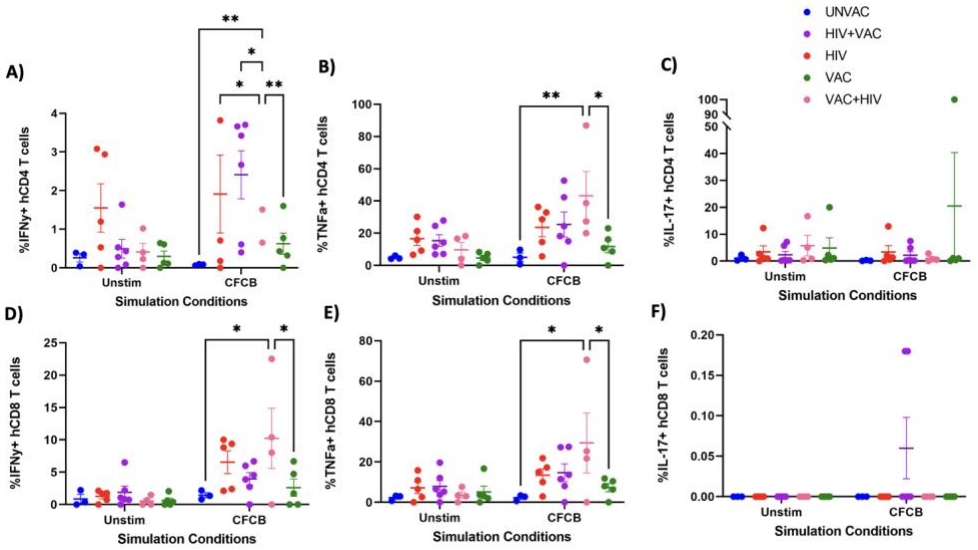

Supplementary Figure 14. **Unstimulated and CFCB stimulated values in the spleen.** Percentage of hCD4+ (A) IFNγ (B) TNFα (C) IL-17. Percentage of hCD8+ (A) IFNγ (B) TNFα (C) IL-17. Data are expressed as +/- SEM. Two-way ANOVA was conducted.
p values = * < 0.05, ** < 0.01, *** < 0.001, **** < 0.001.

Supplementary Table 8. **Engraftment information for each mouse.**

Group	Mouse Symbol	Mouse #	Sex	CB Sample	Approx. Age	%hCD45	hCD45/mL	%hCD3	hCD3/mL	%hCD4	hCD4/mL	%hCD8	hCD8/mL
TB Only (n=3 Hu-DRAG)	●	M48	F	34	19. wks	63.1	199,360	51.6	102,870	37.0	38,062	55.6	57,196
	■	M49	F	8	20. wks	25.3	64,533	29.1	18,779	71.6	13,446	17.7	3,324
	▲	M50	F	34	19. wks	13.4	38,000	44.4	16,872	71.6	12,080	23.2	3,914
HIV+TB (n=3 Hu-DRAG)	●	M51	F	34	19. wks	35.5	137,040	36.3	49,746	70.6	35,120	21.9	10,894
	■	M52	M	34	19. wks	7.7	90,240	49.8	44,940	65.1	29,256	26.5	11,909
	▲	M53	M	34	19. wks	5.3	27,520	66.3	18,246	75.9	13,849	19.3	3,521
VAC+TB (n=2 Hu-DRAG)	●	M54	F	34	19. wks	24.9	121,920	41.5	50,597	68.4	34,608	25.0	12,649
	■	M55	F	34	19. wks	29.7	101,200	34.6	35,015	55.7	19,503	37.4	13,096
HIV+VAC+TB (n=4 Hu-DRAG)	●	M56	F	34	19. wks	42.7	176,000	31.6	55,616	71.5	39,765	16.5	9,177
	■	M57	M	34	19. wks	12.2	91,067	48.6	44,258	66.3	29,343	27.7	12,260
	▲	M58	F	34	19. wks	47.3	74,800	45.5	34,034	72.9	24,811	18.8	6,398
	◆	M59	F	8	20. wks	12.6	36,320	42.3	15,363	79.7	12,245	15.6	2,397

Supplementary Table 9. **Individual RNA Copies/mL for HIV-infected mice at 3- 7-, 10- and 12-weeks post-HIV infection.**

		RNA Copies/mL at Weeks Post HIV-Infection			
Group	**Mouse #**	**3 Weeks**	**7 Weeks**	**10 Weeks**	**12 Weeks**
HIV+TB	M51	58,557	743	603	2,940
	M52	37,892	1,585	0	0
	M53	22,252	2,465	1,319	3,072
HIV+VAC+TB	M56	3,230	2,493	846	2,562
	M57	11,380	2,767	1,071	2,989
	M58	11,523,429	0	2,209	23,584
	M59	7,577	906	2,110	5,269

Supplementary Table 10. **CFU Log_{10} in the lung and spleen of the individual mice at 4 weeks post-*M.tb* infection.**

Group	Mouse #	CFU Log_{10} Lung	CFU Log_{10} Spleen	Average CFU Lung	Average CFU Spleen
TB Only	M48	9.21	6.07	8.70	5.62
	M49	8.41	4.83		
	M50	8.48	5.96		
HIV+TB	M51	8.16	5.52	8.23	5.48
	M52	8.61	5.55		
	M53	7.91	5.38		
VAC+TB	M54	6.92	2.92	7.44	4.96
	M55	7.97	6.99		
HIV+VAC+TB	M56	8.91	5.93	7.62	5.31
	M57	8.21	5.60		
	M58	7.90	4.82		
	M59	5.48	4.90		

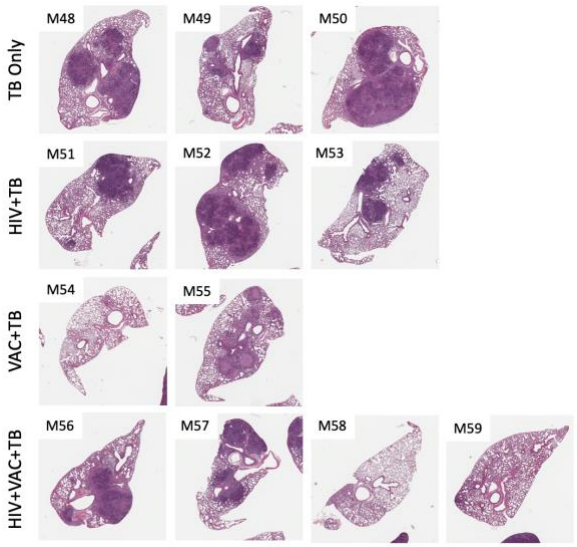

Supplementary Figure 15. **Visualization of the H&E histology of each mouse 4 weeks post-*M.tb* infection.** Middle section of lung segments.

Supplementary Table 11. **Engraftment information for each mouse.**

Group	Mouse Symbol	Mouse #	Sex	CB Sample	Approx. Age (wks)	%hCD45	hCD45/mL	%hCD3	hCD3/mL	%hCD4	hCD4/mL	%hCD8	hCD8/mL
EA+TB (n=4 hu-NRG)	●	M60	M	47	33	2.8	25,440	85.8	21,828	50.9	11,110	36.6	7,989
	■	M61	M	58	21	48.7	174,960	57.5	100,602	52.7	53,017	35.3	35,513
	▲	M62	M	71	18	12.2	91,280	76	69,373	52.9	36,698	40.8	28,304
	◆	M63	M	69	16	5.0	55,440	35.5	19,681	58.5	11,514	27.2	5,353
VAC+TB (n=4 hu-NRG)	●	M64	M	58	21	42.6	132,400	34.4	45,546	62.6	28,512	26.5	12,070
	■	M65	M	68	21	8.3	29,680	34.2	10,151	42.5	4,314	46.5	4,720
	▲	M66	M	64	18	30.5	100,160	85.5	85,637	62.6	53,609	25.9	22,180
	◆	M67	M	69	18	17.4	94,720	33	31,258	52.4	16,379	34.5	10,784
HIV+EA+TB (n=4 hu-NRG)	●	M68	M	58	18	36.1	156,480	65.2	102,025	52.4	53,461	10.5	10,713
	■	M69	M	58	16	5.9	31,440	44.5	13,991	50.9	7,121	33.7	4,715
	▲	M70	M	68	21	5.9	24,400	50.2	12,249	55.6	6,810	34.6	4,238
	◆	M71	M	69	21	31.4	146,160	52.8	77,172	58.9	45,455	31.7	24,464
HIV+VAC+TB (n=4 hu-NRG)	●	M72	M	58	18	41.9	106,320	91.6	97,389	72.6	70,705	17.2	16,751
	■	M73	M	64	18	19.0	79,680	47.2	37,609	41.1	15,457	48.7	18,316
	▲	M74	M	64	21	43.2	156,080	31.1	48,541	55.2	26,795	33.4	16,213
	◆	M75	M	69	21	5.5	24,720	80.9	19,998	56	11,199	30.8	6,160

Supplementary Table 12. **Individual RNA Copies/mL for HIV-infected mice at 3- 6-, and 12-weeks post-HIV infection.**

		RNA Copies/mL at Weeks Post HIV-Infection		
Group	**Mouse #**	**3 Weeks**	**6 Weeks**	**12 Weeks**
HIV+EA+TB	M68	1,915		0
	M69	4,270		721
	M70	6,051		9,324

	M71	8,955		0
HIV+VAC+TB	M72	2,262		0
	M73	4,415		616
	M74	4,714		10,073
	M75	35,689		4,104
EA+TB Pooled	--	0		0
VAC+TB Pooled	--	391		0

Supplementary Table 13. **CFU Log_{10} in the lung and spleen of the individual mice at 4 weeks post-*M.tb* infection.**

Group	Mouse #	CFU Log_{10} Lung	CFU Log_{10} Spleen	Average Lung	Average Spleen
EA+TB	M60	8.11	6.15	7.64	5.74
	M61	8.26	6.72		
	M62	7.37	5.06		
	M63	6.82	5.04		
VAC+TB	M64	8.25	7.13	7.03	5.13
	M65	5.60	4.54		
	M66	7.30	3.12		
	M67	6.97	5.72		
HIV+EA+TB	M68	6.17	2.92	7.48	5.67
	M69	6.87	6.17		
	M70	8.78	6.86		
	M71	8.10	6.72		
HIV+VAC+TB	M72	9.35	7.21	7.86	5.48
	M73	6.51	3.97		
	M74	7.77	5.79		
	M75	7.81	4.95		

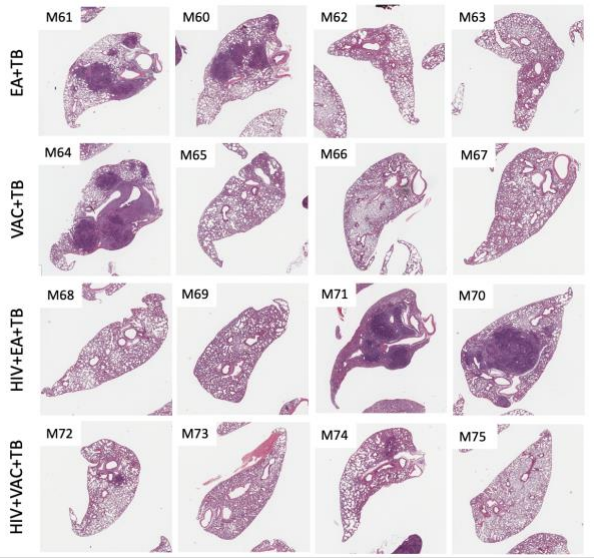

Supplementary Figure 16. **Visualization of the H&E histology of each mouse 4 weeks post-*M.tb* infection.** Middle section of lung segments.

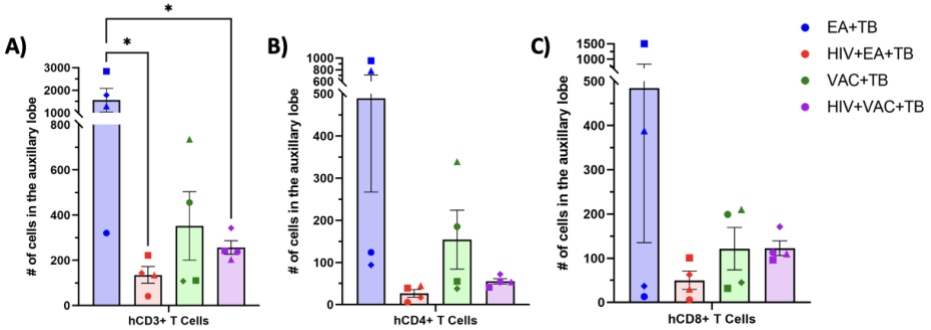

Supplementary Figure 17. **Flow count of T cells in the auxiliary lobe in the lung at 12 weeks post-infection.** Number of (A) hCD3+ (B) hCD4+ (C) hCD8+ T cells in the auxiliary lobe of the lung at endpoint. Data expressed as +/- SEM. Statistical analysis was performed using a one-way ANOVA with Tukeys multiple comparison test. p values = * < 0.05, ** < 0.01, *** < 0.001, **** < 0.001.

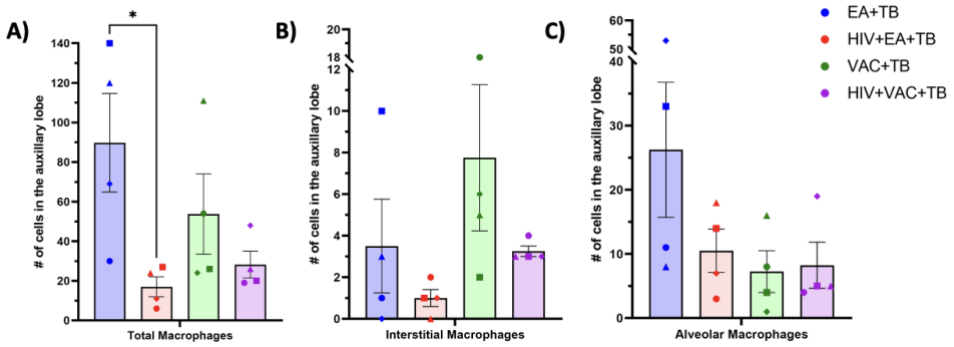

Supplementary Figure 18. **Flow count of macrophage cells in the auxiliary lobe in the lung at 12 weeks post-infection.** Number of (A) total (B) IMØs (C) AMØs in the auxiliary lobes of the lungs at endpoint. Data expressed as +/- SEM. Statistical analysis was performed using a one-way ANOVA with Tukeys multiple comparison test. p values = * < 0.05, ** < 0.01, *** < 0.001, **** < 0.001.

Supplementary Table 14. **Engraftment information for each mouse.**

Group	Mouse Symbol	Mouse #	Sex	CB Sample	%hCD45	hCD45/mL	%hCD3	hCD3/mL	%hCD4	hCD4/mL	%hCD8	hCD8/mL
CONTROL (n=3 hu-NRG)	●	M76	F	82	68.6	692,320	36	249,235	54.2	135,085	37.9	94,460
	■	M77	F	82	78.3	189,900	49.3	93,621	52.4	49,057	41.7	39,040
	▲	M78	F	75	17.0	27,360	73.4	20,082	64.9	13,033	32.3	6,487
ART (n=3 hu-NRG)	●	M79	F	82	57.5	794,880	39.5	313,978	57.2	179,595	36.6	114,916
	■	M80	F	82	64.9	111,680	43.5	48,581	61.4	29,829	31.8	15,449
	▲	M81	F	75	5.3	19,000	85.3	16,207	74.1	12,009	22.2	3,598

Supplementary Table 15. **Individual RNA Copies/mL for HIV-infected mice at 3-, 6-, 8-, 10- and 12-weeks post-HIV infection.**

		RNA Copies/mL at Weeks Post HIV-Infection				
Groups	**Mouse #**	**3 Weeks**	**6 Weeks**	**8 Weeks**	**10 Weeks**	**12 Weeks**
CONTROL	M76	1,156	12,355	24,629	5,664	7,806
	M77	45,586	16,470	16,907	6,1643	19,937
	M78	4,728	1,362	265	3,120	1,692
ART	M79	9,,825	0	0	0	11,000
	M80	8666	0	0	628	2,168
	M81	1,738	0	471	0	821

CHAPTER 6: REFERENCES

1. Weiss RA. How Does HIV Cause AIDS? *Science*. 1993;260(5112):1273-1279. doi:10.1126/science.8493571

2. Nyamweya S, Hegedus A, Jaye A, Rowland-Jones S, Flanagan KL, Macallan DC. Comparing HIV-1 and HIV-2 infection: Lessons for viral immunopathogenesis: Comparisons between HIV-1 and HIV-2 infection. *Rev Med Virol*. 2013;23(4):221-240. doi:10.1002/rmv.1739

3. UNAIDS. Global HIV & AIDS statistics — Fact sheet. Published online 2023.

4. World Health Organization. HIV AND AIDS: Key Facts. Published online 2023.

5. Government of Canada. Estimates of HIV incidence, prevalence and Canada's progress on meeting the 90-90-90 HIV targets. Published online 2020.

6. Chaillon A, Avila-Ríos S, Wertheim JO, et al. Identification of major routes of HIV transmission throughout Mesoamerica. *Infect Genet Evol*. 2017;54:98-107. doi:10.1016/j.meegid.2017.06.021

7. Ramjee G, Daniels B. Women and HIV in Sub-Saharan Africa. *AIDS Res Ther*. 2013;10(1):30. doi:10.1186/1742-6405-10-30

8. Wand H, Ramjee G. Assessing and evaluating the combined impact of behavioural and biological risk factors for HIV seroconversion in a cohort of South African women. *AIDS Care*. 2012;24(9):1155-1162. doi:10.1080/09540121.2012.687820

9. Wessels JM, Nguyen PV, Vitali D, et al. Depot medroxyprogesterone acetate (DMPA) enhances susceptibility and increases the window of vulnerability to HIV-1 in humanized mice. *Sci Rep*. 2021;11(1):3894. doi:10.1038/s41598-021-83242-9

10. Royce RA, Seña A, Cates W, Cohen MS. Sexual Transmission of HIV. *N Engl J Med*. 1997;336(15):1072-1078. doi:10.1056/NEJM199704103361507

11. Fellay J, Shianna KV, Ge D, et al. A Whole-Genome Association Study of Major Determinants for Host Control of HIV-1. *Science*. 2007;317(5840):944-947. doi:10.1126/science.1143767

12. Barnett D, Walker B, Landay A, Denny TN. CD4 immunophenotyping in HIV infection. *Nat Rev Microbiol*. 2008;6(S11):S7-S15. doi:10.1038/nrmicro1998

13. Herbein G, Gras G, Khan KA, Abbas W. Macrophage signaling in HIV-1 infection. *Retrovirology*. 2010;7(1):34. doi:10.1186/1742-4690-7-34

14. Kalichman SC, Rompa D, Cage M, et al. Effectiveness of an intervention to reduce HIV transmission risks in HIV-positive people1 1The full text of this article is available via AJPM Online at www.elsevier.com/locate/ajpmonline. *Am J Prev Med*. 2001;21(2):84-92. doi:10.1016/S0749-3797(01)00324-5

15. Dean M, Carrington M, Winkler C, et al. Genetic Restriction of HIV-1 Infection and Progression to AIDS by a Deletion Allele of the *CKR5* Structural Gene. *Science*. 1996;273(5283):1856-1862. doi:10.1126/science.273.5283.1856

16. Grande F, Occhiuzzi M, Rizzuti B, et al. CCR5/CXCR4 Dual Antagonism for the Improvement of HIV Infection Therapy. *Molecules*. 2019;24(3):550. doi:10.3390/molecules24030550

17. Deeks SG, Overbaugh J, Phillips A, Buchbinder S. HIV infection. *Nat Rev Dis Primer*. 2015;1(1):15035. doi:10.1038/nrdp.2015.35

18. Archin NM, Sung JM, Garrido C, Soriano-Sarabia N, Margolis DM. Eradicating HIV-1 infection: seeking to clear a persistent pathogen. *Nat Rev Microbiol*. 2014;12(11):750-764. doi:10.1038/nrmicro3352

19. Stein BS, Gowda SD, Lifson JD, Penhallow RC, Bensch KG, Engleman EG. pH-independent HIV entry into CD4-positive T cells via virus envelope fusion to the plasma membrane. *Cell*. 1987;49(5):659-668. doi:10.1016/0092-8674(87)90542-3

20. German Advisory Committee Blood (Arbeitskreis Blut), Subgroup 'Assessment of Pathogens Transmissible by Blood'. Human Immunodeficiency Virus (HIV). *Transfus Med Hemotherapy*. 2016;43(3):203-222. doi:10.1159/000445852

21. Frankel AD, Young JAT. HIV-1: Fifteen Proteins and an RNA. *Annu Rev Biochem*. 1998;67(1):1-25. doi:10.1146/annurev.biochem.67.1.1

22. Li G, Piampongsant S, Faria NR, et al. An integrated map of HIV genome-wide variation from a population perspective. *Retrovirology*. 2015;12(1):18. doi:10.1186/s12977-015-0148-6

23. Moir S, Chun TW, Fauci AS. Pathogenic Mechanisms of HIV Disease. *Annu Rev Pathol Mech Dis*. 2011;6(1):223-248. doi:10.1146/annurev-pathol-011110-130254

24. Ciborowski P, Gendelman H. Human Immunodeficiency Virus-Mononuclear Phagocyte Interactions:Emerging Avenues of Biomarker Discovery, Modes of Viral Persistence and Disease Pathogenesis. *Curr HIV Res*. 2006;4(3):279-291. doi:10.2174/157016206777709474

25. Centers for Disease Control and Prevention. HIV Testing: HIV Public Health Partners. Published online 2020.

26. Cordes RJ, Ryan ME. Pitfalls in HIV testing. Application and limitations of current tests. *Postgrad Med*. 1995;98(5):177-180, 185-186, 189.

27. Pyra MN, Haberer JE, Hasen N, Reed J, Mugo NR, Baeten JM. Global implementation of PrEP for HIV prevention: setting expectations for impact. *J Int AIDS Soc*. 2019;22(8). doi:10.1002/jia2.25370

28. Yoshimura K. Current status of HIV/AIDS in the ART era. *J Infect Chemother*. 2017;23(1):12-16. doi:10.1016/j.jiac.2016.10.002

29. Battegay M, Elzi L. Does HIV antiretroviral therapy still need its backbone? *The Lancet*. 2014;384(9958):1908-1910. doi:10.1016/S0140-6736(14)61226-5

30. Hammer SM, Saag MS, Schechter M, et al. Treatment for Adult HIV Infection: 2006 Recommendations of the International AIDS Society–USA Panel. *JAMA*. 2006;296(7):827. doi:10.1001/jama.296.7.827

31. Grabar S. Clinical Outcome of Patients with HIV-1 Infection according to Immunologic and Virologic Response after 6 Months of Highly Active Antiretroviral Therapy. *Ann Intern Med*. 2000;133(6):401. doi:10.7326/0003-4819-133-6-200009190-00007

32. Mocroft A, Phillips A, Gatell J, et al. Normalisation of CD4 counts in patients with HIV-1 infection and maximum virological suppression who are taking combination antiretroviral therapy: an observational cohort study. *The Lancet*. 2007;370(9585):407-413. doi:10.1016/S0140-6736(07)60948-9

33. The Lancet. Mortality of HIV-1-infected patients in the first year of antiretroviral therapy: comparison between low-income and high-income countries. *The Lancet*. 2006;367(9513):817-824. doi:10.1016/S0140-6736(06)68337-2

34. Ivers LC, Kendrick D, Doucette K. Efficacy of Antiretroviral Therapy Programs in Resource-Poor Settings: A Meta-analysis of the Published Literature. *Clin Infect Dis*. 2005;41(2):217-224. doi:10.1086/431199

35. Johnson & Johnson. Janssen Announces Health Canada Approval of CABENUVATM, the First Long-Acting Regimen for the Treatment of HIV. Published online 2020.

36. Morrow WJW, Wharton M, Lau D, Levy JA. Small Animals Are Not Susceptible to Human Immunodeficiency Virus Infection. *J Gen Virol*. 1987;68(8):2253-2257. doi:10.1099/0022-1317-68-8-2253

37. Chahroudi A, Bosinger SE, Vanderford TH, Paiardini M, Silvestri G. Natural SIV Hosts: Showing AIDS the Door. *Science*. 2012;335(6073):1188-1193. doi:10.1126/science.1217550

38. Hatziioannou T, Evans DT. Animal models for HIV/AIDS research. *Nat Rev Microbiol*. 2012;10(12):852-867. doi:10.1038/nrmicro2911

39. Mattapallil JJ, Douek DC, Hill B, Nishimura Y, Martin M, Roederer M. Massive infection and loss of memory CD4+ T cells in multiple tissues during acute SIV infection. *Nature*. 2005;434(7037):1093-1097. doi:10.1038/nature03501

40. Lackner AA, Veazey RS. Current Concepts in AIDS Pathogenesis: Insights from the SIV/Macaque Model. *Annu Rev Med*. 2007;58(1):461-476. doi:10.1146/annurev.med.58.082405.094316

41. Haase AT. Targeting early infection to prevent HIV-1 mucosal transmission. *Nature*. 2010;464(7286):217-223. doi:10.1038/nature08757

42. Van Rompay KKA. Tackling HIV and AIDS: contributions by non-human primate models. *Lab Anim*. 2017;46(6):259-270. doi:10.1038/laban.1279

43. Haase AT. Early Events in Sexual Transmission of HIV and SIV and Opportunities for Interventions. *Annu Rev Med*. 2011;62(1):127-139. doi:10.1146/annurev-med-080709-124959

44. Van Rompay KKA. The Use of Nonhuman Primate Models of HIV Infection for the Evaluation of Antiviral Strategies. *AIDS Res Hum Retroviruses*. 2012;28(1):16-35. doi:10.1089/aid.2011.0234

45. American Lung Association. Learn About Tuberculosis. Published online 2022.

46. Kiazyk S, Ball T. Latent tuberculosis infection: An overview. *Can Commun Dis Rep*. 2017;43(3/4):62-66. doi:10.14745/ccdr.v43i34a01

47. Cao D, Zhang Z, Yang Z, et al. The association between tuberculin skin test result and active tuberculosis risk of college students in Beijing, China: a retrospective cohort study. *BMC Infect Dis*. 2019;19(1):619. doi:10.1186/s12879-019-4238-2

48. World Health Organization. Tuberculosis. Published online 2023.

49. Narasimhan P, Wood J, MacIntyre CR, Mathai D. Risk Factors for Tuberculosis. *Pulm Med*. 2013;2013:1-11. doi:10.1155/2013/828939

50. Government of Canada. Tuberculosis in Canada: Infographic. Published online 2021.

51. Adigun R, Singh R. Tuberculosis. *StatPearls Internet*. Published online 2023.

52. World Health Organization. Global Tuberculosis Report 2022.

53. Heemskerk D, Caws M, Marais B, et al. Chapter 2: Pathogenesis. In: Tuberculosis in Adults and Children. *Lond Springer*. Published online 2015.

54. Koch A, Mizrahi V. Mycobacterium tuberculosis. *Trends Microbiol*. 2018;26(6):555-556. doi:10.1016/j.tim.2018.02.012

55. Cohen SB, Gern BH, Delahaye JL, et al. Alveolar Macrophages Provide an Early Mycobacterium tuberculosis Niche and Initiate Dissemination. *Cell Host Microbe*. 2018;24(3):439-446.e4. doi:10.1016/j.chom.2018.08.001

56. Queval CJ, Brosch R, Simeone R. The Macrophage: A Disputed Fortress in the Battle against Mycobacterium tuberculosis. *Front Microbiol*. 2017;8:2284. doi:10.3389/fmicb.2017.02284

57. Shaler CR, Horvath C, Lai R, Xing Z. Understanding Delayed T-Cell Priming, Lung Recruitment, and Airway Luminal T-Cell Responses in Host Defense against Pulmonary Tuberculosis. *Clin Dev Immunol*. 2012;2012:1-13. doi:10.1155/2012/628293

58. Cavalcanti YVN, Brelaz MCA, Lemoine Neves JKDA, Ferraz JC, Pereira VRA. Role of TNF-Alpha, IFN-Gamma, and IL-10 in the Development of Pulmonary Tuberculosis. *Pulm Med*. 2012;2012:1-10. doi:10.1155/2012/745483

59. Huebner RE, Schein MF, Bass JB. The Tuberculin Skin Test. *Clin Infect Dis*. 1993;17(6):968-975. doi:10.1093/clinids/17.6.968

60. Schluger NW, Burzynski J. Recent Advances in Testing for Latent TB. *Chest*. 2010;138(6):1456-1463. doi:10.1378/chest.10-0366

61. Pai M, Riley LW, Colford JM. Interferon-γ assays in the immunodiagnosis of tuberculosis: a systematic review. *Lancet Infect Dis*. 2004;4(12):761-776. doi:10.1016/S1473-3099(04)01206-X

62. World Health Organization. WHO consolidated guidelines on tuberculosis. Module 3: diagnosis – rapid diagnostics for tuberculosis detection. Published online 2020.

63. Dorman SE, Schumacher SG, Alland D, et al. Xpert MTB/RIF Ultra for detection of Mycobacterium tuberculosis and rifampicin resistance: a prospective multicentre diagnostic accuracy study. *Lancet Infect Dis*. 2018;18(1):76-84. doi:10.1016/S1473-3099(17)30691-6

64. Loddenkemper R, Lipman M, Zumla A. Clinical Aspects of Adult Tuberculosis. *Cold Spring Harb Perspect Med*. 2016;6(1):a017848. doi:10.1101/cshperspect.a017848

65. Lin PL, Ford CB, Coleman MT, et al. Sterilization of granulomas is common in active and latent tuberculosis despite within-host variability in bacterial killing. *Nat Med*. 2014;20(1):75-79. doi:10.1038/nm.3412

66. Zwerling A, Behr MA, Verma A, Brewer TF, Menzies D, Pai M. The BCG World Atlas: A Database of Global BCG Vaccination Policies and Practices. *PLoS Med*. 2011;8(3):e1001012. doi:10.1371/journal.pmed.1001012

67. Barreto ML, Pilger D, Pereira SM, et al. Causes of variation in BCG vaccine efficacy: Examining evidence from the BCG REVAC cluster randomized trial to explore the masking and the blocking hypotheses. *Vaccine*. 2014;32(30):3759-3764. doi:10.1016/j.vaccine.2014.05.042

68. Gasper MA, Hesseling AC, Mohar I, et al. BCG vaccination induces HIV target cell activation in HIV-exposed infants in a randomized trial. *JCI Insight*. 2017;2(7):e91963. doi:10.1172/jci.insight.91963

69. World Health Organization. Safety of BCG vaccination in immunocompromised individuals. Published online 2006.

70. World Health Organization. BCG vaccine: WHO position paper, February 2018 – Recommendations. *Vaccine*. 2018;36(24):3408-3410. doi:10.1016/j.vaccine.2018.03.009

71. Stop TB Partnership, hosted by UNOPS. TB VACCINE CLINICAL PIPELINE. Published online 2023.

72. Wang J, Thorson L, Stokes RW, et al. Single Mucosal, but Not Parenteral, Immunization with Recombinant Adenoviral-Based Vaccine Provides Potent Protection from Pulmonary Tuberculosis. *J Immunol*. 2004;173(10):6357-6365. doi:10.4049/jimmunol.173.10.6357

73. Jeyanathan M, Fritz DK, Afkhami S, et al. Aerosol delivery, but not intramuscular injection, of adenovirus-vectored tuberculosis vaccine induces respiratory-mucosal immunity in humans. *JCI Insight*. 2022;7(3):e155655. doi:10.1172/jci.insight.155655

74. Majhen D, Calderon H, Chandra N, et al. Adenovirus-Based Vaccines for Fighting Infectious Diseases and Cancer: Progress in the Field. *Hum Gene Ther*. 2014;25(4):301-317. doi:10.1089/hum.2013.235

75. Duerr A, Huang Y, Buchbinder S, et al. Extended Follow-up Confirms Early Vaccine-Enhanced Risk of HIV Acquisition and Demonstrates Waning Effect Over Time Among Participants in a Randomized Trial of Recombinant Adenovirus HIV Vaccine (Step Study). *J Infect Dis*. 2012;206(2):258-266. doi:10.1093/infdis/jis342

76. Jeyanathan M, Thanthrige-Don N, Afkhami S, et al. Novel chimpanzee adenovirus-vectored respiratory mucosal tuberculosis vaccine: overcoming local anti-human adenovirus immunity for potent TB protection. *Mucosal Immunol*. 2015;8(6):1373-1387. doi:10.1038/mi.2015.29

77. Romano M, Aryan E, Korf H, et al. Potential of Mycobacterium tuberculosis resuscitation-promoting factors as antigens in novel tuberculosis sub-unit vaccines. *Microbes Infect*. 2012;14(1):86-95. doi:10.1016/j.micinf.2011.08.011

78. Afkhami S, D'Agostino MR, Vaseghi-Shanjani M, et al. Intranasal multivalent adenoviral-vectored vaccine protects against replicating and dormant M.tb in conventional and humanized mice. *Npj Vaccines*. 2023;8(1):25. doi:10.1038/s41541-023-00623-z

79. Jeyanathan M, Yao Y, Afkhami S, Smaill F, Xing Z. New Tuberculosis Vaccine Strategies: Taking Aim at Un-Natural Immunity. *Trends Immunol*. 2018;39(5):419-433. doi:10.1016/j.it.2018.01.006

80. D'Agostino MR, Lai R, Afkhami S, et al. Airway Macrophages Mediate Mucosal Vaccine–Induced Trained Innate Immunity against *Mycobacterium tuberculosis* in Early Stages of Infection. *J Immunol*. 2020;205(10):2750-2762. doi:10.4049/jimmunol.2000532

81. Stürchler DA, Gilsdorf JR. : *Exposure: A Guide to Sources of Infections*. *Clin Infect Dis*. 2007;44(9):1257-1257. doi:10.1086/513587

82. Manabe YC, Kesavan AK, Lopez-Molina J, et al. The aerosol rabbit model of TB latency, reactivation and immune reconstitution inflammatory syndrome. *Tuberculosis*. 2008;88(3):187-196. doi:10.1016/j.tube.2007.10.006

83. Clark S, Hall Y, Williams A. Animal Models of Tuberculosis: Guinea Pigs. *Cold Spring Harb Perspect Med*. 2015;5(5):a018572-a018572. doi:10.1101/cshperspect.a018572

84. Orme IM. The mouse as a useful model of tuberculosis. *Tuberculosis*. 2003;83(1-3):112-115. doi:10.1016/S1472-9792(02)00069-0

85. Ito T, Schaller M, Hogaboam CM, Standiford TJ, Chensue SW, Kunkel SL. TLR9 activation is a key event for the maintenance of a mycobacterial antigen-elicited pulmonary granulomatous response. *Eur J Immunol*. 2007;37(10):2847-2855. doi:10.1002/eji.200737603

86. Feng CG, Kaviratne M, Rothfuchs AG, et al. NK Cell-Derived IFN-γ Differentially Regulates Innate Resistance and Neutrophil Response in T Cell-Deficient Hosts

Infected with *Mycobacterium tuberculosis*. *J Immunol*. 2006;177(10):7086-7093. doi:10.4049/jimmunol.177.10.7086

87. Scanga CA, Mohan VP, Joseph H, Yu K, Chan J, Flynn JL. Reactivation of Latent Tuberculosis: Variations on the Cornell Murine Model. Kaufmann SHE, ed. *Infect Immun*. 1999;67(9):4531-4538. doi:10.1128/IAI.67.9.4531-4538.1999

88. Kaushal D, Mehra S, Didier PJ, Lackner AA. The non-human primate model of tuberculosis: Primate model of TB. *J Med Primatol*. 2012;41(3):191-201. doi:10.1111/j.1600-0684.2012.00536.x

89. Dutta NK, Mehra S, Didier PJ, et al. Genetic Requirements for the Survival of Tubercle Bacilli in Primates. *J Infect Dis*. 2010;201(11):1743-1752. doi:10.1086/652497

90. Straetemans M, Bierrenbach AL, Nagelkerke N, Glaziou P, Van Der Werf MJ. The Effect of Tuberculosis on Mortality in HIV Positive People: A Meta-Analysis. Pai M, ed. *PLoS ONE*. 2010;5(12):e15241. doi:10.1371/journal.pone.0015241

91. Lawn SD, Wood R, De Cock KM, Kranzer K, Lewis JJ, Churchyard GJ. Antiretrovirals and isoniazid preventive therapy in the prevention of HIV-associated tuberculosis in settings with limited health-care resources. *Lancet Infect Dis*. 2010;10(7):489-498. doi:10.1016/S1473-3099(10)70078-5

92. Long R, Boffa J. High HIV-TB Co-infection Rates in Marginalized Populations: Evidence from Alberta in Support of Screening TB Patients for HIV. *Can J Public Health*. 2010;101(3):202-204. doi:10.1007/BF03404374

93. UNAIDS. Fact Sheet - World Tuberculosis Day 2022. Published online 2022.

94. Wilson JW, Nilsen DM, Marks SM. Multidrug-Resistant Tuberculosis in Patients with Human Immunodeficiency Virus. Management Considerations within High-resourced Settings. *Ann Am Thorac Soc*. 2020;17(1):16-23. doi:10.1513/AnnalsATS.201902-185CME

95. Hesseling AC, Marais BJ, Gie RP, et al. The risk of disseminated Bacille Calmette-Guerin (BCG) disease in HIV-infected children. *Vaccine*. 2007;25(1):14-18. doi:10.1016/j.vaccine.2006.07.020

96. Sullivan ZA, Wong EB, Ndung'u T, Kasprowicz VO, Bishai WR. Latent and Active Tuberculosis Infection Increase Immune Activation in Individuals Co-Infected with HIV. *EBioMedicine*. 2015;2(4):334-340. doi:10.1016/j.ebiom.2015.03.005

97. Reid MJ, Shah NS. Approaches to tuberculosis screening and diagnosis in people with HIV in resource-limited settings. *Lancet Infect Dis*. 2009;9(3):173-184. doi:10.1016/S1473-3099(09)70043-X

98. Bares SH, Swindells S. Latent Tuberculosis and HIV Infection. *Curr Infect Dis Rep*. 2020;22(7):17. doi:10.1007/s11908-020-00726-x

99. Lanzafame M, Vento S. Tuberculosis-immune reconstitution inflammatory syndrome. *J Clin Tuberc Mycobact Dis*. 2016;3:6-9. doi:10.1016/j.jctube.2016.03.002

100. Vignesh R, Balakrishnan P, Tan HY, et al. Tuberculosis-Associated Immune Reconstitution Inflammatory Syndrome—An Extempore Game of Misfiring with Defense Arsenals. *Pathogens*. 2023;12(2):210. doi:10.3390/pathogens12020210

101. Bezuidenhout J, Roberts T, Muller L, Van Helden P, Walzl G. Pleural Tuberculosis in Patients with Early HIV Infection Is Associated with Increased TNF-Alpha Expression and Necrosis in Granulomas. Marais B, ed. *PLoS ONE*. 2009;4(1):e4228. doi:10.1371/journal.pone.0004228

102. Diedrich CR, Flynn JL. HIV-1/ *Mycobacterium tuberculosis* Coinfection Immunology: How Does HIV-1 Exacerbate Tuberculosis? Maurelli AT, ed. *Infect Immun*. 2011;79(4):1407-1417. doi:10.1128/IAI.01126-10

103. Kalsdorf B, Scriba TJ, Wood K, et al. HIV-1 Infection Impairs the Bronchoalveolar T-Cell Response to Mycobacteria. *Am J Respir Crit Care Med*. 2009;180(12):1262-1270. doi:10.1164/rccm.200907-1011OC

104. Bell LCK, Pollara G, Pascoe M, et al. In Vivo Molecular Dissection of the Effects of HIV-1 in Active Tuberculosis. Fortune SM, ed. *PLOS Pathog*. 2016;12(3):e1005469. doi:10.1371/journal.ppat.1005469

105. Geldmacher C, Ngwenyama N, Schuetz A, et al. Preferential infection and depletion of *Mycobacterium tuberculosis* –specific CD4 T cells after HIV-1 infection. *J Exp Med*. 2010;207(13):2869-2881. doi:10.1084/jem.20100090

106. Treerat P, Prince O, Cruz-Lagunas A, et al. Novel role for IL-22 in protection during chronic Mycobacterium tuberculosis HN878 infection. *Mucosal Immunol*. 2017;10(4):1069-1081. doi:10.1038/mi.2017.15

107. Nakata K, Rom WN, Honda Y, et al. Mycobacterium tuberculosis enhances human immunodeficiency virus-1 replication in the lung. *Am J Respir Crit Care Med*. 1997;155(3):996-1003. doi:10.1164/ajrccm.155.3.9117038

108. Cambier CJ, Takaki KK, Larson RP, et al. Mycobacteria manipulate macrophage recruitment through coordinated use of membrane lipids. *Nature*. 2014;505(7482):218-222. doi:10.1038/nature12799

109. Kyei GB, Dinkins C, Davis AS, et al. Autophagy pathway intersects with HIV-1 biosynthesis and regulates viral yields in macrophages. *J Cell Biol*. 2009;186(2):255-268. doi:10.1083/jcb.200903070

110. Mazzolini J, Herit F, Bouchet J, Benmerah A, Benichou S, Niedergang F. Inhibition of phagocytosis in HIV-1–infected macrophages relies on Nef-dependent alteration of focal delivery of recycling compartments. *Blood*. 2010;115(21):4226-4236. doi:10.1182/blood-2009-12-259473

111. Martineau AR, Nhamoyebonde S, Oni T, et al. Reciprocal seasonal variation in vitamin D status and tuberculosis notifications in Cape Town, South Africa. *Proc Natl Acad Sci*. 2011;108(47):19013-19017. doi:10.1073/pnas.1111825108

112. Pawlowski A, Jansson M, Sköld M, Rottenberg ME, Källenius G. Tuberculosis and HIV Co-Infection. Hobman TC, ed. *PLoS Pathog*. 2012;8(2):e1002464. doi:10.1371/journal.ppat.1002464

113. Walker NF, Clark SO, Oni T, et al. Doxycycline and HIV Infection Suppress Tuberculosis-induced Matrix Metalloproteinases. *Am J Respir Crit Care Med*. 2012;185(9):989-997. doi:10.1164/rccm.201110-1769OC

114. Toossi Z, Johnson JL, Kanost RA, et al. Increased Replication of HIV-1 at Sites of Mycobacterium tuberculosis Infection: Potential Mechanisms of Viral Activation: *JAIDS J Acquir Immune Defic Syndr*. 2001;28(1):1-8. doi:10.1097/00042560-200109010-00001

115. Tomlinson GS, Bell LCK, Walker NF, et al. HIV-1 Infection of Macrophages Dysregulates Innate Immune Responses to Mycobacterium tuberculosis by Inhibition of Interleukin-10. *J Infect Dis*. 2014;209(7):1055-1065. doi:10.1093/infdis/jit621

116. Poli G, Kinter AL, Fauci AS. Interleukin 1 induces expression of the human immunodeficiency virus alone and in synergy with interleukin 6 in chronically infected U1 cells: inhibition of inductive effects by the interleukin 1 receptor antagonist. *Proc Natl Acad Sci*. 1994;91(1):108-112. doi:10.1073/pnas.91.1.108

117. Duh EJ, Maury WJ, Folks TM, Fauci AS, Rabson AB. Tumor necrosis factor alpha activates human immunodeficiency virus type 1 through induction of nuclear factor binding to the NF-kappa B sites in the long terminal repeat. *Proc Natl Acad Sci*. 1989;86(15):5974-5978. doi:10.1073/pnas.86.15.5974

118. Mlcochova P, Sutherland KA, Watters SA, et al. A G1-like state allows HIV -1 to bypass SAMHD 1 restriction in macrophages. *EMBO J*. 2017;36(5):604-616. doi:10.15252/embj.201696025

119. Gong W, Liang Y, Wu X. Animal Models of Tuberculosis Vaccine Research: An Important Component in the Fight against Tuberculosis. *BioMed Res Int*. 2020;2020:4263079. doi:10.1155/2020/4263079

120. Mattila JT, Diedrich CR, Lin PL, Phuah J, Flynn JL. Simian Immunodeficiency Virus-Induced Changes in T Cell Cytokine Responses in Cynomolgus Macaques with Latent *Mycobacterium tuberculosis* Infection Are Associated with Timing of Reactivation. *J Immunol*. 2011;186(6):3527-3537. doi:10.4049/jimmunol.1003773

121. Mehra S, Golden NA, Dutta NK, et al. Reactivation of latent tuberculosis in rhesus macaques by coinfection with simian immunodeficiency virus: Reactivation of latent TB. *J Med Primatol*. 2011;40(4):233-243. doi:10.1111/j.1600-0684.2011.00485.x

122. Kuroda MJ, Sugimoto C, Cai Y, et al. High Turnover of Tissue Macrophages Contributes to Tuberculosis Reactivation in Simian Immunodeficiency Virus-Infected Rhesus Macaques. *J Infect Dis*. 2018;217(12):1865-1874. doi:10.1093/infdis/jix625

123. Bell LCK, Noursadeghi M. Pathogenesis of HIV-1 and Mycobacterium tuberculosis co-infection. *Nat Rev Microbiol*. 2018;16(2):80-90. doi:10.1038/nrmicro.2017.128

124. Shultz LD, Ishikawa F, Greiner DL. Humanized mice in translational biomedical research. *Nat Rev Immunol*. 2007;7(2):118-130. doi:10.1038/nri2017

125. Schwarz K, Ma Y, Pannicke U, Lieber MR. Human severe combined immune deficiency and DNA repair. *BioEssays*. 2003;25(11):1061-1070. doi:10.1002/bies.10344

126. Blunt T, Finnie NJ, Taccioli GE, et al. Defective DNA-dependent protein kinase activity is linked to V(D)J recombination and DNA repair defects associated with the murine scid mutation. *Cell*. 1995;80(5):813-823. doi:10.1016/0092-8674(95)90360-7

127. Bosma GC, Fried M, Custer RP, Carroll A, Gibson DM, Bosma MJ. Evidence of functional lymphocytes in some (leaky) scid mice. *J Exp Med*. 1988;167(3):1016-1033. doi:10.1084/jem.167.3.1016

128. Priestley A. Molecular and biochemical characterisation of DNA-dependent protein kinase-defective rodent mutant irs-20. *Nucleic Acids Res*. 1998;26(8):1965-1973. doi:10.1093/nar/26.8.1965

129. Hesselton RM, Greiner DL, Mordes JP, Rajan TV, Sullivan JL, Shultz LD. High Levels of Human Peripheral Blood Mononuclear Cell Engraftment and Enhanced Susceptibility to Human Immunodeficiency Virus Type 1 Infection in NOD/LtSz-scid/scid Mice. *J Infect Dis*. 1995;172(4):974-982. doi:10.1093/infdis/172.4.974

130. Katano I, Ito R, Kamisako T, et al. NOD-*Rag2*^{null} *IL-2Rγ*^{null} Mice: An Alternative to NOG Mice for Generation of Humanized Mice. *Exp Anim*. 2014;63(3):321-330. doi:10.1538/expanim.63.321

131. Mombaerts P, Iacomini J, Johnson RS, Herrup K, Tonegawa S, Papaioannou VE. RAG-1-deficient mice have no mature B and T lymphocytes. *Cell*. 1992;68(5):869-877. doi:10.1016/0092-8674(92)90030-G

132. Shinkai Y. RAG-2-deficient mice lack mature lymphocytes owing to inability to initiate V(D)J rearrangement. *Cell*. 1992;68(5):855-867. doi:10.1016/0092-8674(92)90029-C

133. Shultz LD, Banuelos S, Lyons B, et al. NOD/LtSz-Rag1 null Pfp null mice: a new model system with increased levels of human peripheral leukocyte and hematopoietic stem-cell engraftment. *Transplantation*. 2003;76(7):1036-1042. doi:10.1097/01.TP.0000083041.44829.2C

134. Shultz LD, Lyons BL, Burzenski LM, et al. Human Lymphoid and Myeloid Cell Development in NOD/LtSz- *scid IL2R* γ *null* Mice Engrafted with Mobilized Human Hemopoietic Stem Cells. *J Immunol*. 2005;174(10):6477-6489. doi:10.4049/jimmunol.174.10.6477

135. Brehm MA, Cuthbert A, Yang C, et al. Parameters for establishing humanized mouse models to study human immunity: Analysis of human hematopoietic stem cell engraftment in three immunodeficient strains of mice bearing the IL2rγnull mutation. *Clin Immunol*. 2010;135(1):84-98. doi:10.1016/j.clim.2009.12.008

136. Gillgrass A, Wessels JM, Yang JX, Kaushic C. Advances in Humanized Mouse Models to Improve Understanding of HIV-1 Pathogenesis and Immune Responses. *Front Immunol*. 2021;11:617516. doi:10.3389/fimmu.2020.617516

137. Cheng L, Ma J, Li G, Su L. Humanized Mice Engrafted With Human HSC Only or HSC and Thymus Support Comparable HIV-1 Replication, Immunopathology, and Responses to ART and Immune Therapy. *Front Immunol*. 2018;9:817. doi:10.3389/fimmu.2018.00817

138. Choo SY. The HLA System: Genetics, Immunology, Clinical Testing, and Clinical Implications. *Yonsei Med J*. 2007;48(1):11. doi:10.3349/ymj.2007.48.1.11

139. Villaudy J, Schotte R, Legrand N, Spits H. Critical assessment of human antibody generation in humanized mouse models. *J Immunol Methods*. 2014;410:18-27. doi:10.1016/j.jim.2014.06.010

140. Hess NJ, Brown ME, Capitini CM. GVHD Pathogenesis, Prevention and Treatment: Lessons From Humanized Mouse Transplant Models. *Front Immunol*. 2021;12:723544. doi:10.3389/fimmu.2021.723544

141. Victor Garcia J. Humanized mice for HIV and AIDS research. *Curr Opin Virol*. 2016;19:56-64. doi:10.1016/j.coviro.2016.06.010

142. Marsden MD, Zack JA. Humanized Mouse Models for Human Immunodeficiency Virus Infection. *Annu Rev Virol*. 2017;4(1):393-412. doi:10.1146/annurev-virology-101416-041703

143. Lepard M, Yang JX, Afkhami S, et al. Comparing Current and Next-Generation Humanized Mouse Models for Advancing HIV and HIV/Mtb Co-Infection Studies. *Viruses*. 2022;14(9):1927. doi:10.3390/v14091927

144. Kim J, Peachman KK, Jobe O, et al. Tracking Human Immunodeficiency Virus-1 Infection in the Humanized DRAG Mouse Model. *Front Immunol*. 2017;8:1405. doi:10.3389/fimmu.2017.01405

145. Denton PW, Long JM, Wietgrefe SW, et al. Targeted Cytotoxic Therapy Kills Persisting HIV Infected Cells During ART. Douek DC, ed. *PLoS Pathog*. 2014;10(1):e1003872. doi:10.1371/journal.ppat.1003872

146. Denton PW, Olesen R, Choudhary SK, et al. Generation of HIV Latency in Humanized BLT Mice. *J Virol*. 2012;86(1):630-634. doi:10.1128/JVI.06120-11

147. Honeycutt JB, Thayer WO, Baker CE, et al. HIV persistence in tissue macrophages of humanized myeloid-only mice during antiretroviral therapy. *Nat Med*. 2017;23(5):638-643. doi:10.1038/nm.4319

148. Satheesan S, Li H, Burnett JC, et al. HIV Replication and Latency in a Humanized NSG Mouse Model during Suppressive Oral Combinational Antiretroviral Therapy. Silvestri G, ed. *J Virol*. 2018;92(7):e02118-17. doi:10.1128/JVI.02118-17

149. Rajashekar JK, Richard J, Beloor J, et al. Modulating HIV-1 envelope glycoprotein conformation to decrease the HIV-1 reservoir. *Cell Host Microbe*. 2021;29(6):904-916.e6. doi:10.1016/j.chom.2021.04.014

150. Calderon VE, Valbuena G, Goez Y, et al. A Humanized Mouse Model of Tuberculosis. Cardona PJ, ed. *PLoS ONE*. 2013;8(5):e63331. doi:10.1371/journal.pone.0063331

151. Arrey F, Löwe D, Kuhlmann S, et al. Humanized Mouse Model Mimicking Pathology of Human Tuberculosis for in vivo Evaluation of Drug Regimens. *Front Immunol*. 2019;10:89. doi:10.3389/fimmu.2019.00089

152. Yao Y, Lai R, Afkhami S, et al. Enhancement of Antituberculosis Immunity in a Humanized Model System by a Novel Virus-Vectored Respiratory Mucosal Vaccine. *J Infect Dis*. 2017;216(1):135-145. doi:10.1093/infdis/jix252

153. Nusbaum RJ, Calderon VE, Huante MB, et al. Pulmonary Tuberculosis in Humanized Mice Infected with HIV-1. *Sci Rep*. 2016;6(1):21522. doi:10.1038/srep21522

154. Jambo KC, Banda DH, Kankwatira AM, et al. Small alveolar macrophages are infected preferentially by HIV and exhibit impaired phagocytic function. *Mucosal Immunol*. 2014;7(5):1116-1126. doi:10.1038/mi.2013.127

155. Huante MB, Saito TB, Nusbaum RJ, et al. Small Animal Model of Post-chemotherapy Tuberculosis Relapse in the Setting of HIV Co-infection. *Front Cell Infect Microbiol*. 2020;10:150. doi:10.3389/fcimb.2020.00150

156. Guirado E, Schlesinger LS, Kaplan G. Macrophages in tuberculosis: friend or foe. *Semin Immunopathol*. 2013;35(5):563-583. doi:10.1007/s00281-013-0388-2

157. Koppensteiner H, Brack-Werner R, Schindler M. Macrophages and their relevance in Human Immunodeficiency Virus Type I infection. *Retrovirology*. 2012;9(1):82. doi:10.1186/1742-4690-9-82

158. Bell LCK, Noursadeghi M. Pathogenesis of HIV-1 and Mycobacterium tuberculosis co-infection. *Nat Rev Microbiol*. 2018;16(2):80-90. doi:10.1038/nrmicro.2017.128

159. Winkler MS, Rissiek A, Priefler M, et al. Human leucocyte antigen (HLA-DR) gene expression is reduced in sepsis and correlates with impaired TNFα response: A diagnostic tool for immunosuppression? Infante-Duarte C, ed. *PLOS ONE*. 2017;12(8):e0182427. doi:10.1371/journal.pone.0182427

160. Yu YRA, Hotten DF, Malakhau Y, et al. Flow Cytometric Analysis of Myeloid Cells in Human Blood, Bronchoalveolar Lavage, and Lung Tissues. *Am J Respir Cell Mol Biol*. 2016;54(1):13-24. doi:10.1165/rcmb.2015-0146OC

161. World Health Organization. The top 10 causes of death. Published 2020. https://newtbvaccines.org/tb-vaccine-pipeline/

162. World Health Organization. BCG Vaccine. https://www.who.int/teams/health-product-policy-and-standards/standards-and-specifications/vaccines-quality/bcg#:~:text=BCG%20vaccine%20has%20a%20documented,bacillary%20spread%20in%20the%20community.

163. Griffiths KL, Villarreal DO, Weiner DB, Khader SA. A novel multivalent tuberculosis vaccine confers protection in a mouse model of tuberculosis. *Hum Vaccines Immunother*. 2016;12(10):2649-2653. doi:10.1080/21645515.2016.1197454

164. Kruize Z, Kootstra NA. The Role of Macrophages in HIV-1 Persistence and Pathogenesis. *Front Microbiol*. 2019;10:2828. doi:10.3389/fmicb.2019.02828

165. Holguin L, Echavarria L, Burnett JC. Novel Humanized Peripheral Blood Mononuclear Cell Mouse Model with Delayed Onset of Graft-versus-Host Disease for Preclinical HIV Research. Silvestri G, ed. *J Virol*. 2022;96(3):e01394-21. doi:10.1128/JVI.01394-21

166. Danner R, Chaudhari SN, Rosenberger J, et al. Expression of HLA Class II Molecules in Humanized NOD.Rag1KO.IL2RgcKO Mice Is Critical for Development and Function of Human T and B Cells. Chatenoud L, ed. *PLoS ONE*. 2011;6(5):e19826. doi:10.1371/journal.pone.0019826

167. Neal LR, Bailey SR, Wyatt MM, et al. The Basics of Artificial Antigen Presenting Cells in T Cell-Based Cancer Immunotherapies. *J Immunol Res Ther*. 2017;2(1):68-79.

168. Klenerman P, Cerundolo V, Dunbar PR. Tracking T cells with tetramers: new tales from new tools. *Nat Rev Immunol*. 2002;2(4):263-272. doi:10.1038/nri777

169. Duerr A, Huang Y, Buchbinder S, et al. Extended Follow-up Confirms Early Vaccine-Enhanced Risk of HIV Acquisition and Demonstrates Waning Effect Over Time Among Participants in a Randomized Trial of Recombinant Adenovirus HIV Vaccine (Step Study). *J Infect Dis*. 2012;206(2):258-266. doi:10.1093/infdis/jis342

170. Murphy DM, Mills KHG, Basdeo SA. The Effects of Trained Innate Immunity on T Cell Responses; Clinical Implications and Knowledge Gaps for Future Research. *Front Immunol*. 2021;12:706583. doi:10.3389/fimmu.2021.706583

171. Brainard DM, Seung E, Frahm N, et al. Induction of Robust Cellular and Humoral Virus-Specific Adaptive Immune Responses in Human Immunodeficiency Virus-Infected Humanized BLT Mice. *J Virol*. 2009;83(14):7305-7321. doi:10.1128/JVI.02207-08

172. Saito S, Murase K. Detection and Early Phase Assessment of Radiation-Induced Lung Injury in Mice Using Micro-CT. Muñoz-Barrutia A, ed. *PLoS ONE*. 2012;7(9):e45960. doi:10.1371/journal.pone.0045960

173. Plumlee CR, Duffy FJ, Gern BH, et al. Ultra-low Dose Aerosol Infection of Mice with Mycobacterium tuberculosis More Closely Models Human Tuberculosis. *Cell Host Microbe*. 2021;29(1):68-82.e5. doi:10.1016/j.chom.2020.10.003

174. Saini D, Hopkins GW, Seay SA, et al. Ultra-low dose of Mycobacterium tuberculosis aerosol creates partial infection in mice. *Tuberculosis*. 2012;92(2):160-165. doi:10.1016/j.tube.2011.11.007

175. HIV.gov. The Global HIV and AIDS Epidemic. Published 2023. https://www.hiv.gov/hiv-basics/overview/data-and-trends/global-statistics/

176. CATIE. Common HIV drugs available in Canada for adults. Published 2023. https://www.catie.ca/your-guide-to-hiv-treatment/common-hiv-drugs-available-in-canada-for-adults